

CQUniversity Australia



High Performance Brushless DC Motor Control

Submitted by
Patrick Fisher

Final year research project report submitted in partial fulfilment of the coursework requirements for the degree of Bachelor of Engineering

May 2014

School of Engineering & Technology
CQUniversity Australia

Executive Summary

This thesis presents a method for controlling synchronous brushless DC machines via advanced control techniques that are usually reserved for use in high end industrial AC machine drives. The DC machines this research is aimed at are commonly found in model aircraft, including advanced research aircraft such as 'drones'. However, this research is not limited to model aircraft or vehicles and has applications anywhere BLDC motors are used.

It was hypothesised that by utilising an advanced control technique on a purpose built custom motor controller, superior motor performance could be achieved when compared to that which is possible with the current generation of commercial motor controllers. For the purposes of this research, 'superior performance' was defined as improved dynamic response, more stable (closed loop) control, higher efficiency and the ability to commutate motors stably at lower speeds. In addition, the controller to be developed aimed to be comparable with commercial options in terms of size, weight and cost and to be able to be used wherever commercial controllers are currently used.

Current research was reviewed with particular focus on literature comparing *Field Oriented Control* and *Direct Torque Control* which are the two most common methodologies for advanced motor control. The intent was to investigate their potential application to small brushless DC machines. Based on the results of the literature review conducted, *Field Oriented Control* (FOC) was the chosen control technique to be applied. On the basis of further research, a commercial FOC solution by Texas Instruments was chosen.

Using the commercial *Field Oriented Control* development solution, InstaSPIN™ by Texas Instruments, the feasibility of the project was first assessed on a TI development board. Following a partially successful initial evaluation, a prototype custom controller was developed to better suit the requirements of the research. This controller was then evaluated against commercially available options in order to determine the viability of *Field Oriented Control* for the stated purpose.

This thesis documents the initial evaluation of TI's InstaSPIN-FOC using a TI development board, the development of several prototype controllers as well as their empirical evaluation. It outlines relevant theory and describes the methodology used in the development of a prototype custom motor controller together with the reasoning that informed design choices that were made. It also includes all data, descriptions of the data collection methods and data analysis.

Acknowledgements

This work would not have been possible without the assistance and support of a number of people. I would like to thank Dr D.M.G Preethichndra (CQU), Mr Chris Clearman (Texas Instruments), Mr Nicholas Oborny (Texas Instruments), Mr Ian Tomlinson (CQU) and Mr Simon Cumming (CQU) for their guidance and encouragement.

Declaration

I certify that this work is my own and has not been submitted to any other university, publication or professional body for assessment. All work derived from, or directly quoted from any other publications has been appropriately referenced and credit given to the author(s) of the publication.

Material submitted for assessment in *ENEG14003 - Engineering Project Planning* has been included in this submission. This work includes the literature review and part of the Theory chapter and was submitted in the project planning phase and was always intended to be submitted with this thesis.

Contents

Executive Summary.....	ii
Acknowledgements.....	iii
Declaration.....	iv
List of Figures	viii
List of Tables	x
Abbreviations	xi
1 Introduction	1
1.1 Background	1
1.2 Objective of the Research	2
1.3 Significance of the Research	2
1.4 Limitations of the Research	2
1.5 Structure of the Thesis.....	2
2 Literature Review.....	3
2.1 Scalar Control.....	3
2.1.1 Six Step Commutation.....	3
2.1.2 Sinusoidal Commutation.....	4
2.2 Vector Control.....	5
2.2.1 Field Oriented Control Functional Overview	5
2.2.2 Direct Torque Control Functional Overview	7
2.2.3 FOC and DTC Comparison	8
2.3 Rotor Position Estimation	11
2.3.1 Hall Effect Sensors.....	11
2.3.2 Back-EMF Zero Crossing.....	12
2.3.3 Extended Kalman Filter	13
2.3.4 Sliding Mode Observer.....	13
2.3.5 TI FAST.....	14
2.4 Power Control Schemes	14
2.4.1 Low/High Dedicated Driver.....	15
2.4.2 Low-Side Devices.....	15
2.4.3 High-Side Devices	16
2.5 Literature Review Conclusion and Control Method Selection.....	17
3 Theory	18
3.1 FOC Operation Theory	18

3.2	Space Vector Pulse Width Modulation	20
3.3	Sensorless Rotor Position Estimation	22
4	InstaSPIN™-FOC	23
4.1	InstaSPIN-FOC Overview and Functions	23
4.2	FAST Estimator	23
4.3	Control Loops	25
4.3.1	Torque Controller.....	26
4.3.2	Speed Controller	29
4.4	Motor Identification.....	35
5	Methodology.....	38
5.1	Evaluation Board	38
5.2	Initial InstaSPIN-FOC Evaluation	42
5.2.1	Motor Identification.....	43
5.2.2	Torque Controller.....	43
5.2.3	Speed Controller	44
5.2.4	Initial InstaSPIN FOC Evaluation Conclusion	44
5.3	Custom Controller Development	44
5.3.1	Microcontroller	45
5.3.2	Gate Driver	46
5.3.3	Current Sense.....	47
5.3.4	Voltage Sense.....	50
5.3.5	Switching Devices (MOSFETs)	51
5.3.6	Miscellaneous	51
5.3.7	PCB Layout	53
5.3.8	Prototyping	58
5.3.9	InstaSPIN™-FOC User Configuration	63
5.3.9.1	Software Execution Timing	63
5.3.9.2	InstaSPIN-FOC Hardware Parameters.....	64
5.3.9.3	InstaSPIN-FOC Motor Parameters and ID Settings	65
5.9.3.9	Added Abstractions.....	66
6	Results and Discussion	68
6.9	Test Motors and Controllers	69
6.10	Identification Results	70
6.11	Unloaded.....	70

6.12	Loaded.....	75
6.13	Cost and Physical Comparison	81
7	Conclusions and Recommendations for Future Work.....	82
7.9	Recommendations for Future Work	82
Bibliography	84	
APENDIX I	87	
Appendix II	92	
Appendix III	93	

List of Figures

Figure 1. Research Drone with Commercial Motor Controllers Visible (SERL, 2014)	1
Figure 2 – Six-Step Commutation. (Microcontroller Solutions, n.d.).....	4
Figure 3 –Sinusoidal vs. back-EMF Waveforms. (Torres, 2009).....	5
Figure 4-Direct (d) and orthogonal (q) force components (John, et al., 2011).....	6
Figure 5-Functional block diagram of a generic FOC drive. (Lepka, 2009)	6
Figure 6. DTC Control Scheme for PMSM (Paturca, et al., 2006).....	7
Figure 7. Inverter voltage vectors and stator flux vectors (Paturca, et al., 2006).	8
Figure 8. Three-phase Hall sensor timing chart with 120° angle separation (Lee & Lemley, n.d.).....	12
Figure 9. Circuit model during PWM ON-time (Ungurean, et al., 2010).....	12
Figure 10. FAST™ Sensorless Observer. (Texas Instruments, 2013)	14
Figure 11. IR2101 implementation for one phase of a MOSFET power stage (Lock, 2012).	15
Figure 12. High-side p-channel device (left) and high-side n-channel device (right) implementation (Lock, 2012).....	16
Figure 13-Clarke's Transformation. (Zambada & Deb, 2010)	19
Figure 14 - Park's Transformation. (Zambada & Deb, 2010).....	19
Figure 15. PWM used to generate a varying analogue equivalent. (Acroname, 2007)	20
Figure 16. Basic Three Phase Inverter.....	21
Figure 17. Non-zero voltage vectors in the α, β plane. (Virginia Tech, n.d.).....	21
Figure 18. Current, Voltage and Rotor Flux (ΨR) in the d-q Rotating Reference Frame and Their Relationship with A(a), B(b),C(c) and (α, β) Stationary Reference Frame. (Akin & Bhardwaj, 2013) ..	22
Figure 19. InstaSPIN™-FOC Block Diagram (Texas Instruments, 2013)	23
Figure 20. Speed controller cascaded with a current controller (Texas Instruments, 2013).	25
Figure 21. Generic Series PI control (Texas Instruments, 2013).....	26
Figure 22. Torque Control System (Texas Instruments, 2013).	27
Figure 23. Parallel PI Control (Texas Instruments, 2013).....	30
Figure 24. Mass, spring, damper mechanical system (Texas Instruments, 2013)	31
Figure 25. Ideal Speed Controller Bode Plot (Texas Instruments, 2013).....	33
Figure 26. Estimator State Diagram (Texas Instruments, 2013)	35
Figure 27. InstaSPIN Motor Identification Sequence (Texas Instruments, 2013).....	36
Figure 28. Evaluation Board	39
Figure 29. 45A AttoPilot Current Sense board (AttoPilotInternational, 2011)	39
Figure 30. AMT-103 Rotary Encoder.....	40
Figure 31. Quadrature Encoding (CUI INC, 2010)	40
Figure 32. 128*128 Pixel OLED Display.....	41
Figure 33. DRV8301-69M-KIT (Texas Instruments, 2014).....	42
Figure 34. Initial InstaSPIN™-FOC evaluation (Evaluation and Development boards visible).	42
Figure 35. TI's DRV8301 BOOSTXL (Texas Instruments, 2014).	45
Figure 36. DRV8301 Simplified Application Schematic (Texas Instruments, 2011).....	47
Figure 37. Inverter Stage with Low Side Shunt Resistors Circled in Blue.....	48
Figure 38. Differential Amplifier (Texas Instruments, 2013).	48
Figure 39. OPA2374 External Amplifier	49
Figure 40. Bus and Phase Feedback Voltage Dividers.....	50
Figure 41. DRV8301 Buck Converter.....	52

Figure 42. Custom FOC controller (Revision 2C) PCB layout.....	53
Figure 43. DRV8301 Pre-Driver and Associated Components (Revision 2C).	53
Figure 44. Cross Section of PowerPAD™ Package Mounted to PCB and Resulting Heat Transfer (Kummerl, 2011)	54
Figure 45. F28027F MCU Placement (Revision 2C).....	54
Figure 46. Low Side MOSFET Placement (Revision 2C).....	54
Figure 47. R ₃₆ With (Left) and Without (Right) Thermal Relief.	55
Figure 48. Differential Signal Parameters.	56
Figure 49. High Current Traces (Revision 2C).....	56
Figure 50. Phase Voltage Sense Dividers.	57
Figure 51. 2.54mm and SAMTEC Headers.	58
Figure 52. Custom Motor Controller Unpopulated Boards.	58
Figure 53. Custom FOC Controller Revision 2A Top Side.....	60
Figure 54. Custom FOC Controller Revision 2A Bottom Side.....	60
Figure 55. Custom Controller Revision 2C Top Side.....	62
Figure 56. Custom Controller Revision 2C Bottom Side.....	62
Figure 57. Phase-Gnd Waveform: Custom FOC Controller.....	64
Figure 58. Evaluated Motors, Controllers and Loads.....	68
Figure 59. PropDrive Motor Unloaded Data.....	71
Figure 60. Unknown Motor Unloaded Data.	72
Figure 61. 2278 Motor Unloaded Data.....	73
Figure 62. PropDrive Motor Loaded Data.....	76
Figure 63. Unknown Motor Unloaded Data.	77
Figure 64. 2278 Motor Loaded Data.....	78
Figure 65. Multi-Step Response of controller/motor combinations.	79

List of Tables

Table 1. Torque settling time at different speeds (Garcia, et al., n.d.).....	9
Table 2. Steady state performance indexes (Garcia, et al., n.d.).....	9
Table 3. Comparison of FOC and DTC as implemented for a PMSM (Garcia, et al., n.d.) & (Merzoug & Naceri, 2008).....	10
Table 4. SVPWM Switching Vectors. Ref: Figure 16.....	21
Table 5. FAST Estimator Compared to Typical Solutions (Texas Instruments, 2013)	24
Table 6. C2000 InstaSPIN-FOC Capable Microcontroller comparison.....	46
Table 7. Selected Hobby Motors and Known Parameters.....	69
Table 8. Selected Motor Controllers and Known Parameters.	69
Table 9. Identification Results.....	70
Table 10. Unloaded Motor Results.	70
Table 11. Loaded Motor Results.	75

Abbreviations

ADC	Analogue to Digital Converter
BLAC	Brushless Alternating Current (motor)
BLDC	Brushless Direct Current (motor)
CAD	Computer Aided Design
CMOS	Complementary Metal Oxide Semiconductor
CNC	Computer Numerical Control
CQU	Central Queensland University
DCA	Direct Chip Attach
DTC	Direct Torque Control
ESC	Electronic Speed Controller
FOC	Field Oriented Control
FPU	Floating Point Unit
GPIO	General Purpose Input Output
I ² C	Inter-Integrated Circuit
IC	Integrated Circuit
JTAG	Joint Test Action Group
LED	Light Emitting Diode
LiPo	Lithium Polymer
MCU	Microcontroller Unit
MOSFET	Metal Oxide Semiconductor Field Effect Transistor
OLED	Organic Light Emitting Diode
PIE	Peripheral Interrupt Expansion
PMSM	Permanent Magnet Synchronous Motor
PWM	Pulse Width Modulation
RC	Radio Control
RAM	Random Access Memory
ROM	Read Only Memory
RPM	Revolutions Per Minute
SCI	Serial Communications Interface
SCL	Serial Clock Line
SDA	Serial Data Line
SMD	Surface Mount Device
SON	Small Outline – No Leads
SPI	Serial Peripheral Interface
SVPWM	Space Vector Pulse Width Modulation
TSSOP	Thin Shrink Small Outline Package
TTL	Transistor Transistor Logic
UART	Universal Asynchronous Receiver Transmitter

1 Introduction

1.1 Background

Over the past several decades, the brushed DC motor has been phased out in virtually all applications in favour of the brushless DC (BLDC) motor. This is because the BLDC motor is superior to its brushed counterpart in almost every way, including efficiency, power density, controllability and reliability.

The BLDC motor has become the standard motor type for use in all small-scale electric vehicles from low performance model aeroplanes to advanced research ‘drones’. The BLDC motor is perfectly suited to these applications as it is inherently efficient, has a very high power-to-weight-ratio and the lack of mechanical commutators (brushes) makes them extremely reliable. However, the current state of commercial electronic controllers for these motors offer only limited controllability and are not able to drive the motors to their full potential. This effectively limits the potential of all applications of these motors, having a particularly noticeable effect on high performance vehicles. Figure 1 below shows an advanced research drone with typical commercial motor controllers (red ‘box’ on each of the four struts) and BLDC motors (of a size this research is focussed on).



Figure 1. Research Drone with Commercial Motor Controllers Visible (SERL, 2014)

The performance issues associated with commercial controllers are a direct result of the relatively simplistic control techniques that are invariably used. These controllers use a scalar control technique called six-step control (see 2.1.1 Six Step Commutation) which, by nature, results in poor dynamic response, sub-optimal efficiency and a high torque ripple leading to increased vibrations and subsequently shorter motor life. In addition, these controllers are not capable of low speed commutation. This is not a direct result of the six-step control technique, but reflects the simplistic rotor position estimation technique used, back-EMF zero crossing detection (see 2.3.2 Back-EMF Zero Crossing).

1.2 Objective of the Research

This research aimed to show that advanced motor control techniques, currently reserved for high-end industrial AC machine drives, can be successfully utilised in small DC machine controllers designed for synchronous permanent magnet motors, with a particular focus on ‘hobby’ sized BLDC motors (see Figure 1 for reference). This required the development of custom hardware which utilised an advanced control technique as well as the empirical evaluation of the controller against the current generation of commercial controllers.

A secondary aim of this research is to allow very low speed commutation by utilising a more capable rotor position estimation technique.

1.3 Significance of the Research

If successful, this research will effectively increase the general performance all small-electric vehicle applications which currently utilise standard commercial controllers. It is anticipated that this research will be particularly useful for advanced research or hobbyist vehicles, notably, multicopters. In addition, low speed commutation will allow a direct drive mechanical system to be used where gearboxes or expensive electro-mechanical rotor position sensors were once required, reducing maintenance requirements and costs. Small-scale autonomous submersible vehicles are an example.

1.4 Limitations of the Research

This research was limited by both time and money. There was a total of five months allocated to the research (not inclusive of preparatory research time). This limited the total scope of the research as well as the testing that could be conducted, due to unavailability of laboratory instruments. In addition, this research was only aimed at BLDC motors of the type and size found in scale electric vehicles. These motors vary widely in appearance, ratings and parameters, but, in general they are ‘outrunner’ types with rated current consumption of less than 20A and a bus voltage rating less than 21V.

1.5 Structure of the Thesis

The design of a custom motor controller for ‘hobby’-sized 3-phase synchronous permanent magnet motors utilising an advanced control technique is outlined in this thesis. This includes the initial research undertaken in preparation for the thesis (Chapter 2, [Literature Review](#)), the underlying theory for the control technique chosen (Chapter 3, [Theory](#)), theory specifically pertaining to the chosen solution (Chapter 4, [InstaSPIN™-FOC](#)), the research methodology including justification for all decisions made (Chapter 5, [Methodology](#)), results of the research and discussion about their meaning (Chapter 6, [Results and Discussion](#)) and finally, the conclusion and recommendations for future work (Chapter 7, [Conclusions and Recommendations for Future Work](#)).

2 Literature Review

DC motors can be categorised in terms of the shape of the back-EMF waveform generated, either sinusoidal or trapezoidal. Often, motors which ‘naturally’ produce sinusoidal back-EMF are referred to as permanent magnet synchronous motors (PMSM) and motors with ‘natural’ trapezoidal back-EMF are referred to as brushless DC motors (BLDCM). However, the literature on BLDC motor commutation is not always consistent in this respect and the only physical difference between so-called PMSM and BLDC motors is in the way the stator windings are wound. This does serve to make each individual motor more suited to a particular commutation method but it does not limit the motor to a particular commutation method. It should also be noted that it is ultimately the commutation method employed that dictates the back-EMF waveform generated (Liu & Zhu, 2008). In an effort to maintain consistency, when referring to motors with ‘natural’ sinusoidal back-EMF, the term Permanent Magnet Synchronous Motor (PMSM) will be used and when referring to motors with ‘natural’ trapezoidal back-EMF, the term Brushless DC (BLDC) motor will be used. However, both motors are powered by a DC source and electrically commutated. Hence, both BLDC and PMSM motors are brushless DC machines under any rigid definition.

2.1 Scalar Control

Scalar motor control drives only manipulate the voltage magnitude and frequency supplied to the motor.

2.1.1 Six Step Commutation

Conventional BLDC motor control is a form of scalar control and relies on a method known as six-step commutation. This results in the characteristic trapezoidal shape of the back-EMF waveform. In six-step commutation, the three phases of the BLDC motor are energised in 120^0 degree sequences and each winding remains ‘high’ for 120^0 degrees (See Figure 2). Current is passed through two of the three windings at any time with one winding held at a high electrical potential and the other at a low electrical potential (and the third off). This results in six-possible commutation states or six sequential steps per revolution. The timing of these high/low sequences is critical to the motor’s operation and requires knowledge of the rotor position relative to the stator windings. There are several methods for obtaining this position including Hall Effect sensors, encoders, resolvers and several sensorless options (Yedamale, 2003). Rotor position estimation is critical to most DC motor control techniques and is discussed in section 2.3 (Rotor Position Estimation) below.

Six-step commutation has gained significant popularity due to its relative simplicity and cost effectiveness. However, six-step commutation does have drawbacks, having only two windings energised at any given time results in lower torque production and increased torque ripple. The increased torque ripple leads to increased vibration, noise and subsequently a shorter motor lifespan. The discrete nature of this commutation method also results in imprecise control and poor performance at low speeds. A variation of 120^0 six-step commutation is 180^0 six-step commutation and operates as the name suggests. This method generates more torque but results in even higher torque ripple, noise and further decreases motor lifespan (Lee & Lemley, n.d.).

Figure 2 below provides a graphical representation of the principles of trapezoidal or six-step commutation for a BLDC motor including the six-transistor power bridge.

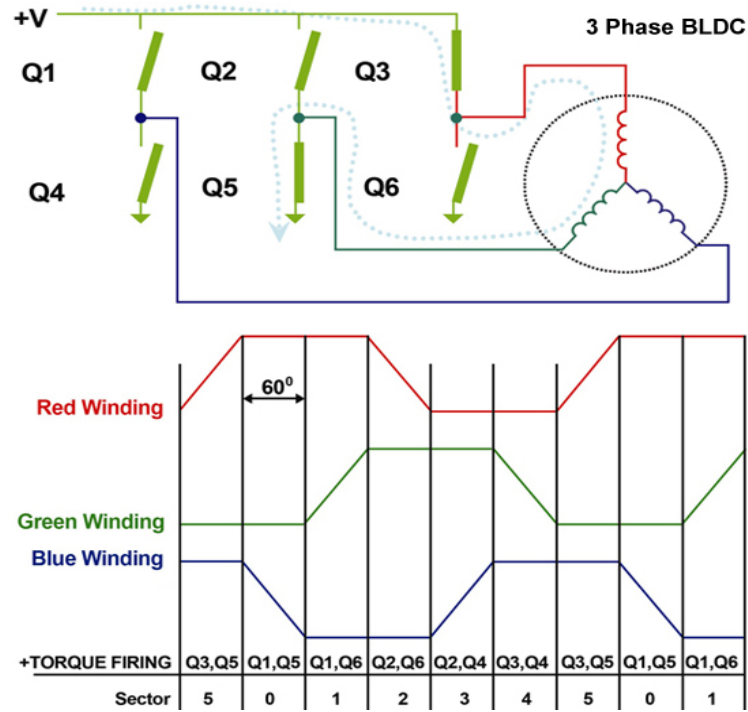


Figure 2 – Six-Step Commutation. (Microcontroller Solutions, n.d.)

2.1.2 Sinusoidal Commutation

The second common form of scalar control, aimed at PMS motors (sinusoidal back EMF) replaces the flat peaks of the trapezoidal back-EMF of six-step commutation with sinusoids. The nature of sinusoidal back-EMF requires that the commutation of phases be overlapped and that more than one pair of switching semiconductors be on at any given time. This allows for substantially reduced torque ripple and more precise control than trapezoidal commutation can achieve. However, sinusoidal commutation also requires more complicated control algorithms and more precise rotor position information. This calls for optical encoders, resolvers or (more) complex sensorless methods to be used to provide rotor position feedback and this adds to the overall cost of the control method (ATMEL, 2007).

Figure 3 below provides a graphical representation of the back-EMF of both the trapezoidal and sinusoidal scalar commutation methods. Note, sinusoidal commutation has been labelled as permanent magnet synchronous motor (PMSM) commutation. The figure also shows the slightly different ‘natural’ stator flux linkage waveforms of PMSM and BLDC motors.

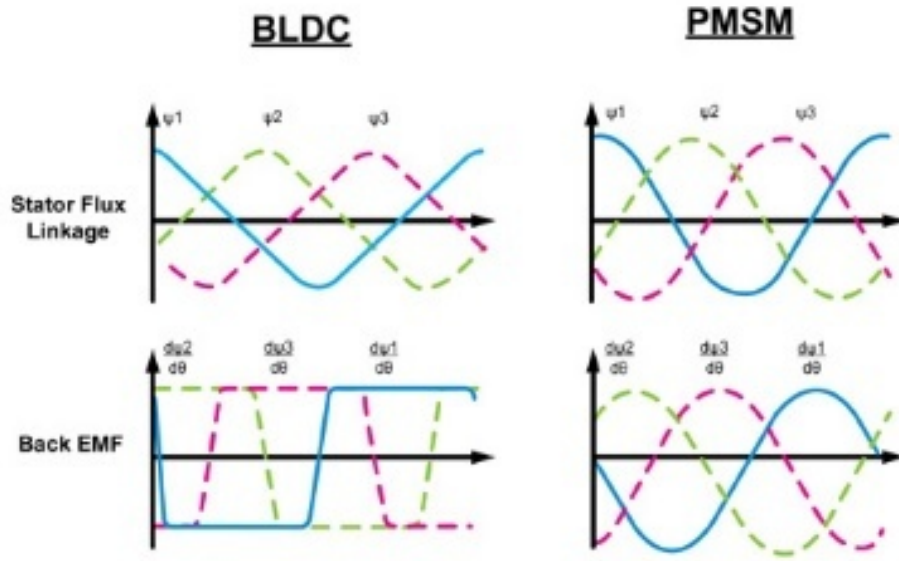


Figure 3 –Sinusoidal vs. back-EMF Waveforms. (Torres, 2009)

2.2 Vector Control

Over the past decade, research into the high performance control of brushless DC motors and permanent magnet synchronous motors has focussed on two competing methodologies: Field Oriented Control (FOC) and Direct Torque Control (DTC). Both FOC and DTC are forms of vector control and aim to effectively control certain motor parameters directly in order to force the motor to the application setting regardless of external conditions. Proponents of each methodology claim superiority over the other and each method (in terms of performance) is indisputably superior to legacy DC motor control methods (scalar control). However, each control strategy does have distinct advantageous and disadvantageous which need to be considered (Merzoug & Naceri, 2008).

2.2.1 Field Oriented Control Functional Overview

Field Oriented Control or Vector Control manipulates space vectors in the direct (d) and quadrature (q) axes in order to accomplish very precise and efficient motor control. Controlling the voltage and current space vectors directly in the d-q reference frame avoids a fundamental problem with sinusoidal commutation in that the currents are no longer controlled in a time variant reference frame. This overcomes bandwidth limitations of PID (Proportional-Integral-Derivative) controllers and allows for precise motor control across a much wider speed range than scalar commutation can offer. The torque and precision control that FOC offers are a direct result of the nature of FOC in that the windings are ‘managed’ to keep the flux produced by the rotor’s permanent magnets orthogonal to the stator field. This provides exceptionally precise torque control and is the real advantage of operating in the d-q reference frame (Copley Controls Corp, n.d.).

The direct and quadrature components discussed above are simply the decomposition of the flux linkage state vector into two discrete components, the flux (d) and torque (q) producing components. Figure 4 below provides a graphical representation of the direct and quadrature components. Note the intrinsically orthogonal nature of the direct and quadrature axes (John, et al., 2011).

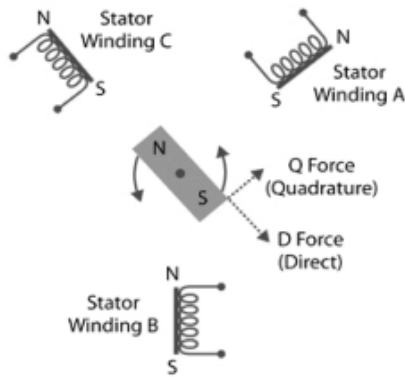


Figure 4-Direct (d) and orthogonal (q) force components (John, et al., 2011)

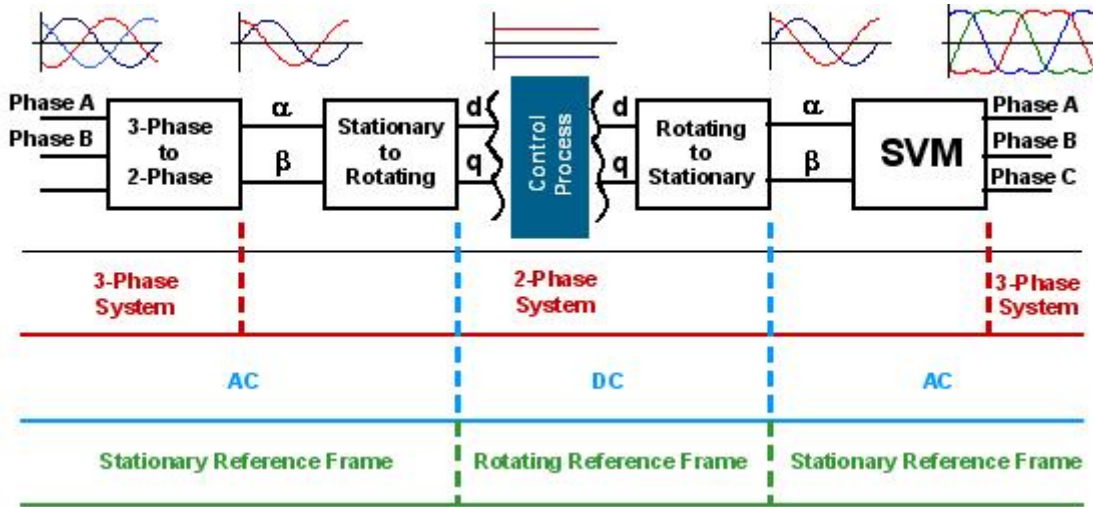


Figure 5-Functional block diagram of a generic FOC drive. (Lepka, 2009)

Figure 5 above provides a basic operational overview of FOC. Field oriented control requires the measured phase currents to be transformed from the 3-phase static reference frame of the stator to a static 2-phase reference (α, β) and finally to a rotating two-phase reference system aligned with the rotor flux (d-q). FOC processing is carried out entirely in this reference frame. It follows, that in order for the d-q reference frame to be aligned with the rotor, detailed information about the rotor position is required at every sampling time. Significant research into rotor position estimation has been carried out over the past 50 years, and recently, particularly in the past decade, research into sensorless rotor position estimation has been undertaken. This research is reviewed in section 2.3 (Rotor Position Estimation) below. It should be noted that the two-phase d-q system is only rotating with respect to the stator and that it is actually stationary with respect to the rotor. Transformations from the static 3-phase reference frame into the two phase d-q reference frame result in two flux vector ‘components’, the direct and quadrature components. The direct (d) component offers no useful torque and only serves to increase wear on the motor bearings. It follows that it is beneficial to minimise this component. The quadrature component is responsible for ‘actual’ motor torque and this component is set by the application. The direct and quadrature components are then fed with reference to zero and the application torque setting respectively into two PI (Proportional-Integral) blocks. This results in a vector output that is (optimally) exclusively in the quadrature axis with a

resulting torque tracked to the application setting. The output of these PI blocks is two components (d and q) of a voltage vector in the rotating d-q reference frame (Zambada & Deb, 2010). The output of the two PI ‘blocks’ are the (new) direct and quadrature voltage components of the required stator voltage space vector. In order to actually drive the motor, these components are back-transformed to the stator reference frame and used for Space Vector Pulse Width Modulation (SVPWM).

In the past decade, FOC has been successfully implemented in both PMSM and BLDC motor drives in both sensed and sensorless forms. Many semiconductor companies including TI, Atmel and Microchip provide retail microcontrollers with routines flashed on ROM that allow for simpler implementations of FOC. However, at the time of writing, no commercially available Electronic Speed Controllers for small (<100A) DC machines could be found that utilise field oriented control.

2.2.2 Direct Torque Control Functional Overview

Realistically, DTC is the only competition to FOC in terms of performance motor control for brushless DC machines. Fundamentally, DTC aims to control the flux linkage and electromagnetic torque directly by changing the relative angle between the stator flux and the permanent magnet flux vectors. (Garcia, et al., n.d.) DTC directly controls motor torque by rapidly manipulating the stator flux vector orientation by changing the voltage provided to the motor stator windings.

DTC operates by comparing reference (application set) values of the stator flux and torque with observed values. Hence, the only feedback parameters required for DTC are the torque and flux (T and Ψ) which are derived directly from the stator flux linkage. The stator flux linkage is estimated by the equation $\Psi_s = \int(v_a - R_a i_a)dt$ where Ψ_s is the estimated stator flux vector, v_a is the measured stator voltage vector, R_a is the stator resistance and i_a is the stator current vector (Inoue, et al., 2011). DTC does not require rotor speed or position information to achieve torque control and is considered an inherently sensorless control scheme.

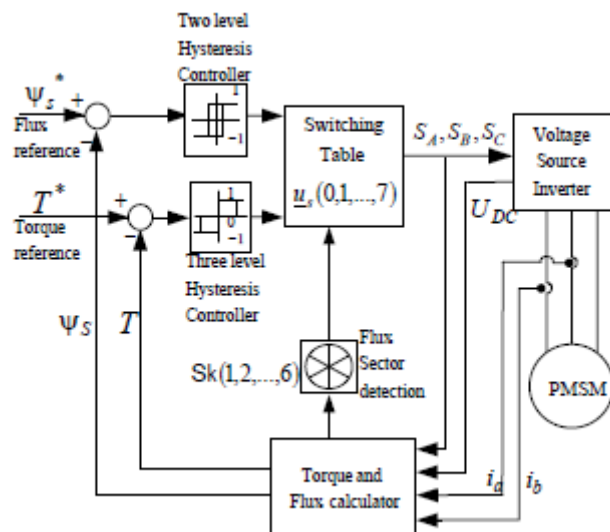


Figure 6. DTC Control Scheme for PMSM (Paturca, et al., 2006)

Figure 6 above provides a basic operational overview of DTC. It can be seen that DTC requires a torque and stator flux vector estimator, a look-up table (switching table) and hysteresis comparators (Paturca, et al., 2006). At each sample time, the stator currents i_a and i_b as well as the DC-bus voltage are sampled. Using these values and the manufacturer data for the stator resistance, the

stator flux is calculated in the α, β reference frame. By nature, the stator flux is rotating, ideally, with the rotor. Referring to Figure 7 below, DTC breaks the full stator flux rotation into six possible discrete ‘inverter voltage vectors’ (Paturca, et al., 2006). The calculated $\alpha - \beta$ components of the stator flux are used to determine the ‘sector’ ($S_1 - S_6$) in which the current flux vector is located.

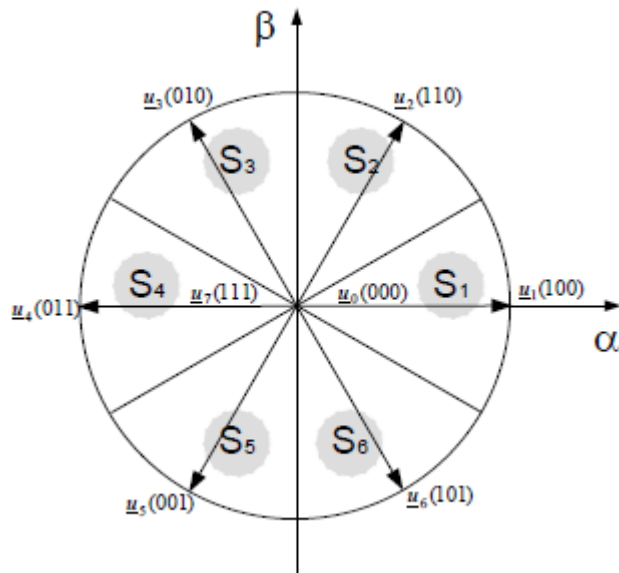


Figure 7. Inverter voltage vectors and stator flux vectors (Paturca, et al., 2006).

The magnitude of the stator flux and electromagnetic torque is then calculated and compared with reference values in the relative hysteresis comparators (see Figure 6). Finally, the output of the comparators with the current flux vector ‘sector’ is fed to a lookup table and the appropriate inverter voltage vector is selected. No PWM is required with DTC, instead, PWM is replaced with a simple lookup table.

Many variations of DTC exist, but all are based on the general principals outlined above. Like FOC, DTC has seen implementation in both PMSM and BLDC motor drives with the former being more common. DTC is often employed for large machine drives but currently has not been employed in any commercially available small DC machine electronic speed controllers.

2.2.3 FOC and DTC Comparison

Casadei, Profumo, Serra and Tani (2002) argue that due to the identical goals and the ability to use one scheme directly in place of the other, a direct comparison between FOC and DTC is valid and that, in terms of performance, ultimately DTC or FOC can be deemed superior depending on the application requirements. The aim of this project is the development of a low cost, high performance single board ESC for small DC machines. Hence, the superiority of either DTC or FOC will be judged on the scheme’s ability to meet these requirements. Casadei, Profumo, Serra and Tani go on to make the comparison between DTC and FOC and reach the conclusion that while the ‘whole performance of the two schemes is comparable’, DTC is preferred for high dynamic load applications but does result in a higher current and torque ripple than FOC (Casadei, et al., 2002). However, further research has been conducted in an attempt to establish either FOC or DTC as a superior control method with varying conclusions reached. In addition, it should be noted that very little research has been done considering small DC machines specifically. While the conclusions reached

must be considered with this fact in mind, the literature can be used to make a case for either DTC or FOC for application in low cost, high performance, electronic speed controllers designed for small DC machines.

In much of the literature surrounding DTC and FOC, the major stated advantage of DTC over FOC is simplicity. DTC does not require any reference frame transformations or rotor position estimation. This allows for lower capability (and cost) processors to be used in DTC and also requires less development time. In addition, PWM is completely replaced in DTC with a simple lookup table (Cassadei, et al., 2002). In contrast, FOC commutation requires substantial processing power in order to perform the required transformations and control algorithms. However, as the price of microcontrollers, DSPs and FPGAs have fallen while processing power has been increasing, computational complexity is no longer a decisive metric and performance based criteria needs to be considered.

Garcia, Zigmund, Terlizzi, Pavlanin and Salvatore (n.d) performed several comparison tests on DTC and FOC. These experiments were done using a relatively large (2kW) PMSM motor in simulation. Table 1 below provides the results of the simulations for the torque settling time of both DTC and FOC at different speeds.

Table 1. Torque settling time at different speeds (Garcia, et al., n.d.).

Electrical Speed	DTC	FOC
0 rad/s	0.22ms	6ms
300 rad/s	0.32ms	5ms
1200 rad/s	1ms	15ms

The authors make specific note of the fact that while DTC offers a considerably faster response time, the torque ripple observed was substantially higher than that observed with FOC. Further, torque ripple for DTC was observed to increase at lower speeds which meant that DTC performance was seen to reduce as speed was lowered from nominal. The results obtained for the steady state performance testing of FOC and DTC may be seen in Table 2 below.

Table 2. Steady state performance indexes (Garcia, et al., n.d.).

	DTC	FOC
Stator Flux Average Error	0.3%	0.1%
Stator Flux Standard Deviation	4.85%	0.15%
Torque Average Error	1.8%	0.08%
Torque Standard Deviation	12.8%	2.81%

Table 2 shows that the steady state performance of FOC is considerably higher than that of DTC.

Further, the authors found that the torque distortion is ‘considerably bigger for DTC’ and that FOC has more consistent performance across a wider speed range than DTC (Garcia, et al., n.d.).

Garcia, Zigmund, Terlizzi, Pavlanin and Salvatore are not alone in reaching these conclusions. In fact, most comparisons between FOC and DTC reach the same conclusions but place different weightings on the advantages and short-comings of each method, thus reaching different overall conclusions. While the superiority of one method is largely dependent on the application, the literature surrounding FOC and DTC almost invariably contains a note on the fact that DTC results in higher torque and current ripple than FOC and lower performance at low speeds. This problem is exacerbated when DTC is applied to BLDC motors ('natural' trapezoidal back-EMF) due to the fact that ‘the amplitude of the stator flux linkage cannot easily be controlled due to the sharp changes and the curved shape of the flux vector between two consecutive commutation points in the stator flux linkage locus [in regards to BLDC motors]’ (Ozturk & Toliyat, 2007). In an attempt to overcome this issue, Ozturk and Toliyat (2007) introduced a method of DTC designed specifically for BLDC motors. This method has similarities with legacy six-step commutation in that only two of the stator windings are current carrying at any given time, producing the characteristic trapezoidal shape back-EMF and allowing for better DTC performance when applied to BLDC motors. The authors argue that by properly selecting the inverter voltage space vectors from a [newly designed] lookup table, two-phase conduction DTC can offer a much faster torque response than conventional DTC. Further, the method is suggested for reducing the low frequency torque ripple commonly seen in six-step commutation in an effort to increase the performance speed range of DTC. The assertions made in the journal article are validated in both simulation and experimentation. While this method is promising, it has many of the limitations of six-step commutation including lower net torque production (compared to 3-phase conduction) and increased torque ripple compared to FOC.

While numerous variations of FOC and DTC can be found in literature, each attempting to solve a particular shortcoming, both methods have disadvantages as a result of the underlying principles. These are outlined in Table 3 below.

Table 3. Comparison of FOC and DTC as implemented for a PMSM (Garcia, et al., n.d.) & (Merzoug & Naceri, 2008).

	DTC	FOC
Dynamic response for Torque	Quicker	Slower
Steady-state behaviour for torque, stator flux and currents	High ripple and distortion	Low ripple and distortion
Requirement of rotor position	No	Yes
Current control	No	Yes

PWM modulator	No	Yes
Coordinate transformation	No	Yes
Switching frequency	Variable, depending on the operating point and during transients	Constant
Audible noise	Spread spectrum, high noise especially at low speed	Low noise at a fixed frequency
Control tuning	Hysteresis Bands	PI gains
Complexity and processing requirements	Lower	Higher
Parameter Sensitivity	Lower	High
Performance at lower speeds	Not good	Good

2.3 Rotor Position Estimation

Rotor position estimation is critical to most methods of DC motor commutation, with a single notable exception, which is DTC. In fact, even DTC systems benefit from accurate rotor position and speed information, with many ‘high-end’ implementations of DTC utilising complex rotor position estimators to improve performance. In scalar and more specifically FOC based drives, inaccurate rotor position estimation will result in very poor performance and in some cases lead to complete drive failure. Many methods of rotor position estimation exist, from conventional sensored methods to more complex sensorless techniques. The overwhelming majority of recent research into brushless DC motor control applies some form of sensorless rotor position estimation.

2.3.1 Hall Effect Sensors

The simplest and most common forms of rotor position estimation utilise physical sensors. The most common position sensor seen in rotating machines is the Hall Effect Sensor. When a current-carrying conductor is placed into a magnetic field a voltage is generated perpendicular to both the current and the field. This is known as the Hall Effect and has been used extensively in large machines for rotor position estimation. For rotor position estimation, three Hall Effect sensors are placed on the stator and generate a High or Low signal whenever rotor magnetic poles pass close by. Figure 8 below shows the electrical output of a three Hall Effect sensor rotor position estimation system (Lee & Lemley, n.d.).

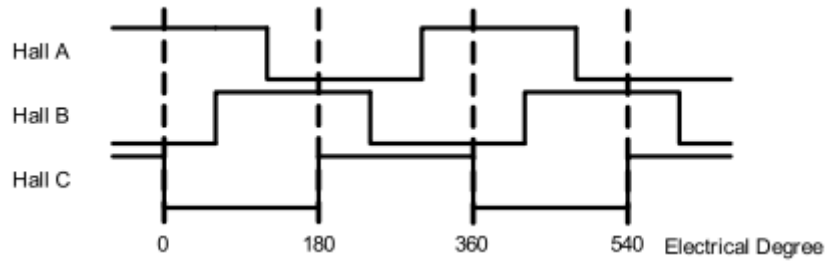


Figure 8. Three-phase Hall sensor timing chart with 120° angle separation (Lee & Lemley, n.d.).

The most obvious drawback to the Hall Effect rotor position estimator is that it requires Hall Effect sensors to be added by manufacturers which adds to the overall cost of the motor. While this cost is negligible in larger machines, in small DC machines the cost is significant and hence Hall Effect sensors are rarely found in small DC machines. Hall Effect sensors also require their own power supply and add additional wiring to the motor. Further, in the classical 3-Hall Effect sensor configuration, rotor position is only estimated to an accuracy of 60° .

2.3.2 Back-EMF Zero Crossing

Back-EMF zero crossing is a sensorless method of rotor position estimation that has seen significant development over the past two decades. When a brushless DC motor rotates, each winding generates a back-EMF which opposes the voltage supplied to the winding in accordance with Lenz's law. Back-EMF zero crossing rotor position estimation is particularly suited to two-phase conduction implementations of the commutation methods discussed. This is because the third 'un-powered' phase can be used for back-EMF detection. The zero-crossing is found by feeding the voltage of the un-powered winding with respect to a virtual ground and half the DC bus voltage to a comparator. At the point the output of the comparator changes state, the zero crossing has occurred and the next commutation sequence can begin. (Ungurean, et al., 2010) Figure 9 below shows back-EMF zero crossing detection with winding power flow.

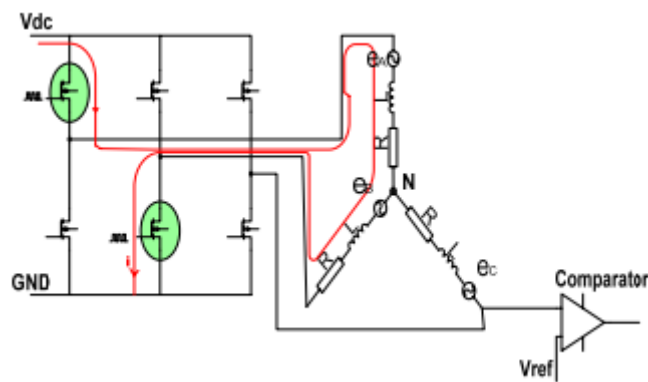


Figure 9. Circuit model during PWM ON-time (Ungurean, et al., 2010).

Back-EMF zero crossing detection overcomes a lot of the problems associated with conventional techniques in that it does not require physical sensors to be mounted in or on the motor and also offers high accuracy at high speed. However, this method does have two serious draw-backs.

1. The back-EMF generated is proportional to the rotor speed. This means that back-EMF simply does not work when the rotor is stationary (starting) and that accuracy is diminished

at lower speeds (the problems associated with this have already been established). Some methods have been identified to (somewhat) overcome this. For example, Urgurean, Coroban-Schramel and Boldea (2010) propose a novel solution in which Hall-Effect sensors are used at zero and low speeds and the back-EMF zero crossing is used to provide high accuracy rotor position estimation when an appropriate speed has been reached. However, this introduces the problems associated with Hall-Effect sensors (at low speed) and results in more complicated control and additional expenses. Various other back-EMF methods have been proposed but all suffer from the same fundamental problem, inaccuracy at low speeds due to insufficient back-EMF generation.

2. The method requires a phase to be non-current-carrying in order to detect the back-EMF. While almost all of the methods discussed have two-phase conduction variants, they all result in lower torque generation and increased torque ripple. Further, two-phase conduction results in trapezoidal back-EMF which results in diminished efficiency and performance when applied to PMS motors.

2.3.3 Extended Kalman Filter

The Extended Kalman Filter (EKF) rotor position estimator is based on an extension of R.E. Kalman's recursive solution to the discrete-data linear filtering problem published in his famous 1960 paper. This 'extension' takes the Kalman filter and applies it to non-linear state-space systems, in this case brushless DC motor variables. EKFs have been employed in both BLDC and PMSM motor drives but due to the relative complexity of the method, EKFs are normally reserved for high end drives or experimentation. The real advantage of the EKF is that regardless of the precision of the variables measured, EKF algorithms will provide an accurate estimate of the future state of the variables (Jacob, et al., 2013). A common EKF used in the rotor position estimation of BLDC motors is presented by Terzic and Jadric (2001). 'An extended Kalman filter (EKF) is employed to estimate the motor state variables by only using measurements of the stator line voltages and currents' (Terzic & Jadric, 2001). The authors note that 'when applying the EKF, it was necessary to solve some specific problems related to the voltage and current waveforms of the BLDCM'. This assertion leads to an important point about sensorless rotor position and speed estimation techniques. That is, they are very complicated and tailor made for each application. The methods discussed are only a broad outline of the underlying theory and the application of any of the sensorless methods discussed to this point requires significant design to ensure successful operation.

2.3.4 Sliding Mode Observer

Determining the rotor position and other motor parameters (e.g. speed) is the job of the motor 'observer'. All of the sensorless rotor position estimation techniques discussed up to this point are motor observers. Spurgeon (2008) makes the point that Sliding Mode Observers (SMOs) are unique 'in that the ability to generate a sliding motion on the error between the measured plant output and the output of the observer ensures that a sliding mode observer produces a set of state estimates that are precisely commensurate with the actual output of the plant' (Spurgeon, 2008). The Sliding Mode Observer (SMO) is in fact a branch of control theory with many rotor position and speed estimation techniques falling under its umbrella. For instance, Ilioudis and Margaris (2008) employ an SMO consisting of two discrete steps, 'flux/current and speed/position estimation'. In this method the 'stator flux/current and resistance error converges to zero and afterwards speed and position estimation is carried out using a modified back electromotive force (EMF) observer' (Ilioudis

& Margaris, 2008). Yet, another SMO method proposed by Lee and Lee (2013) is iterative in nature and allegedly ‘improves the performance in estimating the motor speed and angle by reducing the estimation error in the back electromotive force by iteratively applying the observer in the sensorless operation’ (Lee & Lee, 2013). This goes to show the broad nature of SMO theory and the significant design required for the successful implementation of any observer.

2.3.5 TI FAST

Rotor *Flux*, *Angle*, *Speed* and *Torque* (FAST) is Texas Instruments (TI) proprietary observer which is in ROM on selected C2000 Piccolo devices (6x and 2x series). As the FAST observer is TI proprietary technology, limited literature exists with the exception of TI marketing and application notes. Figure 10 below is taken from an InstaSPIN™ application note and provides an overview of the advantages of the FAST™ sensorless observer.

F Rotor Flux <ul style="list-style-type: none"> • High integrity signal for stable field control A Rotor Angle <ul style="list-style-type: none"> • Locks within one electrical cycle of rotation • Stable through zero • Robust under dynamics • Recovery after stall events S Rotor Speed <ul style="list-style-type: none"> • Mechanical and electrical speed estimations • Near zero phase lag T Rotor Torque <ul style="list-style-type: none"> • Accurate for load monitoring, flow rate, unbalanced load, motor diagnostics 	FAST™ Software Encoder (Sensorless Observer) <ul style="list-style-type: none"> • Universal 3-phase motor software encoder supports <ul style="list-style-type: none"> ◦ Synchronous (BLDC, SPM, IPM) ◦ Asynchronous (ACI) motors ◦ Unique, high-quality feedback signals for use in control systems • Performance <ul style="list-style-type: none"> ◦ Tracks below 1 Hz ◦ Tracks through zero on speed reversals ◦ Stable feedback to control system when rotor is at zero speed • Motor parameters <ul style="list-style-type: none"> ◦ Relies on fewer parameters than other observers ◦ Off-line commissioning learns the needed electrical motor parameters ◦ Optional on-line observer tracks parameter changes to ensure estimation accuracy over time and temperature • Tuning <ul style="list-style-type: none"> ◦ No tuning of the observer required <p>Included in ROM on select Piccolo™ MCUs, with software API</p>	
---	--	---

Figure 10. FAST™ Sensorless Observer. (Texas Instruments, 2013)

FAST is a very promising observer as it offers very high performance for low implementation time. Fast offers precise rotor position estimation over a very wide speed range for both PMSM and BLDC motors. Further, it is integrated with the InstaSPIN™ FOC environment which offers routines to assist with the implementation of FOC. InstaSPIN™ and FAST are available on selected TI Piccolo microcontroller units (MCU).

2.4 Power Control Schemes

Without exception, the penultimate output of any three-phase motor drive is the switching signals required to drive the power stage of the drive. The method to generate these signals is unique in each method, ranging from a simple lookup table for DTC to PWM for scalar and more complex SVPWM for FOC based drives. The ultimate step of the motor drive is the controlled passing of current through stator windings to produce rotor movement. This is done by switching semiconductors at a high frequency in response to control signals.

2.4.1 Low/High Dedicated Driver

To pass current through a stator winding, one winding must be held high and the other held low. Many methods to accomplish this have been established and proven, from Application Specific Integrated Circuits (ASIC) to custom logic implementations.

Dedicated driver ICs offer many advantages including:

- very fast switching time;
- allowing the use of high-side n-channel MOSFETs or IGBTs;
- intrinsically safe, internal low-voltage cut-off;
- capable of handling large supply voltages ($V+ < 600V$);
- easy implementation.

However, IC drivers do have disadvantages in that they are expensive and require substantial space on the board (Lock, 2012).

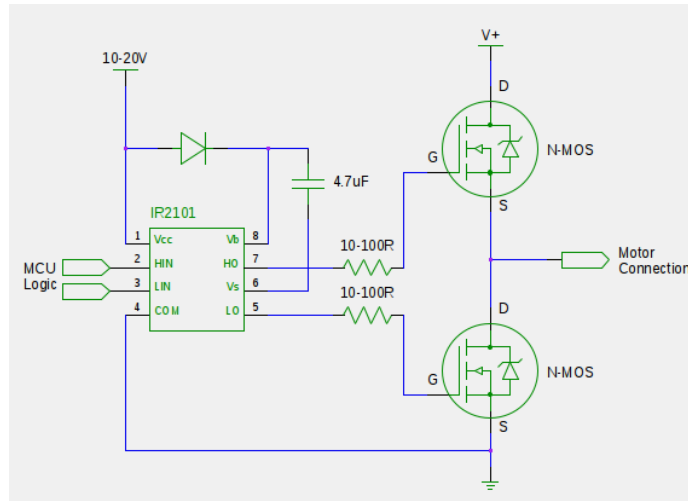


Figure 11. IR2101 implementation for one phase of a MOSFET power stage (Lock, 2012).

Figure 11 shows the implementation of an IR2101 dedicated MOSFET driver utilising n-channel MOSFETs as both the high and low side switching semiconductors. Dedicated drivers are generally recommended when using a supply voltage above 15V (Lock, 2012).

A distinction must be made between high side drivers (IR2101) and all in one IC drivers. High side drivers ‘take-up’ space only because they are required to drive the high side switching devices. All in one drivers include all driving logic and additional functionality such as current amplifiers. In addition, all in one three-phase drivers exist, such as TIs DRV8301. This driver allows independent control through 6 PWM signals, has integrated ‘bootstrapping’, integrated dual shunt current amplifiers and much more functionality which could not be implemented using discrete components in a comparable size. These drivers, considering functionality, actually save substantial space on the board.

2.4.2 Low-Side Devices

A popular method for switching the power board without utilising IC drivers is the use of logic-level switching devices on the low-side. These devices have a much lower gate drive requirement and can

be efficiently driven by MCU level logic. This eliminates the need for extra ICs on the board which can be a big factor especially in small form-factor boards. However, this method is slower than a dedicated driver and results in a less efficient drive (Lock, 2012).

Low-side devices as the name suggests are only used on the low side of the power inverter and a high side devices is required to complete each ‘leg’ of the bridge.

2.4.3 High-Side Devices

P-Channel devices can be used as the high side switch but they are less popular than n-channel devices and hence more expensive. Further, it is very difficult to find p and n-channel devices with matching voltage and current ratings. This means that it is difficult to design and implement a high performance power inverter utilising both p and n-channel devices.

A more popular choice for the high-side switch is to use an n-channel device. These allow matched high and low side switches. However, a high-side n-channel device will not switch on a logic level signal and requires a ‘bootstrapping’ circuit in order to saturate. The ‘bootstrapping’ circuit works as a high voltage floating supply and is necessary in order to switch the device on and off. Further, the high-side n-channel device operates active-low. That is, the logic signal is reversed.

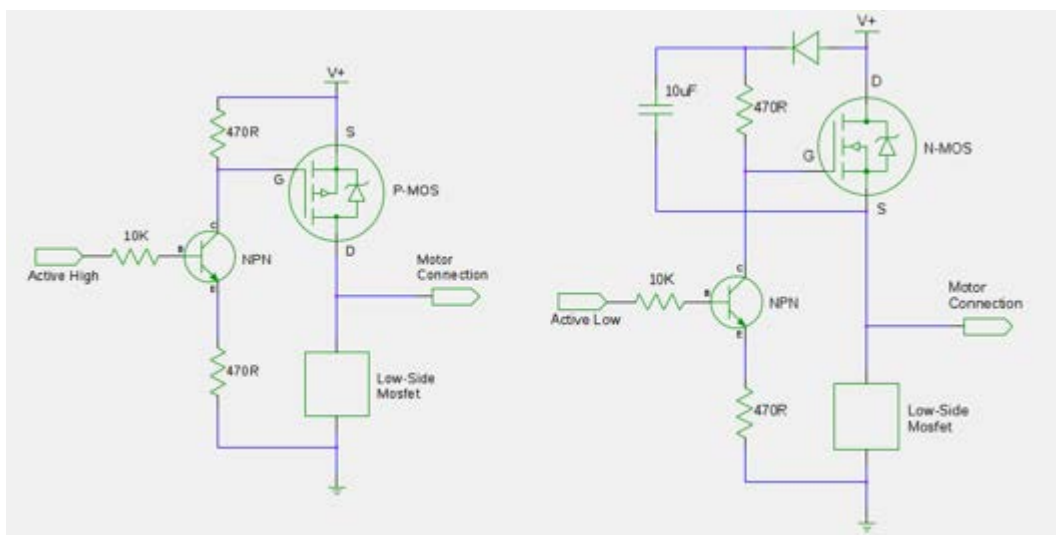


Figure 12. High-side p-channel device (left) and high-side n-channel device (right) implementation (Lock, 2012).

Figure 12 above provides a basic generic circuit diagram for both p and n-channel devices.

2.5 Literature Review Conclusion and Control Method Selection

Upon reviewing the current literature on performance DC motor control, several conclusions have been drawn. In the past decade, research into performance motor control has almost exclusively focussed on one of two competing methodologies: DTC or FOC. Further, significant research has been conducted on the comparison of the two methods, with neither of the methods consistently found superior by the community. Another important revelation that came from the literature review is that very little research has been conducted on the performance control of small DC machines.

Conducting the literature review has allowed for an informed decision to be made regarding the suitability of FOC and DTC for application in small DC machine drives. Small DC machines are constantly employed in applications requiring a wide speed range (model aircraft for example) and the superiority of FOC in this regard cannot be ignored. Steady-state stability and torque ripple are also important factors pertaining to the decision and the literature consistently showed FOC outperforming DTC in these areas. In addition, what would have been a major draw-back for FOC even a decade ago, the high processing power required, has largely been overcome with modern MCUs.

The literature review has also resulted in many insights into the observer method chosen. While a custom observer based on the extended Kalman Filter or Sliding Mode Observer theory may offer some performance increases, it is not realistically possible to design an observer based on any of these methods in addition to the other components of the ESC in the available time. For this reason, TI's FAST observer will be used within the InstaSPIN™ environment. This means that a TI Piccolo MCU will be used as the controller for the ESC.

While conducting research for the literature review, it was found that the majority of small DC machines are BLDC and not PMSM. For this reason, the ESC will be developed specifically for BLDC motors. However, as established, the PMSM is very similar to the BLDC motor and the ESC will be capable of driving PMS motors.

3 Theory

The basic theory underpinning field oriented control has already been established in section 2.2.1 (Field Oriented Control Functional Overview) above. What follows is an extension of this theory and should not be read prior to section 2.2.1.

3.1 FOC Operation Theory

FOC requires the current space vectors to be manipulated directly in the d-q reference frame. It follows that it is necessary to transform the measured (sensed) currents from the static three-phase stator reference to a rotating (aligned with the rotor) two axis d-q reference frame. This is possible through computationally intense mathematics known as Parks and Clarkes transformations. It is these transformations that call for the high processing power of DSPs, microcontrollers or FPGAs in FOC motor control (John, et al., 2011).

The first step in this transformation takes the 3-phase stator currents, i_a , i_b and i_c (time variant, A, B, C) out of the two-dimensional stator reference frame and into a two-phase equivalent system still referenced to the stator (Zambada & Deb, 2010). The two phase variables are denoted as α and β and are by nature orthogonal. This is the Clarke transform and is defined mathematically as follows:

$$\begin{aligned} v_\alpha &= v_a \\ v_\beta &= \frac{2v_b + v_a}{\sqrt{3}} \end{aligned}$$

A zero sequence component is added in order to make the transformation *invertible*.

$$[f_{\alpha\beta 0}] = T_{\alpha\beta 0}[f_{abc}]$$

where f represents voltage, current, flux linkages or electric charge. In this case, f will represent the three-phase stator currents. The transformation matrix T is given as:

$$T_{\alpha\beta 0} = \frac{2}{3} \begin{bmatrix} 1 & -\frac{1}{2} & -\frac{1}{2} \\ 0 & \frac{\sqrt{3}}{2} & -\frac{\sqrt{3}}{2} \\ \frac{1}{2} & \frac{1}{2} & \frac{1}{2} \end{bmatrix}$$

(Dan, 2008).

Figure 13 below provides a geometric overview of Clarke's transformation.

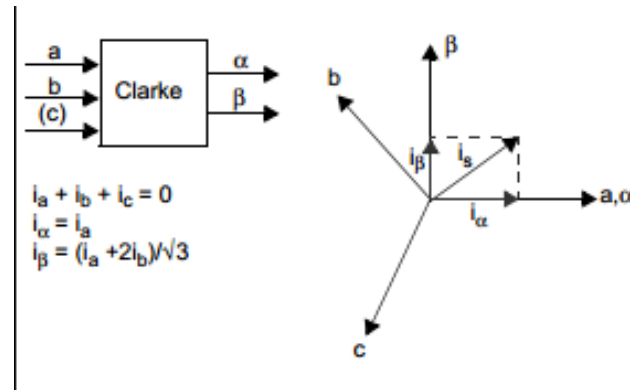


Figure 13-Clarke's Transformation. (Zambada & Deb, 2010)

Next it is necessary to transform the (now) two-phase orthogonal system (α, β) from the stationary stator reference frame to a two-phase system that is rotating aligned with the rotor flux. This is possible using Park's transformation. Mathematically:

$$i_{sd} = i_\alpha \cos(\theta) + i_\beta \sin(\theta)$$

$$i_{sq} = -i_\alpha \sin(\theta) + i_\beta \cos(\theta)$$

(Dan, 2008).

Figure 14 below provides a geometric overview of Park's transformation.

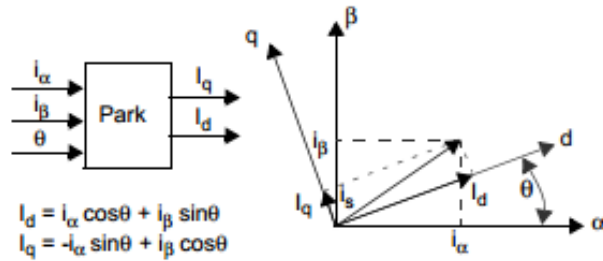


Figure 14 - Park's Transformation. (Zambada & Deb, 2010)

The angle θ , in the Park's transformation is the rotor flux angle as referenced to some constant point on the stator. This is why accurate rotor position estimation is integral to the operation of FOC.

With the stator current vectors now in a two-phase system aligned with the rotor flux (in the d-q reference frame), FOC processing can begin. The direct (d) component is minimised as it offers no useful torque generation. The quadrature component is responsible for 'actual' motor torque and it is this component that is set by the application. The direct and quadrature components are fed with reference to zero and the application torque setting respectively into two PI blocks. In order to achieve stable motor control, these PI block require 'tuning' to achieve the required response. Methods for this range from manual adjustments to semi-automatic tuning. The output of these PI blocks is a two component (d and q) voltage vector in the rotating d-q reference frame (Zambada & Deb, 2010).

With FOC processing now complete it is necessary to 'back' convert to a stator referenced two-phase system for Space Vector Pulse Width Modulation (SVPWM) generation.

As discussed, the output of the two PI ‘blocks’ are the (new) direct and quadrature voltage components of the required stator space vector. In order to actually drive the motor, these components are transformed to the stator reference frame using an inverse Park’s transformation. The inverse Park’s transformation is defined as follows:

$$V_\alpha = V_d \cos(\theta) - V_q \sin(\theta)$$

$$V_\beta = V_d \sin(\theta) + V_q \cos(\theta)$$

The two-phase system can now be used to generate SVPWM signals to switch the power components and drive the motor.

3.2 Space Vector Pulse Width Modulation

The outputs of the two PI controllers discussed in section 3.1 above represent a voltage space vector with respect to the rotor. Using the inverse Park transform, these signals are transformed from the rotating d-q reference frame to the stationary stator reference (α, β) frame for SVPWM signal generation (John, et al., 2011). It is these PWM signals that control the power electronics in order to drive the motor.

PWM is used to signal power semiconductors (transistors) to switch on and off at a high frequency. This allows a DC source to be ‘converted’ to an AC source of a desired frequency and rms voltage. This is best described graphically as shown in Figure 15 below:

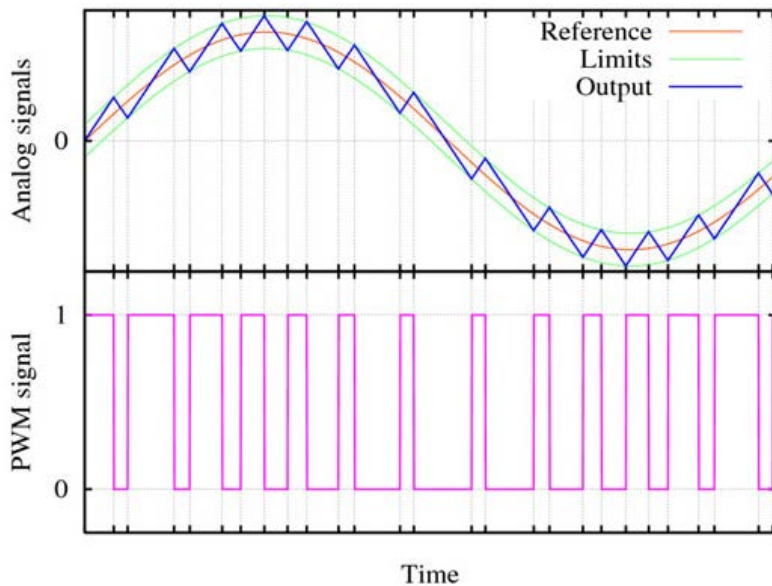


Figure 15. PWM used to generate a varying analogue equivalent. (Acroname, 2007)

In the case of three-phase DC motor control, six PWM signals are required to drive the switching components in the power stage (see Power Electronics). Because the voltage signals are in the α, β reference frame, it is necessary to use space vector PWM control techniques. The basic 3-phase inverter shown in Figure 16 must be controlled so that at no point both switches in the same leg are closed as this would result in a very low impedance short. It follows that there are eight switching vectors with six of these being non-zero.

High Performance Brushless DC Motor Control

Table 4. SVPWM Switching Vectors. Ref: Figure 16

Vector	+A	+B	+C	-A	-B	-C	V_{AB}	V_{BC}	V_{CA}	
$V_0 = 000$	OFF	OFF	OFF	ON	ON	ON	0	0	0	Zero Vector
$V_1 = 100$	ON	OFF	OFF	OFF	ON	ON	$+V_{DC}$	0	$-V_{DC}$	Active Vector
$V_2 = 110$	ON	ON	OFF	OFF	OFF	ON	0	$+V_{DC}$	$-V_{DC}$	Active Vector
$V_3 = 010$	OFF	ON	OFF	ON	OFF	ON	$-V_{DC}$	$+V_{DC}$	0	Active Vector
$V_4 = 011$	OFF	ON	ON	ON	OFF	OFF	$-V_{DC}$	0	$+V_{DC}$	Active Vector
$V_5 = 001$	OFF	OFF	ON	ON	ON	OFF	0	$-V_{DC}$	$+V_{DC}$	Active Vector
$V_6 = 101$	ON	OFF	ON	OFF	ON	OFF	$+V_{DC}$	$-V_{DC}$	0	Active Vector
$V_7 = 111$	ON	ON	ON	OFF	OFF	OFF	0	0	0	Zero Vector

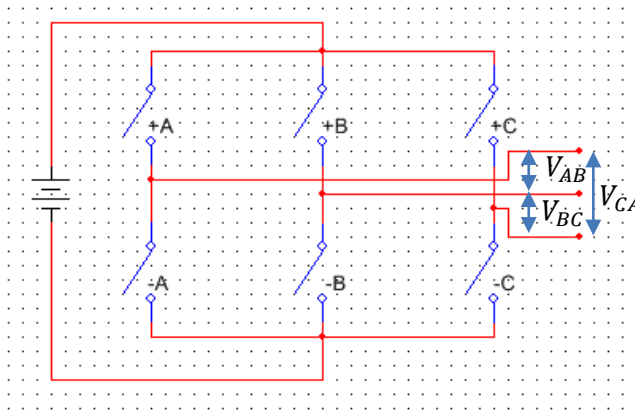


Figure 16. Basic Three Phase Inverter.

The non-zero vectors ($V_1 - V_6$) are shown graphically in the α, β plane in below.

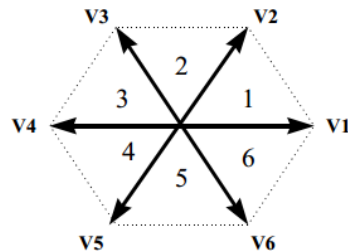


Figure 17. Non-zero voltage vectors in the α, β plane. (Virginia Tech, n.d.)

Several different SVPWM ‘schemes’ exist to generate a three-phase output at the bridge for a desired line-to-line output voltage represented in the α, β reference frame. This is an extensive subject in and of itself and requires the consideration of many factors that can only be determined during the implementation phase of the project. Within the InstaSPIN™ environment, SVPWM is split

into a space vector modulation scheme which is a part of InstaSPIN™ and general PWM which is external to InstaSPIN™. A detailed PWM (whether utilising InstaSPIN™ SVM or not) scheme will be determined during the implementation phase of the project.

3.3 Sensorless Rotor Position Estimation

FOC algorithms, like all electronic commutation methods, require information on the rotor position relative to the stator. In fact, if the rotor flux position is not accurate, the PI blocks will be working with incorrect flux (d) and torque (q) components of the stator current. This will obviously lead to very poor motor control (Akin & Bhardwaj, 2013). In reviewing the literature on motor observers, it was determined that it is not feasible to design an observer from the ground up and that TI's FAST observer will be used.

The limited literature available on FAST has been examined in section 2.3.5 (TI FAST) above.

Figure 18 below shows the (A, B, C), (α, β) and (d, q) reference frames aligned with the correct rotor flux position. The stator current and stator voltage space vectors (shown) rotate synchronously with the d - q reference. This can only be achieved with an accurate observer such as TI FAST.

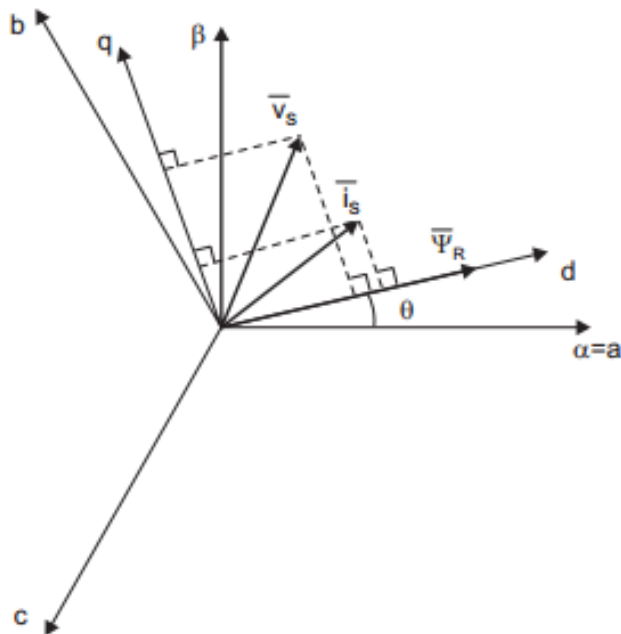


Figure 18. Current, Voltage and Rotor Flux ($\bar{\Psi}_R$) in the d - q Rotating Reference Frame and Their Relationship with A(a), B(b), C(c) and (α, β) Stationary Reference Frame. (Akin & Bhardwaj, 2013)

4 InstaSPIN™-FOC

The literature review provided significant insight into the current areas of study into advanced motor control techniques. After careful consideration of the available literature, *field oriented control* was deemed the most suitable control methodology for this project. The rationale for this decision can be seen in *Literature Review Conclusion and Control Method Selection* in the literature review above. It was decided that TI's InstaSPIN™-FOC would be evaluated initially and, conditioned on promising results, ultimately used for the motor controller.

While the underpinning theory required for a generic implementation of FOC has been established in the literature review and theory chapters, no theory specifically regarding InstaSPIN-FOC has been provided. The relevant theory specifically relating InstaSPIN™-FOC follows.

4.1 InstaSPIN-FOC Overview and Functions

InstaSPIN-FOC is a motor control solution by *Texas Instruments* which allows for the rapid development of advanced FOC based motor controllers. This solution includes a proprietary unified observer structure, *FAST*, and all required FOC 'blocks'. These 'blocks' include Clarke and Park transformations as well as the required PI controllers. InstaSPIN-FOC is best summarised by Figure 19 below.

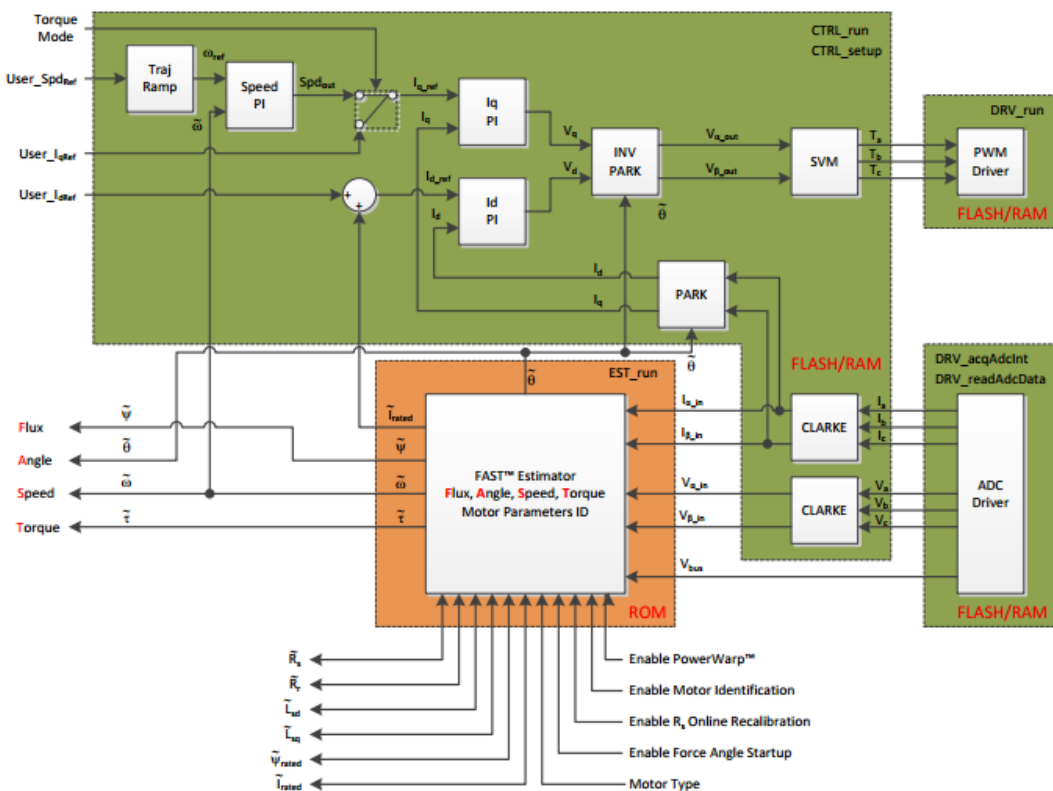


Figure 19. InstaSPIN™-FOC Block Diagram (Texas Instruments, 2013)

4.2 FAST Estimator

The FAST estimator is arguably the 'heart' of InstaSPIN-FOC and, continuing established nomenclature, is a unified observer structure. That is, FAST provides feedback on the Flux, Angle, Speed and Torque of a motor which is required for high efficiency motor control. Importantly, this is done entirely 'sensorlessly' with no encoders or resolvers required. Instead of expensive

High Performance Brushless DC Motor Control

electromechanical sensors, FAST only requires phase voltage and current feedback. TI's FAST estimator remains closed source and is supplied on ROM of selected C2000 Piccolo devices. As such, the specifics of the observer remain unclear. It should be noted that the FAST estimator is the only element of InstaSPIN™-FOC without fully documented source code provided. The following table (taken directly from InstaSPIN™ manual) shows a comparison of TIs FAST estimator with typical estimator methods.

Table 5. FAST Estimator Compared to Typical Solutions (Texas Instruments, 2013)

Topic	Typical Software Sensors and FOC	Solutions Fast Estimator and InstaSPIN-FOC Solution
Electrical Motor Parameters	Motor-model based observers heavily dependent on motor parameters.	Relies on fewer motor parameters. Off-line parameter identification of motor – no data sheet required. On-line parameter monitoring and re-estimation of stator resistance
Estimator Tuning	Complex observer tuning, done multiple times for speed/loads, for each motor	No estimator tuning required. Once motor parameters are identified, it works the same way every time, across speed/torque dynamics.
Estimator Accuracy	<p>Angle-tracking performance is typically only good at over 5-10Hz with challenges at higher speeds and compensation for field weakening.</p> <p>Dynamic performance influenced by hand tuning of observer, Motor stalls typically crash observer.</p>	<p>FAST provides reliable angle tracking which converges within one electrical cycle of the applied waveform, and can track at less than 1 Hz frequency (depending on quality and resolution of analogue sensing).</p> <p>Angle tracking exhibits excellent transient response (even with sudden load transients which can stall the motor, thus enabling a controlled restart with full torque).</p>
Start-up	Difficult or impossible to start from zero speed. Observer feedback at zero speed is not stable, resulting in poor rotor angle accuracy and speed feedback.	<p>InstaSPIN-FOC includes:</p> <ul style="list-style-type: none"> • Zero Speed start with forced-angle • 100% torque at startUp • FAST rotor flux angle tracking converges within one electrical cycle. <p>FAST is completely stable through zero speed, providing accurate speed and angle estimation.</p>
Current Loop	Tuning FOC current control is challenging-especially for novices	Automatically sets the initial tuning of current controllers based on the parameters identified. User may update gains or use own controllers if desired. The identification process to fully tune the observer and torque controller takes less than two minutes.
Feedback Signals	System offset and drifts are not managed.	FAST includes automatic hardware/software calibration and offset compensation. FAST requires 2-phase currents (3 for 100% and over-modulation), 3-phase voltages to support full dynamic performance, DCbus voltage for

		ripple compensation in current controllers. FAST includes an on-line stator resistance tracking algorithm.
Motor Types	Multiple techniques for multiple motors: standard back-EMD, Sliding Mode, Saliency tracking, Induction flux estimators, or “mixed mode” observers.	FAST works with all 3-phase motor types, synchronous and asynchronous, regardless of load dynamics. Supports salient IPM motors with different Ls-d and Ls-q. Includes PowerWarp™ for induction motors = energy savings.
Field-Weakening	Field-weakening region challenging for observers – as Back-EMF signals grow too large, tracking and stability effected	FAST estimator allows easy field weakening or field boosting applications due to the stability of the flux estimation in a wide range.
Motor Temperature	Angle tracking degrades with stator temperature changes	Angle estimation accuracy is improved from online stator resistance recalibration
Speed Estimation	Poor speed estimation causes efficiency losses in the FOC system and less stable dynamic operation	High quality low noise Speed estimator, includes slip calculation for induction motors
Torque Estimation	Torque and vibration sensors typically required	High bandwidth motor Torque estimator

4.3 Control Loops

InstaSPIN™-FOC has both torque and speed control loops available with full access to PI loop gains to allow user tuning. As a true FOC implementation, the torque controller maintains two state variables, the direct and quadrature components of the torque. The direct component is minimised as it provides no useful torque and the quadrature component is controlled to the application set-point. With InstaSPIN™-FOC configured directly as a torque controller, the quadrature component is simply the user supplied set-point. InstaSPIN’s speed controller is simply cascaded with the torque controller as shown in Figure 20 below.

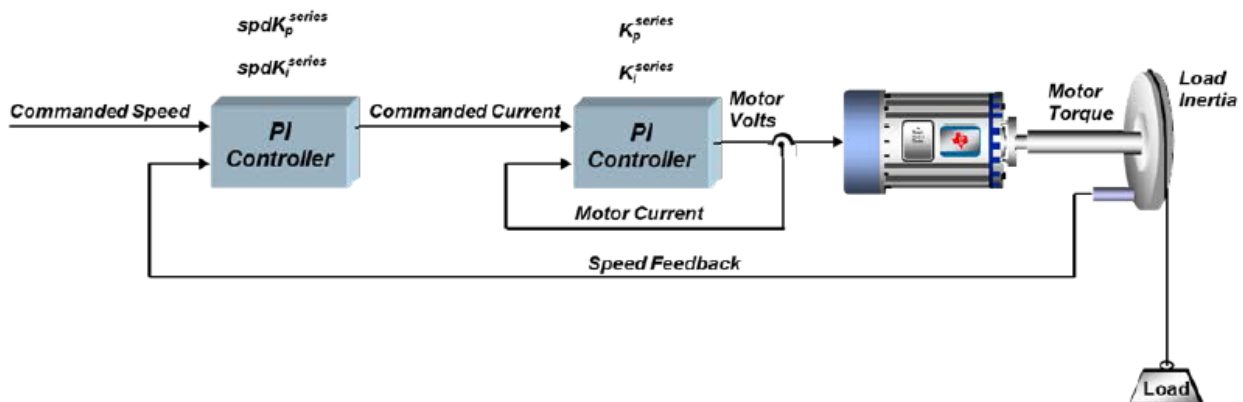


Figure 20. Speed controller cascaded with a current controller (Texas Instruments, 2013).

All commercial BLDC controllers for hobby motors are torque controllers, in fact, virtually every ‘speed’ controller with a user set throttle, is a torque controller. To illustrate this point, consider the ‘speed’ controller in a car. With a constant ‘set-point’ (throttle pedal depression) the vehicle will increase or decrease speed depending on the incline of the traversed plane. In this analogy, cruise

control is a true speed controller. While cascaded speed loops add complexity to the system, there are scenarios where they are very useful, usually when the load is highly dynamic.

4.3.1 Torque Controller

The torque controller can best be analysed by considering a series PI control loop such as the one shown in Figure 21 below.

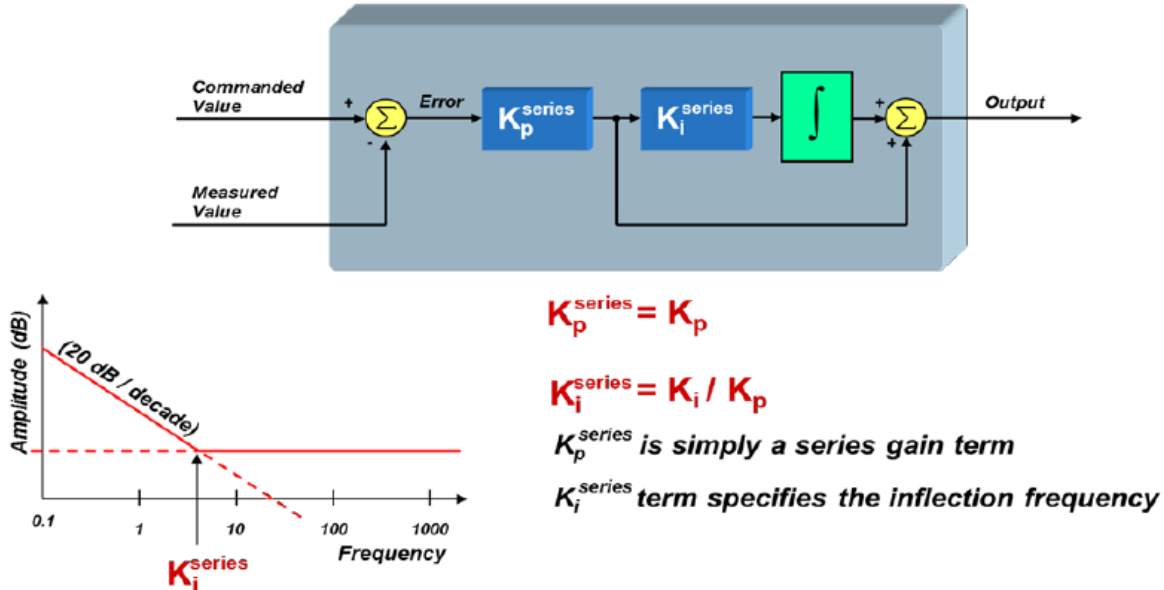


Figure 21. Generic Series PI control (Texas Instruments, 2013).

The gain of the PI controller, K_p^{series} and K_i^{series} as per Figure 21, have a substantial effect on the controller's performance. K_p^{series} sets the gain for all frequencies and K_i^{series} defines the inflection point (zero, see Figure 21) of the controller in rad/sec (Texas Instruments, 2013).

The s-domain transfer function of the controller is given by:

$$PI(s) = \frac{K_p^{series} * K_i^{series}}{s} + K_p^{series} = \frac{K_p^{series} * K_i^{series} \left(1 + \frac{s}{K_i^{series}} \right)}{s} \quad \text{Equation 1}$$

From this, it is clear that a pole exists at $s = 0$ and a zero exists at $s = K_i^{series}$. The figure below shows the PI controller and the equivalent stator coil circuit (first order approximation of stator winding using a series inductance, resistance and back-EMF voltage source).

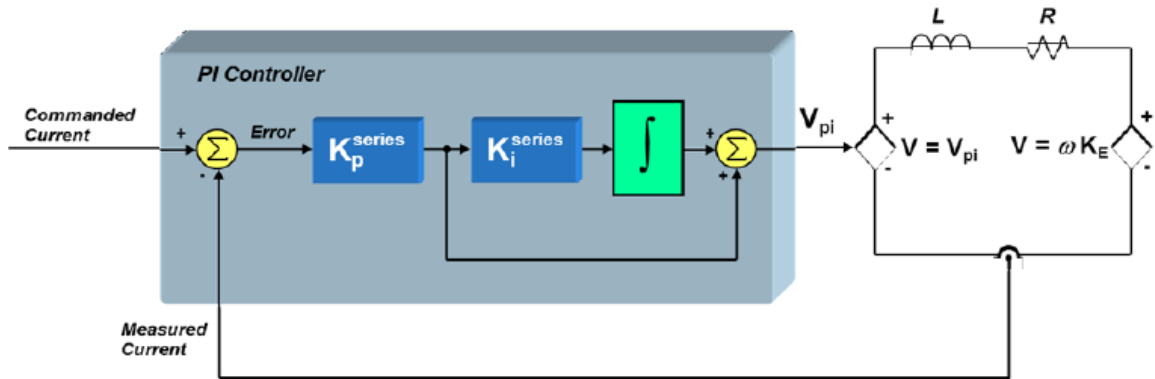


Figure 22. Torque Control System (Texas Instruments, 2013).

The small-signal transfer function from motor voltage to motor current is given by:

$$\frac{I(s)}{V(s)} = \frac{\frac{1}{R}}{1 + \frac{L}{R}s} \quad \text{Equation 2}$$

The loop gain of the controller is the product of the defined PI controller transfer function and the voltage to current transfer function for the stator coil equivalent circuit, established immediately above:

$$G_{loop}(s) = PI(s) * \frac{I(s)}{V(s)} = \left(\frac{K_p^{series} * K_i^{series} \left(1 + \frac{s}{K_i^{series}} \right)}{s} \right) \left(\frac{\frac{1}{R}}{1 + \frac{L}{R}s} \right) \quad \text{Equation 3}$$

The closed loop response can be found by:

$$G(s) = \frac{G_{loop}(s)}{1 + G_{loop}(s)} \quad \text{Equation 4}$$

assuming $H(s)=1$.

Substituting Equation 3 into Equation 4 yields the torque controller's closed loop transfer function:

$$\therefore G(s) = \frac{\left(\frac{K_p^{series} K_i \left(1 + \frac{s}{K_i^{series}} \right)}{s} \right) \left(\frac{1}{\frac{R}{L} s} \right)}{1 + \left(\frac{K_p^{series} K_i^{series} \left(1 + \frac{s}{K_i^{series}} \right)}{s} \right) \left(\frac{1}{\frac{R}{L} s} \right)}$$

Equation 5

After some algebraic manipulation, the transfer function can be defined as:

$$G(s) = \frac{1 + \frac{s}{K_i^{series}}}{\left(\frac{L}{K_p^{series} K_i^{series}} \right) s^2 + \left(\frac{R}{K_p^{series} K_i^{series}} + \frac{1}{K_i^{series}} \right) s + 1}$$

Equation 6

From Equation 6, it is clear that the denominator is a second order expression, meaning that there are two poles in the transfer function. Therefore, correct selection of K_p^{series} and K_i^{series} is critical to avoiding complex poles and to maintain a stable control system. It is necessary to choose poles that are not situated near the $j\omega$ axis to avoid large resonant spikes.

The denominator of Equation 6 can be factored into the following expression:

$$G(s)(denominator) = \left(\frac{L}{K_p^{series} K_i^{series}} \right) s^2 + \left(\frac{R}{K_p^{series} K_i^{series}} + \frac{1}{K_i^{series}} \right) s + 1$$

$$= (1 + Cs)(1 + Ds)$$

Equation 7

where C and D are real numbers. Multiplying out the expression and equating terms:

$$\frac{L}{K_p^{series} K_i^{series}} = C * D$$

Equation 8

and,

$$\frac{R}{K_p^{series} K_i^{series}} + \frac{1}{K_i^{series}} = C + D$$

Equation 9

$$\therefore \frac{R}{K_p^{series} K_i^{series}} = C \text{ and } \frac{1}{K_i^{series}} = D$$

Equation 10

Substituting the factored equivalent denominator (Equation 10) into Equation 6 yields:

$$G(s) = \frac{1 + \frac{s}{K_i^{series}}}{\left(1 + \left(\frac{R}{K_p^{series} K_i^{series}} \right) s \right) \left(1 + \left(\frac{1}{K_i^{series}} \right) s \right)}$$

Equation 11

As can be seen in Equation 11, the ‘D’ substitution has resulted in a pole that cancels out one of the zeroes of the original transfer function. Therefore, with the correct selection of ‘C’ and ‘D’, a closed loop system with no zeroes and only one real (i.e. non-complex) pole can be achieved. This is a system with no resonant responses and a single-pole low-pass roll off response (Texas Instruments, 2013).

Further, substituting the expressions for C and D established in Equation 10 into Equation 8 results in the following equality:

$$K_i^{series} = \frac{R}{L} \quad \text{Equation 12}$$

The frequency at which the controller zero occurs (K_i^{series}) is given by Equation 12. In order to achieve the desired response (no-zero, one real pole), it is a simple matter of setting K_i^{series} to the pole of the plant (Texas Instruments, 2013).

Continuing with substitutions made to this point:

$$G(s) = \frac{1}{\frac{L}{K_p^{series}}s + 1} \Rightarrow K_p^{series} = L * \text{Bandwidth} \quad \text{Equation 13}$$

Considering Equation 12 and Equation 13 it is clear that K_i^{series} should be set to the pole of the plant and that K_p^{series} sets the bandwidth of the current controller. It is clear that the loop gains, K_i^{series} and K_p^{series} and the motor’s series impedance and inductance are critical to the performance of the controller. Traditionally, these values would be obtained from manufacturers data sheets. However, manufacturers of small hobby grade BLDC motors rarely (if ever) provide data sheets with their product. To overcome this, InstaSPIN™-FOC incorporates an ‘identify’ routine which allows for quick and easy identification of pertinent motor parameter’s which can then be used to establish initial values for the loop gains discussed. PI loop gains must be fine-tuned in order to achieve the maximum possible performance from the controller.

Texas Instruments provides fully open source sample code to implement InstaSPIN-FOCs torque controller.

4.3.2 Speed Controller

InstaSPIN’s speed controller can best be described as a parallel PI controller as shown in Figure 23 below.

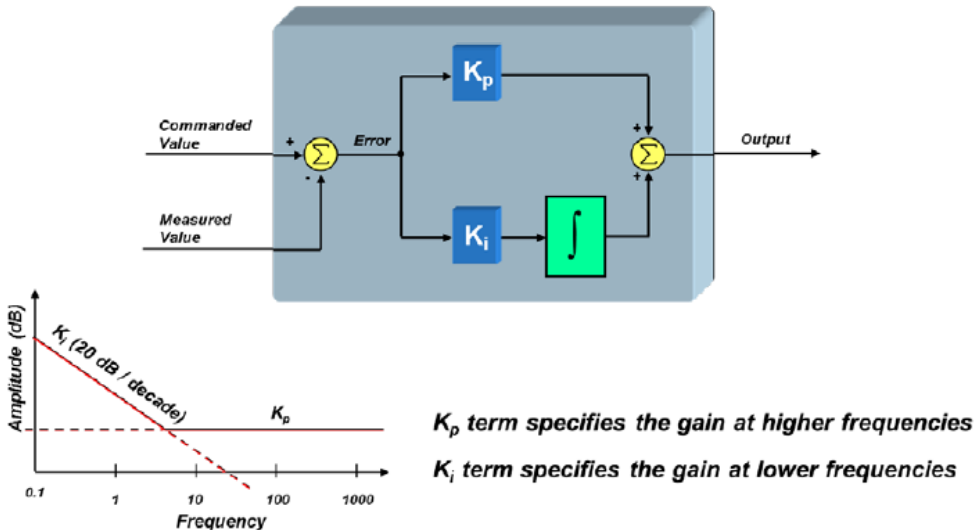


Figure 23. Parallel PI Control (Texas Instruments, 2013).

As shown in Figure 20 above, the speed controller is cascaded with the current (torque) controller. It is also important to note that the speed controller resides in the mechanical domain where time constants are much slower. The transfer function describing the cascaded speed controller is:

$$G_{loop}(s) = PI(s) * K_{curr} * Mech(s) = K_i \left(\frac{\left(1 + \frac{K_p}{K_i}s\right)}{s} \right) * K_{curr} * \left(\frac{K}{s}\right)$$

$$G_{loop}(s) = \frac{K * K_{curr} * K_i}{s^2} \left(1 + \frac{K_p}{K_i}s\right)$$
Equation 14

(Texas Instruments, 2013)

Where K_{curr} is a constant gain representing the current controller and K is a gain representing the motor's voltage constant and inertia.

$$G_{loop}(s) = \frac{KK_{curr}K_i \left(\left(1 + \frac{K_p}{K_i}s\right) \right)}{s^2 + KK_{curr}K_p s + KK_{curr}K_i}$$
Equation 15

The free-body diagram of an analogous mechanical mass, spring and damper system is shown in Figure 24 below.

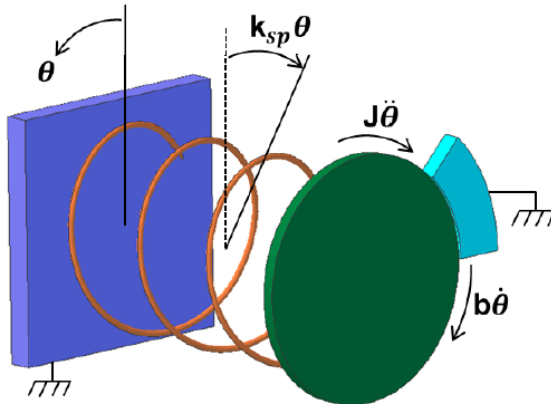


Figure 24. Mass, spring, damper mechanical system (Texas Instruments, 2013)

The transfer function defining Figure 24 above is:

$$T_{mech}(s) = \frac{1}{\frac{J}{s^2 + \frac{b}{J}s + \frac{k_{sp}}{J}}} \quad \text{Equation 16}$$

Equating terms in the denominators of Equation 15 and Equation 16 allows the following relationships to be defined:

$$\begin{aligned} K_p &\propto b \\ K_i &\propto k_{sp} \end{aligned} \quad \text{Equation 17}$$

It is clear that increasing k_i has the same system effect as increasing a spring constant. That is, increasing k_i has the effect of stiffening the system. Increasing K_p has the effect of increasing the dampening of the system. Selecting the correct K_p and K_i is important and requires tuning for each motor.

The closed loop transfer function for the current controller is given by Equation 13 above where K_p^{series} is the PI controller's error multiplier in the PI structure. With correct inductance and resistance values, the torque controllers K_i^{series} does not impact the speed controller as it is set to cause pole/zero cancellation. The transfer function used to define the torque controller can also be used to define the speed controller as follows.

$$\begin{aligned} PI(s) &= \frac{spdK_p^{series} * spdK_i^{series}}{s} + spdK_p^{series} \\ &= \frac{spdK_p^{series} * spdK_i^{series} \left(1 + \frac{s}{spdK_i^{series}} \right)}{s} \end{aligned} \quad \text{Equation 18}$$

For a BLDC motor under FOC Control, the transfer function between quadrature-axes current and motor torque is given by:

$$Mtr(s) = \frac{3}{2} \frac{P}{2} \lambda_r = \frac{3}{4} P \lambda_r$$

Equation 19

(Texas Instruments, 2013)

Where P is the total number of rotor poles and λ_r is the rotor flux. The transfer function from motor torque to load speed is:

$$Load(s) = \frac{\frac{1}{J} \frac{1}{s}}{s}$$

Equation 20

Where J is the inertia of the load and the motor (Texas Instruments, 2013).

Combining (multiplying) Equation 13, Equation 29, Equation 30 and Equation 31 yields the composite open-loop transfer function:

$$GH(s) = \left(\frac{spdK_p^{series} * spdK_i^{series} \left(1 + \frac{s}{spdK_i^{series}} \right)}{s} \right) \left(\frac{1}{\frac{L}{K_p^{series}} s + 1} \right)^K$$

Equation 21

Where K represents all motor and load parameters:

$$K = \left(\frac{3}{4} P \lambda_r \right) \left(\frac{1}{J} \frac{1}{s} \right)$$

Equation 22

Some algebraic manipulation yields:

$$GH(s) = \frac{K * spdK_p^{series} * spdK_i^{series} \left(1 + \frac{s}{spdK_i^{series}} \right)}{s^2 \left(1 + \frac{L}{K_p^{series}} s \right)}$$

Equation 23

Equation 23 shows two poles at $s = 0$, 1 pole $s = \frac{K_p^{series}}{L}$ (the current controllers pole) and a zero at $s = spdK_i^{series}$. For stable operation, the pole at $s = \frac{K_p^{series}}{L}$ must be of a higher frequency than the zero at $s = spdK_i^{series}$. Figure 25 below shows the Bode plot for the system providing that the unity gain frequency occurs somewhere between $s = spdK_i^{series}$ and $s = \frac{K_p^{series}}{L}$.

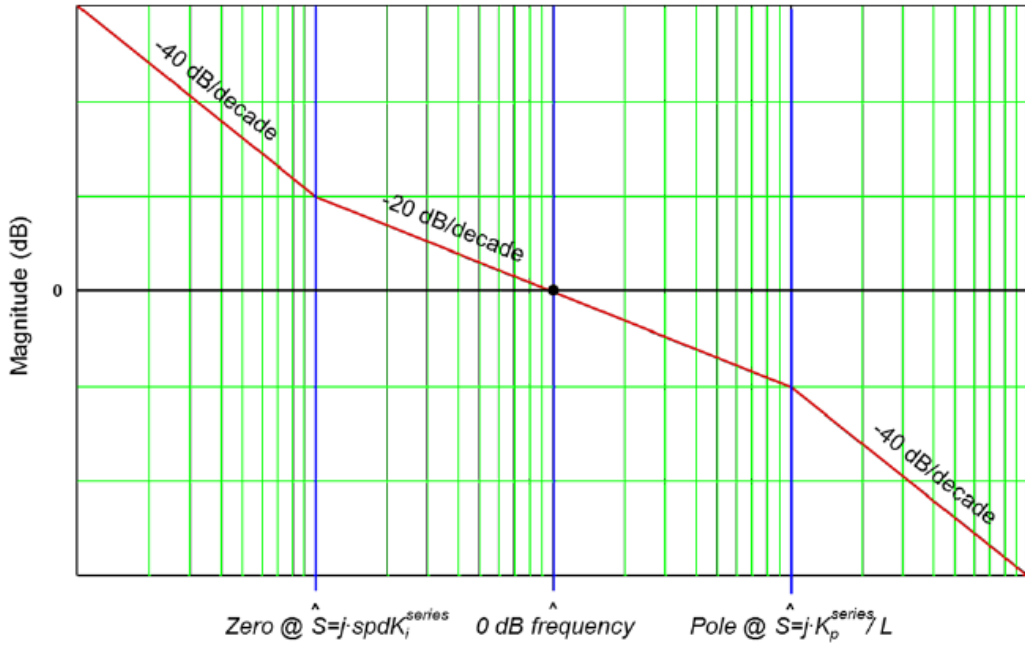


Figure 25. Ideal Speed Controller Bode Plot (Texas Instruments, 2013).

$$\omega_{pole} = \delta\omega_{0dB}$$

$$\omega_{0dB} = \delta\omega_{zero}$$

$$\omega_{pole} = \delta^2\omega_{zero}$$

Equation 24

From Equation 1 above, ω_{pole} and ω_{zero} have been defined in terms of the PI coefficients:

$$spdK_i^{series} = \frac{K_p^{series}}{\delta^2 L} \quad \text{Equation 25}$$

where δ is the system damping factor. By increasing δ , system stability can be increased but at the cost of controller bandwidth. Equation 29 shows that Equation 23 will be unity gain at a frequency equal to the zero inflection point frequency multiplied by δ :

$$1 = \left| \frac{K * spdK_p^{series} * spdK_i^{series} \left(1 + \frac{s}{spdK_i^{series}} \right)}{s^2 \left(1 + \frac{L}{K_p^{series}} s \right)} \right|_{s=j\delta spdK_i^{series}} \quad \text{Equation 26}$$

Solving Equation 26 yields the last remaining loop gain:

$$1 = \frac{\delta K spdK_p^{series}}{\delta^2 \left(\frac{K_p^{series}}{\delta^2 L} \right)}$$

$$\therefore spdK_p^{series} = \frac{K_p^{series}}{L \delta K} = \frac{\delta spdK_i^{series}}{K} \quad \text{Equation 27}$$

TI (InstaSPIN-FOC user's manual) provide the following equation (Equation 28) to determine the speed controllers bandwidth.

$$BW_c = \frac{K_p^{series}}{L} = BW_s \left(\delta + 2.16e^{\frac{\delta}{2.8}} - 1.86 \right) \left(rad/sec \right)$$

$$\therefore spdK_p^{series} = \frac{K_p^{series}}{L\delta K} = \frac{\delta spdK_i^{series}}{K}$$
Equation 28

where:

BW_c is the current controller bandwidth;

K_p^{series} is a current loop PI coefficient;

L is the motor inductance;

BW_s is the speed controller bandwidth;

δ is the damping factor;

Using Equation 25, Equation 27 and Equation 28 the PI loop gains can be calculated for both the speed and torque controllers.

This is, of course, done automatically by InstaSPIN™-FOC after parameters are given or identified. A full speed controller is provided open-source as part of the InstaSPIN™ package, defined as above.

4.4 Motor Identification

InstaSPIN's Motor identification functionality is particularly critical to this research as small BLDC motors are rarely (if ever) provided with any more information than current and voltage ratings and the number of poles. (This is sometimes not provided but is easily found). As established above, the identified parameters have a direct effect on the system poles, and hence, the overall performance of the controller. A state diagram for InstaSPINs motor parameter estimator may be seen in Figure 26 below. Additionally, Figure 27 below shows the sequence of events that happen inside of the controller and estimator state machines.

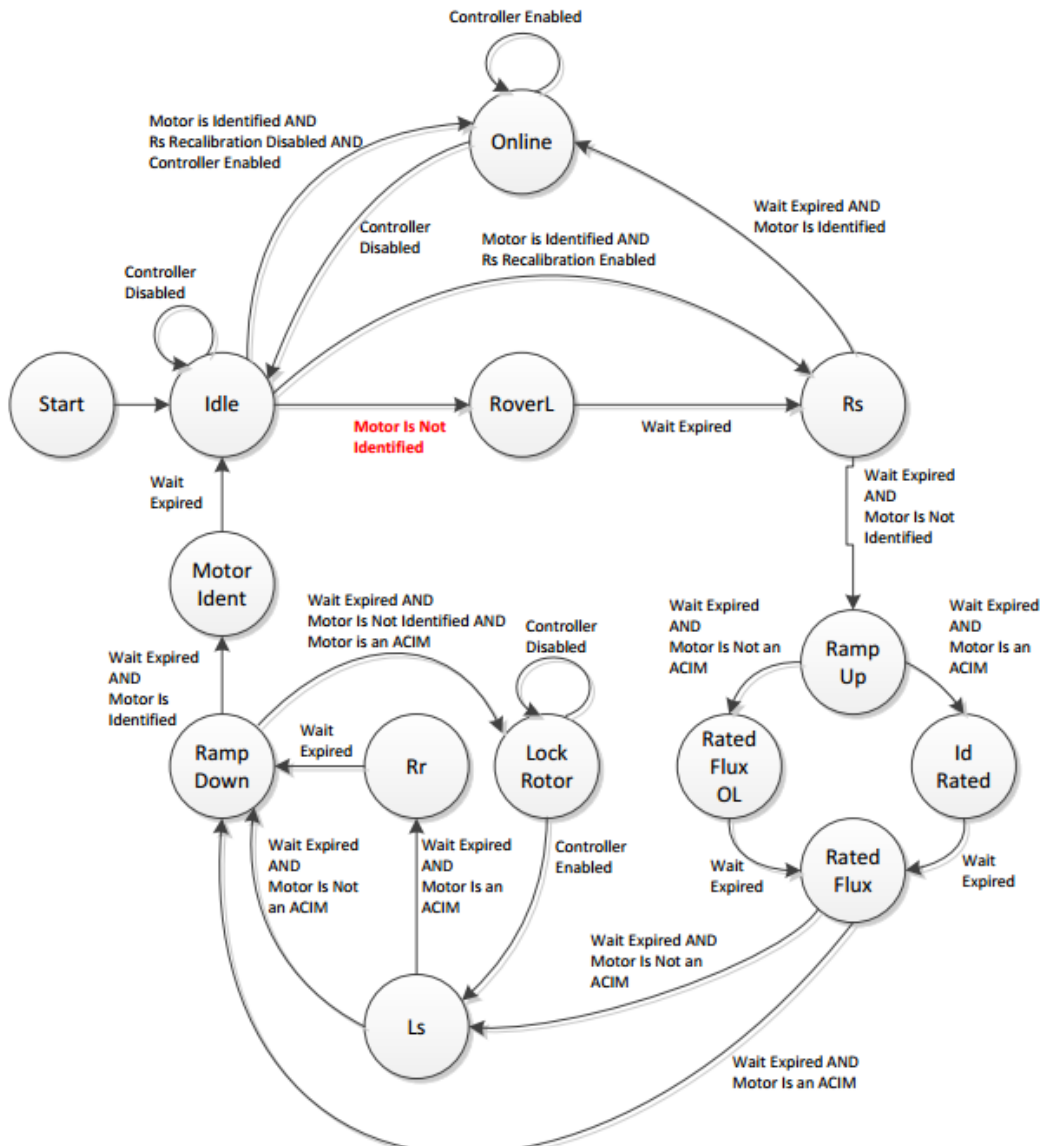


Figure 26. Estimator State Diagram (Texas Instruments, 2013)

Figure 26 above is a general overview of InstaSPIN's estimator and includes functionality not relevant to this research. That is, anything regarding ACIM motors (lock rotor for example) is not relevant.

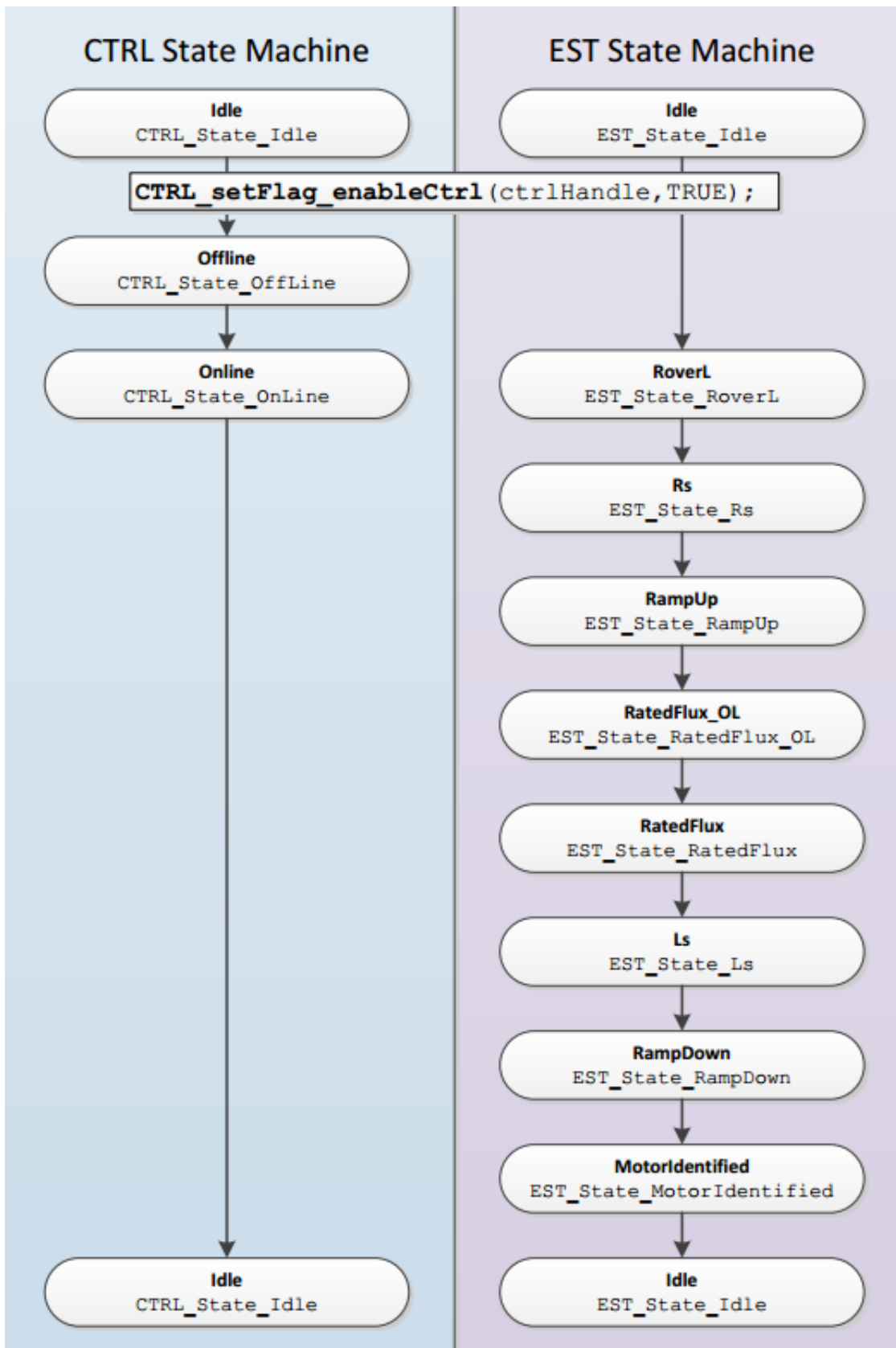


Figure 27.InstaSPIN Motor Identification Sequence (Texas Instruments, 2013).

High Performance Brushless DC Motor Control

Figure 26 and Figure 27 above show the general processes and estimator state steps required for motor identification. However, the intricacies of InstaSPIN's motor identification routine cannot be outlined in a meaningful way here due to their inherent complexity. (Full explanations could easily fill this document). Instead, it is recommended that the reader review the relevant literature provided freely by Texas Instruments at <http://www.ti.com/lit/ug/spruhj1d/spruhj1d.pdf>, specifically, chapter 6.

5 Methodology

This research was designed to be conducted in three distinct phases. These are outlined below.

1. Initial InstaSPIN™-FOC Evaluation
 - InstaSPIN™-FOC was evaluated using hobby BLDC motors and a TI development kit;
 - InstaSPIN-FOC sample code was used for motor identification and torque and speed controllers;
 - An evaluation platform was developed to empirically test InstaSPIN's performance;
 - Substantial familiarity was gained with Texas Instrument's Code Composer Studio (CCS) IDE, specifically with the MotorWare package;
2. Custom Motor Controller Hardware Development
 - Hardware for a custom controller was developed and fabricated;
 - Several PCB layouts were trialled;
 - Two revisions were fully populated and evaluated.
3. Custom Motor Controller Evaluation
 - The final (to this point) Custom Motor Controller revision (2C) was empirically tested on several hobby BLDC motors and compared with commercial BLDC controllers.

5.1 Evaluation Board

Before InstaSPIN™ could be effectively evaluated, it was necessary to develop a method for determining its performance empirically. From the outset, several requirements for the evaluation board were identified:

- Accurate to 50mA bus current sensing and capable of up to 20A;
- Accurate to 0.5RPM rotor speed evaluation and capable of up to 30kRPM;
- Real time feedback;
- Data logging;
- Accomplished using the TI F28027 LaunchPad (LP) Development board.
- PCB to be developed using the CNC mill available at CQU.

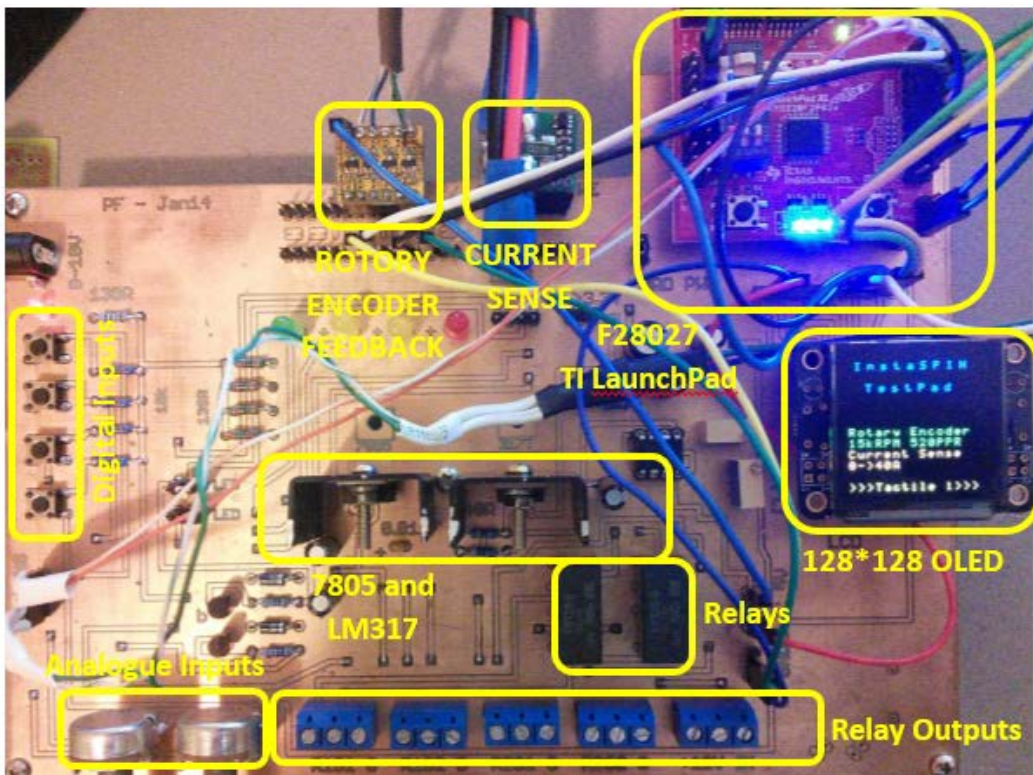


Figure 28. Evaluation Board

Figure 28 above shows a labelled photograph of the evaluation board developed. This was designed in Eagle CAD and fabricated using the CNC mill at CQU. Bus current sense was achieved using an AttoPilot Current Sense breakout from *Sparkfun*. This is a high side current shunt resistor and op-amp which scales 0-45A to 0-3.3V. The current limit is set by the I^2R losses of the shunt resistor, in this case 0.0001Ω at 2W. The schematic for the current sense board may be seen in Figure 29 immediately below.

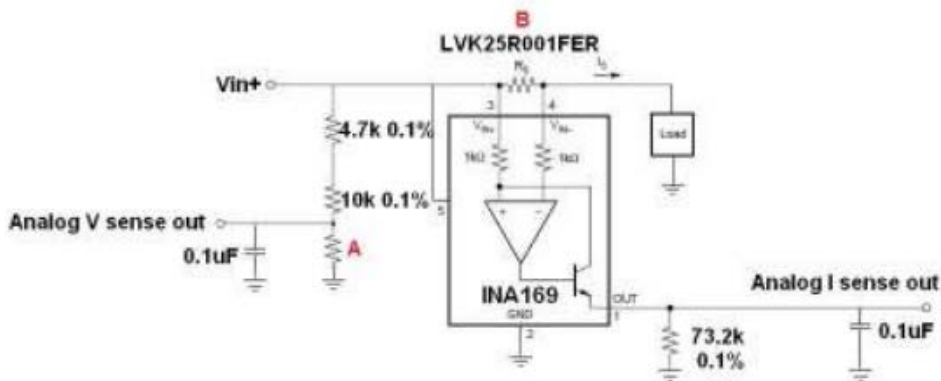


Figure 29. 45A AttoPilot Current Sense board (AttoPilotInternational, 2011)

Initial ADC sampling of the potential difference across the shunt resistor using the F28027 LP proved inconsistent and noisy. By adding a low pass filter and oversampling, a very clean and accurate result was obtained. The accuracy of the current sense was verified at 50mA using known loads and bench meters. In addition, loads of up to 35A (DC) have been tested without issue.

An AMT-103 capacitive rotary encoder was used for rotor speed sensing. The encoder is mounted directly on the rotor shaft of the motor to be tested and is rated for speeds up to 30kRPM (speeds over 35kRPM have been successfully tested). The AMT-103 only supports TTL level logic which is not compatible with the CMOS (3.3V) voltage levels of the F28027 LP. It was necessary to use a logic level converter to take the 5V out from the encoder to 3.3V.



Figure 30. AMT-103 Rotary Encoder.

The AMT-103 produces two standard quadrature encoded signals, offset from each other by 90°.

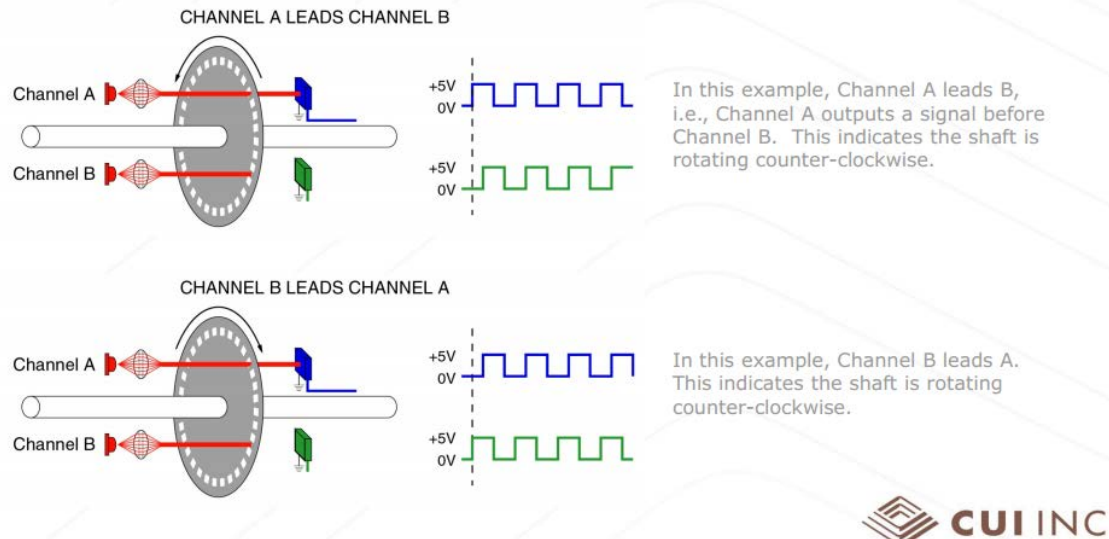


Figure 31. Quadrature Encoding (CUI INC, 2010)

As Figure 31 shows, this offset allows the direction of the motor to be identified, if channel A is High while B is low, the motor is spinning clockwise and vice-versa. This functionality was successfully implemented in early code revisions. However, it was not required for the evaluation of the motors and was discarded in later code revisions, allowing rotor speed sensing to be achieved using only a single GPIO. The number of pulses per revolution (PPR) is user selectable via a dip switch. The PPR for this application was set to 48PPR, to provide high resolution across the widest possible speed range. A 32bit timer was used to provide a 50ms count window.

$$Speed = \frac{C}{\frac{PPR}{t} \cdot \frac{60}{60}}$$

Equation 29

where C is the number of pulses counted in a given time t .

$$\text{Speed} = \frac{\frac{C}{48}}{\frac{0.05}{60}} = 25C$$
Equation 30

To ensure accuracy, an external interrupt was used on the selected GPIO instead of simple polling which may well miss a pulse. The 48PPR provides much higher resolution than the required 0.5RPM. The indicated speed has been verified using an optical tachometer as well as comparing against the rotor speed estimated by InstaSPIN-FOC's FAST observer.

The real time feedback requirement was achieved using a 128*128 pixel OLED display module by freelectronics. This screen utilises 16,384 full colour RGB pixels in a 1.5" screen. As no support was offered for TI microcontrollers, several functions were written to create textbox's, shapes and read a font header. The screen uses the SPI communications protocol clocked at 8MHz. The dedicated SPI peripheral on the F28027 LP was used to communicate with the screen.

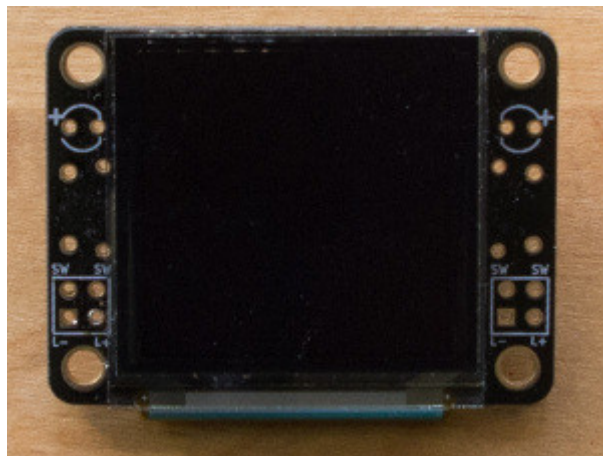


Figure 32. 128*128 Pixel OLED Display

The OLED screen used on the evaluation board displays rotor speed and bus current to two decimal places as well as graphing the rotor speed in real time.

Data logging was handled using a terminal program and the SCI (UART) peripheral on the F28027 LP. Bus current and rotor speed is sampled and sent every 50mS with a time stamp. A baud rate of 9600 baud was selected for the protocol, this proved more than fast enough for the 50ms window.

5.2 Initial InstaSPIN-FOC Evaluation

InstaSPIN-FOC was evaluated using a DRV8301-69M-KIT development board (see Figure 33 right) selected during the planning phase of this research. This is an InstaSPIN- FOC enabled 60V, 40A continuous inverter designed specifically for evaluating InstaSPIN technology. During the initial evaluation of InstaSPIN-FOC, several problems were encountered, including;



Figure 33. DRV8301-69M-KIT (Texas Instruments, 2014)

- Misidentifying BLDC motor;
 - Complete failures to identify motors or identified values were incorrect and inconsistent.
 - A PMSM motor was successfully identified without issue. However, the problems with identification existed with all BLDC motors tested.
- Very poor performance with speed controller in loop;
 - Resonant control responses, physically observable rotor vibrations and generally poor performance was observed using InstaSPIN's speed controller.
- Complete motor failure (dielectric breakdown in motor windings leading to fire);
 - Single incident, unknown cause.

These problems, with the exception of motor identification, were overcome gradually and were simply problems with initial InstaSPIN configurations.

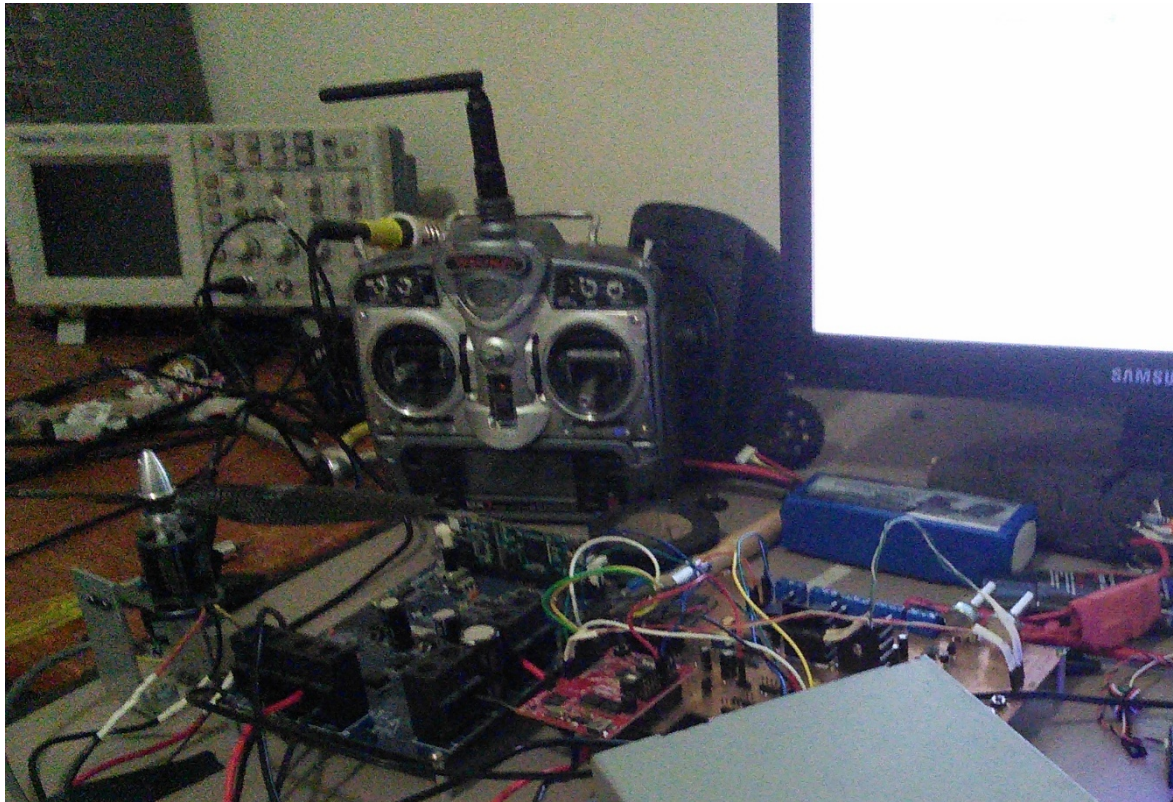


Figure 34. Initial InstaSPIN™-FOC evaluation (Evaluation and Development boards visible).

5.2.1 Motor Identification

Several weeks were spent specifically trying to identify small hobby sized BLDC motors using the DRV8301-69M-KIT development board. This was because motor identification was particularly important to this research as the manufacturers of the motors this research is aimed at only provide very basic nameplate data. During the initial evaluation, motor identification would invariably fail to accurately estimate the inductance of the motors. This would result in both the torque and speed (speed more so) controllers operation being very unstable (see 4.3 Control Loops) and resulted in extremely poor general motor performance. In one notable case, the motor identification routine resulted in complete dielectric failure of one of the tested PropDrive motors which resulted in a small fire on the rubber grommet surrounding the phase wires. The cause of this remains unknown and was a single (and unrepeatable) event. It is important to note that the development board was configured to allow only half of the motors rated current to pass through each phase. It is unlikely that the fault was caused by a significant overcurrent event. It may have been a result of a manufacturing fault within the motor. Also note that the TI development board was not damaged by the event.

Several methods were tried to identify the trailed motors including reducing software voltage feedback scaling, adding external inductors to each of the three phase wires, loading the motor to produce more feedback and much more. Further, the user configuration file *user.h* was experimented with (generally, changes were checked or advised by TI engineers) and several variations were tried. Ultimately, no success was had and some trailed methods were in fact detrimental to the identification routine results (notably, loading the motor). After discussion with Texas Instruments engineers, it was decided that the most likely cause was the very low inductance of hobby BLDC motors and the feedback scale of the development kit which is (hardware) scaled for 60V bus voltage and 40A continuous current. The motors this research is aimed at are very rarely driven from more than a 21V (5 cell LiPo) source and generally consume less than 20A continuous under steady-state conditions. In addition, the target motors produce very little back-EMF at low speeds (<100RPM) resulting in identification issues. It was decided that the best solution to this problem was to simply guess the motor parameters such that loop gains would be in the ‘ballpark’ and the torque and current controller could be more effectively evaluated using BLDC motors.

5.2.2 Torque Controller

As discussed above, motor parameters used by InstaSPIN for setting PI loop gains were guessed as a result of automatic motor identification being unsuccessful. Nonetheless, excellent performance was achieved using InstaSPIN’s torque controller (with guessed parameters). With the motor unloaded, the InstaSPIN-FOC development board (DRV8301-69M-KIT) was able to drive the motor up to some upper limit and remain stable while running at the motors upper speed limit. No noticeable vibrations were present and step responses appeared critically damped with no control oscillations present. Time was invested in PI loop tuning, however, no substantial improvements to the controller’s performance were noted. With the motor loaded with a model aeroplane propeller, performance was also excellent, in this case however, step responses were considerably faster and smoother with some PI loop gain tuning.

Note, PI loop gain tuning was conducted as advised in Texas Instruments InstaSPIN Users Guide. This can be found here: <http://www.ti.com/lit/ug/spruhj1d/spruhj1d.pdf> - Chapter 12, Tuning Regulators.

5.2.3 Speed Controller

The speed controller's performance (again using guessed motor parameters) was found to be stable only between about 1500RPM and 8000RPM (maximum speed found using the torque controller was 15000RPM) using the unloaded PropDrive motor. When speeds outside of this range were commanded, the motor would become unstable, the further outside of this range, the more unstable the motor would become. With the motor loaded, the controller was able to commutate from about 800RPM to 4000RPM, again, losing stability outside of this range. PI tuning was able to extend this range from 500RPM to 5000RPM, but the motor was still not able reach its speed limit (or inverter current limits). It is believed that PI tuning was not able to tune the loop gain to optimum values because the initial loop gains (derived from guessed motor parameters) were too far away from their optimal values for tuning to converge. Additionally, a stated goal of the research was sensorless low speed commutation. What exactly constituted 'low speed' was not explicitly stated, but it was hoped that stable speeds below 100RPM could be achieved.

A PMSM motor was tried with the development board with great success. This motor was able to run stably from 80RPM to 4000RPM (its rated top speed) with identification running smoothly with very consistent results. Some very minor PI tuning (again, following procedures outlined by Texas Instruments) resulted in excellent step responses and very fast ramp-up times. This was done just to assess InstaSPIN on a PMSM motor as anecdotal evidence had suggested that these motors would be easier to identify. However, the stated goal of the project was to commutate BLDC motors using advanced control techniques, and so, only very little time was spent evaluating with the PMSM motor.

5.2.4 Initial InstaSPIN FOC Evaluation Conclusion

After discussing the aforementioned issues extensively with Texas Instruments (InstaSPIN) engineers and the project supervisor, it was decided to persevere with Texas Instrument's InstaSPIN FOC. This was justified by the fact that problems encountered with the speed controller were almost certainly a result of the failed motor identification routine, itself likely a result of less than optimal hardware scaling. This did mean that the DRV8301-69M-KIT could not be used as the basis for custom hardware design (as initially planned) as the same issues would undoubtedly ensue.

5.3 Custom Controller Development

Several iterations of custom hardware were developed, with two 'versions' being fully populated and tested. Texas Instruments establishes several hardware prerequisites necessary for the correct operation of InstaSPIN;

- Bidirectional phase current sense;
- At least two phase current sense, preferably three;
- Correct polarity current sense;
- Three phase voltage sense;
- Voltage filter pole location;
- Bus voltage sense (optional);

Due to the limited time-frame available for this project, a complete 'ground up' (*i.e.* '*start from scratch*') hardware design was not feasible nor planned. It was known that the development kit initially evaluated was not a suitable design (for this application). Instead, the BOOSTXL-DRV8301

Motor Drive BoosterPack by TI was used as a reference guide. This Booster pack was designed with far more suitable scaling and also utilised the DRV8301 gate-driver which had been previously selected for use on the basis of the Literature Review and experience with the IC gained using DRV8301-69M-KIT. The BOOSTXL-DRV8301 design files are released by TI. In fact, TI recommends using their hardware designs as a ‘starting point’ for custom designs.

The BOOSTXL-DRV8301 did not meet several design requirements for the custom speed controller, including;

- Form factor was far too big;
 - PCB layout was completely redesigned.
- No microcontroller – this is a Booster Pack, designed to be used with TI LaunchPads and not as a standalone device (analogous to the popular Arduino ‘shields’).
 - A C2000 piccolo and associated components (including full JTAG header) were added to the design.
- Availability of components
 - Some components were not available and were substituted.
- Power stage is quite small.
 - A larger power stage was designed but not implemented – this is a suggested improvement (see 7.9 Recommendations for Future Work).



Figure 35. TI’s DRV8301 BOOSTXL (Texas Instruments, 2014).

5.3.1 Microcontroller

TI currently only offers InstaSPIN on selected MCUs in their C2000 Piccolo range. Within this subset, InstaSPIN technology is available on the F28027F and the F28069F models (F indicates InstaSPIN™). A brief comparison between the F28027F and F28069F C2000 microcontrollers can be seen in Table 6 below.

Table 6. C2000 InstaSPIN-FOC Capable Microcontroller comparison.

	F28027F	F28069F
SPEED (MHz)	60	90
FPU	NO	YES
FLASH (KB)	64	256
GPIO	22	40
SCI (UART)	YES	YES
SPI	YES	YES
CAN	NO	YES
ADC	12-Bit 13 Channel	12-Bit 16 Channel
I²C	YES	YES
Footprint (mm²)	90.16	201.64

Given the requirement for a physically small motor controller, the F28027F was chosen. This is despite the fact that the development board initially experimented with utilised the F28069F MCU which has substantially more capability and supports CAN bus. A full list of each of the MCUs features may be seen on Texas Instrument's website.

The F28027F microcontroller is more than capable for this application, and, while its performance is less than that of the F28069, it is more suitable in this application. No planned feature of the custom FOC controller was rejected due to the selection of the F28027F microcontroller.

5.3.2 Gate Driver

Several methods for driving MOSFET gates were investigated during the literature review. After considering the merits of the various options considered, a pre-driver was decided upon. Specifically, TI's DRV8301 was chosen as the most suitable pre-driver as it includes several protection schemes as well as two current amplifiers on chip which can be used as part of the phase current feedback circuit. Specifically, the DRV8301 was chosen because it offers;

- A wide supply range voltage of 6V-60V;
- Integrated Dual Shunt Current Amplifiers with adjustable gain and offset;
- Integrated buck converter to support 1.5A external load;
- Independent control of three or 6 PWM inputs;
- Bootstrap Gate Driver with 100% Duty Cycle Support;
- Programmable Dead Time to Protect External FETs from Shoot Through;
- Slew Rate Control for EMI Reduction;
- Support for both 3.3V and 5V Digital Interface;

- SPI Interface;
- Thermally Enhanced 56-Pin TSSOP PAD DOWN DCA Package.

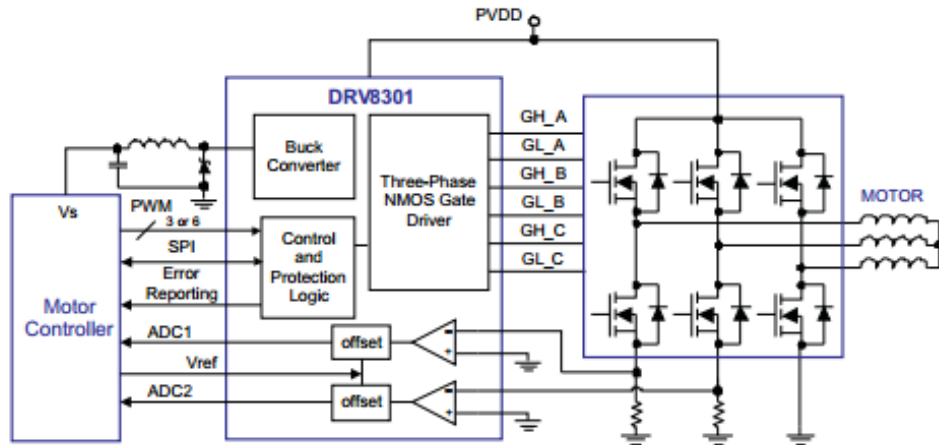


Figure 36. DRV8301 Simplified Application Schematic (Texas Instruments, 2011).

The DRV8301 provides three half bridge drivers each capable of supporting two N-type MOSFETs, allowing N-Channel FETs to be used as both the high and low side switching device. This is advantageous as N-Channel FETs are faster than P-Channel FETs. Additionally, using identical FETs allows for impedance matching on the high and low side devices. Several important protection and auxiliary systems are implemented on-chip. These include automatic handshaking when high or low side FET is switching to prevent current shoot through; active current limiting; integrated dual shunt current amplifiers with adjustable gain and offset; integrated buck converter (1.5A) and an SPI interface. Through the SPI interface, several parameters may be set, including slew rate, dead time, overcurrent protection (detected by drain-to-source voltage), gain (current amplifiers, 4 settings) and DC calibration settings. Fault reporting is also available through the SPI interface. While this is not used per se (system will shut down on fault but SPI registers are not checked), it was invaluable during the prototyping stages of the project.

5.3.3 Current Sense

A prerequisite of most sensorless motor controllers, including InstaSPIN, is accurate phase current feedback. Phase current feedback is provided for all three phases using precision shunt resistors and op-amps. Due to the nature of three-phase BLDC motors, it is necessary to measure bidirectional phase currents in some fashion. As the ADCs on the F28027F microcontroller cannot handle bidirectional currents natively, a reference voltage of 1.65V was used to allow the measurement of both positive and negative flowing currents. This reference voltage allows the measurement of bidirectional currents by denoting the maximum negative current as 0V and the maximum positive current as 3.3V. The required 1.65V reference was achieved using a voltage follower scheme, using the same external op-amp as used for the external current amplifier (see Figure 39. OPA2374 External Amplifier below) and two 10k precision resistors in a voltage divider format. A precision (10K) voltage divider is also used to provide the DRV8301 internal current amplifiers with the required 1.65V reference voltage (see APENDIX I FOC Speed Controller Full Schematic (1/5)).

Phase currents are measured by observing the voltage drop across a low side shunt resistor placed on the ground leg of each of the three half-bridges as shown in Figure 37 below.

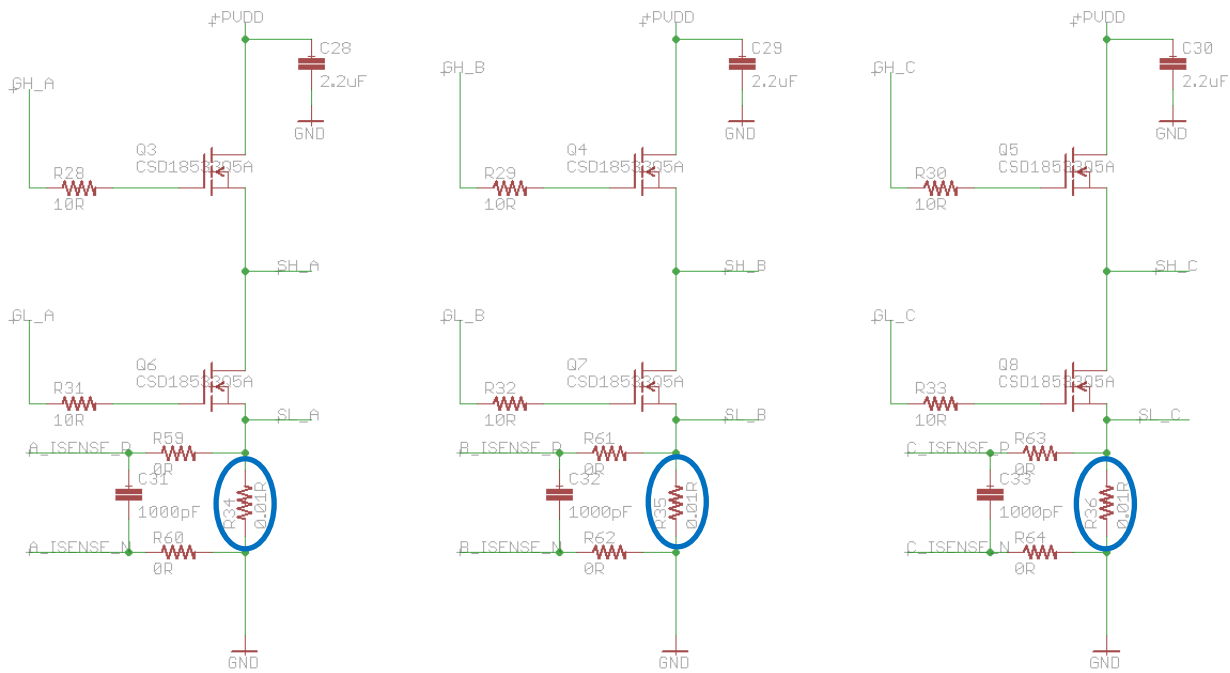


Figure 37. Inverter Stage with Low Side Shunt Resistors Circled in Blue.

Figure 37 also shows 0Ω resistors on both the high and low side of each shunt resistor, this is to allow for true differential routing and will be explained further in section 5.3.7 (*PCB Layout*) below. Sizing the shunt resistors correctly is critical to the operation of the speed controller. The shunt resistor size determines the resolution of the current feedback and is also one of the primary current ‘bottlenecks’. As all phase current must flow through the shunt resistor to ground, its ability to dissipate heat is a critical design criteria. The differential amplifier configuration used for phase current feedback may be seen in Figure 38 below.

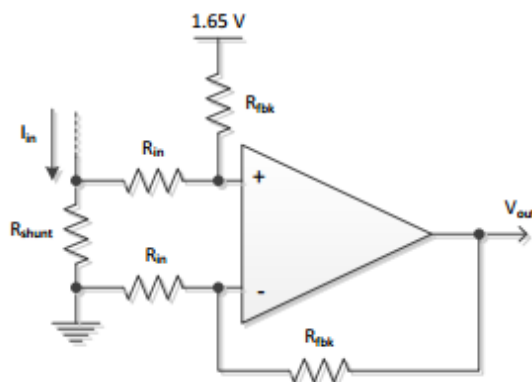


Figure 38. Differential Amplifier (Texas Instruments, 2013).

A small controller rated for 10A continuous and 14A peak current was required for the first prototype. Therefore, the output from the differential amplifiers is required to be 0V for -14A phase

current and +3.3V for +14A phase currents. In addition, the amplifier should maintain linearity for all mid-range phase currents. Considering Figure 38, the output (V_{out}) is given by:

$$\begin{aligned}
 V_{out} &= 1.65 + \frac{(R_{fbk} + R_{in}) * R_{fbk}}{(R_{fbk} + R_{in}) * R_{in}} * V_{R_{shunt}} \\
 V_{R_{shunt}} &= I_{in} * R_{shunt} \\
 \therefore V_{out} &= 1.65 + \frac{(R_{fbk} + R_{in}) * R_{fbk}}{(R_{fbk} + R_{in}) * R_{in}} * I_{in} R_{shunt} \\
 V_{out} &= 1.65 + I_{in} R_{shunt} \frac{R_{fbk}}{R_{in}}
 \end{aligned}
 \tag{Equation 31}$$

As can be seen in Figure 37, a shunt resistor value of 0.01Ω was chosen initially as the value for the shunt resistor. Additionally, setting the input resistance to $1.0k\Omega$ and assuming a maximum peak current of 15.4A (+10% of peak current), Equation 31 can be solved for the required feedback resistor value:

$$\begin{aligned}
 3.3 &= 1.65 + 15.4 * 0.01 \frac{R_{fbk}}{1k} \\
 R_{fbk} &= 10.7k\Omega \approx 10k\Omega
 \end{aligned}
 \tag{Equation 32}$$

Using a $10k\Omega$ feedback resistor will allow -16.5A to + 16.5A to be scaled to 0-3.3V respectively.

An OPA2374 op-amp is used as the third current amplifier and is set to mimic the internal amplifiers of the DRV8301. A gain of 10 is set with a reference voltage of 1.65V (using a voltage follower as discussed).

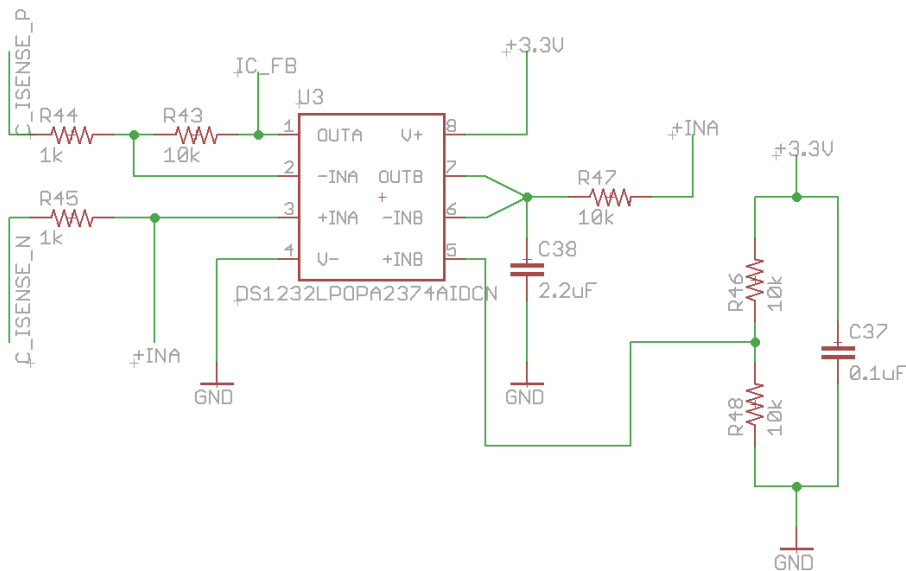


Figure 39. OPA2374 External Amplifier

As stated previously, the shunt resistors must be capable of sinking the entire phase-ground current. This means 10A continuous (RMS), 14A peak and scaled for 16.5A. There is much literature on the correct size and impedance of a low-side shunt resistor. The primary considerations are the required resolution and the maximum current required. With a smaller value resistor, I^2R losses are much smaller, but the result is a smaller potential difference across the resistor and therefore a lower

resolution. To achieve the greatest resolution (required as the motors produce only a small back-EMF at low speeds) possible, the largest resistor that will handle the required current should be selected:

$$P = I^2R$$

$$P = 16.5^2 * 0.01$$

$$P = 2.7W \approx 3W$$

Equation 33

A 3W 0.01R resistor was used in a 2512 package was chosen to ensure that no thermal limits will be reached even under prolonged heavy load use.

5.3.4 Voltage Sense

Phase voltage feedback is a prerequisite for the FAST observer with bus voltage feedback being optional but enabling InstaSPIN's™ DC bus compensation feature. As such, the custom motor controller provides voltage feedback for all three phases as well as DC bus voltage feedback. Voltage feedback is accomplished using precision voltage dividers as can be seen in Figure 40 below.

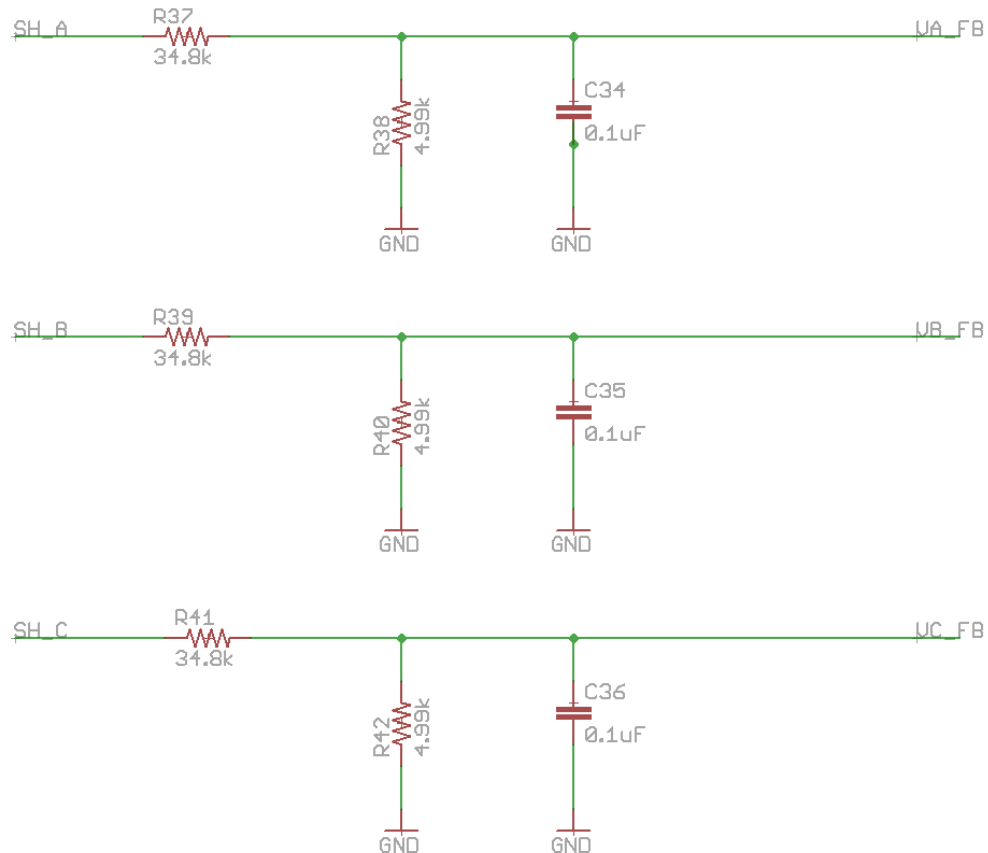


Figure 40. Bus and Phase Feedback Voltage Dividers.

The output of the voltage dividers shown in Figure 40 above for the designed maximum bus voltage, 24V, is:

$$\begin{aligned}
 VA_{FB} &= \frac{R_{38}}{R_{37} + R_{38}} SH_A \\
 &= \frac{4.99k}{34.8k + 4.99k} 24 \\
 &= 3.01V
 \end{aligned}
 \tag{Equation 34}$$

And, with the set scaling, software scaling (see section 5.3.9 - InstaSPIN™-FOC User Configuration) needs to be set to:

$$\begin{aligned}
 VA_{FB} &= \frac{R_{38}}{R_{37} + R_{38}} SH_A \\
 3.3V &= \frac{4.99k}{34.8k + 4.99k} SH_A \\
 SH_A &= 26.314V
 \end{aligned}
 \tag{Equation 35}$$

Figure 40, Equation 34 and Equation 35 above show the operation of the voltage dividers used for phase voltage feedback. Bus voltage feedback is obtained in an identical manner. Capacitors C_{34} , C_{35} and C_{36} shown in the figure above (as well as C_{23} (see Appendix I)) are used to form the low pass filter. The pole location for these low-pass filters are used by InstaSPIN-FOC and can be calculated as shown in Equation 36 below.

$$\begin{aligned}
 f_c &= \frac{1}{2\pi RC} \\
 &= \frac{1}{2\pi \left(\frac{1}{4.99k} + \frac{1}{34.8k} \right)^{-1} * 0.1\mu} \\
 &= 364.68Hz
 \end{aligned}
 \tag{Equation 36}$$

5.3.5 Switching Devices (MOSFETs)

Six TI CSD18533Q5A NexFETs™ were used for the power inverter. These are N channel Power MOSFETs ($<6.5m\Omega$) in a SON5*6(mm) package and were chosen simply because this is what is used in the BOOSTXL-DRV8301. This decision was made to minimise development time while maximising the chances of the controller functioning as intended. The power inverter may be seen in Figure 40 in the section immediately above.

The CSD18533Q5A NexFETs™ were initially only intended for use in Revision 2 controllers and a more capable (higher current rating) inverter was designed using BSC016N04LS G FETs by Infineon to be utilised on Revision 3 boards. A complete power stage update was designed, including the necessary changes required to the phase current feedback circuitry. However, due to longer than expected Revision 2 build times, revision 3 boards were never fabricated.

5.3.6 Miscellaneous

Power for the control electronics was provided by the isolated internal buck regulator included in the DRV8301 pre-driver. The buck is capable of supplying 1.5A to external loads, more than enough for the MCU, Op-amps, JTAG and other control electronics used.

High Performance Brushless DC Motor Control

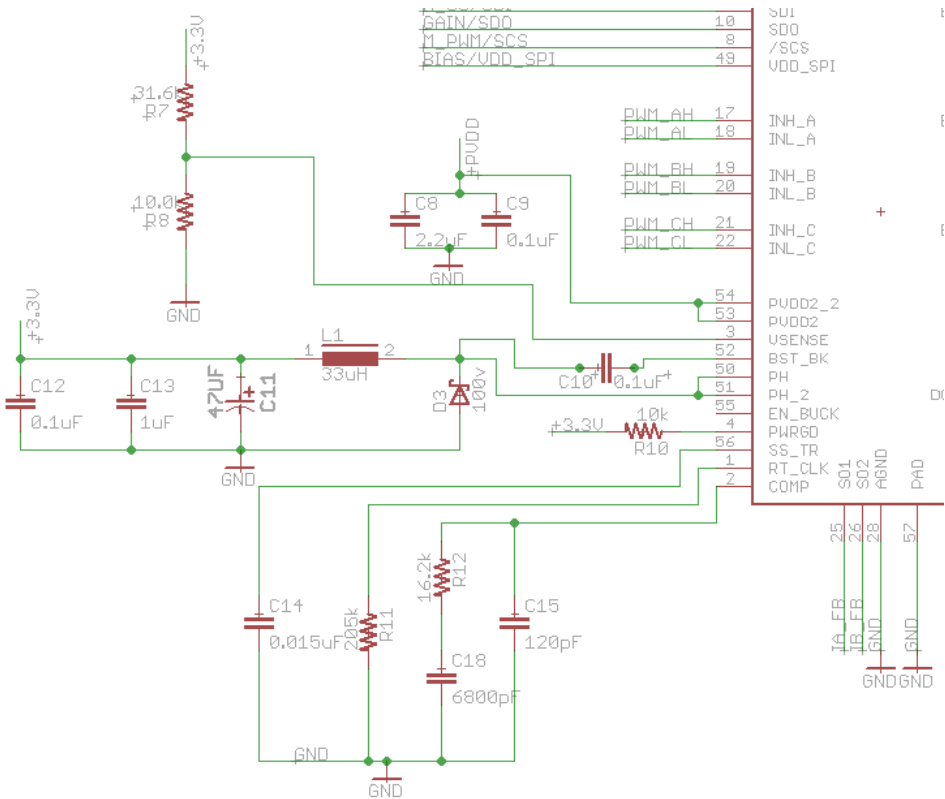


Figure 41. DRV8301 Buck Converter

The output voltage is adjusted using a precision divider from the output node to VSENSE. In this case, all control electronics require 3.3V:

$$\begin{aligned}
 R_1 &= R_2 \left(\frac{(V_{OUT} - 0.8V)}{0.8V} \right) \\
 &= 10k \left(\frac{(3.3V - 0.8V)}{0.8V} \right) \\
 R_1 &= 31.25k\Omega
 \end{aligned}
 \tag{Equation 37}$$

where 0.8V is the chip-set reference voltage.

A 31.6kΩ resistor was used to complete the voltage divider, giving a theoretical output voltage of 3.328V ~3.3V. Values for the buck converter capacitor C11, Inductor L1 and catch Diode D3 were taken directly from the DRV8301 application note. This could be reviewed, and components sized for this specific application, but no performance issues were identified during testing. The Buck switching frequency is determined by the external timing resistor R₁₁, in this case 570kHz, again, this value was simply taken from the device application note.

The board has many other features, including PNP transistors (Q₁, Q₂) used to turn LEDs (1, 2) on to indicate active low faults reported by the DRV8301, large SMD bus capacitors (C₂₀, C₂₁) for supply filtering, transient voltage suppression IC (U₂) and several more secondary systems components.

5.3.7 PCB Layout

As can be seen in Figure 52 below, several versions of the custom FOC controller were designed and fabricated. All versions of the custom FOC controller were designed in Eagle CAD by *CadSoft* and were routed by ‘hand’. That is, the auto-router available in Eagle was not used as initial testing showed less than optimal results. In addition, every revision of the board went through multiple iterations in order to achieve good component placement and optimal signal routing. Figure 42 immediately below shows the custom FOC controller (revision 2C) Eagle CAD board layout. *Note, all dimensions are in mm.*

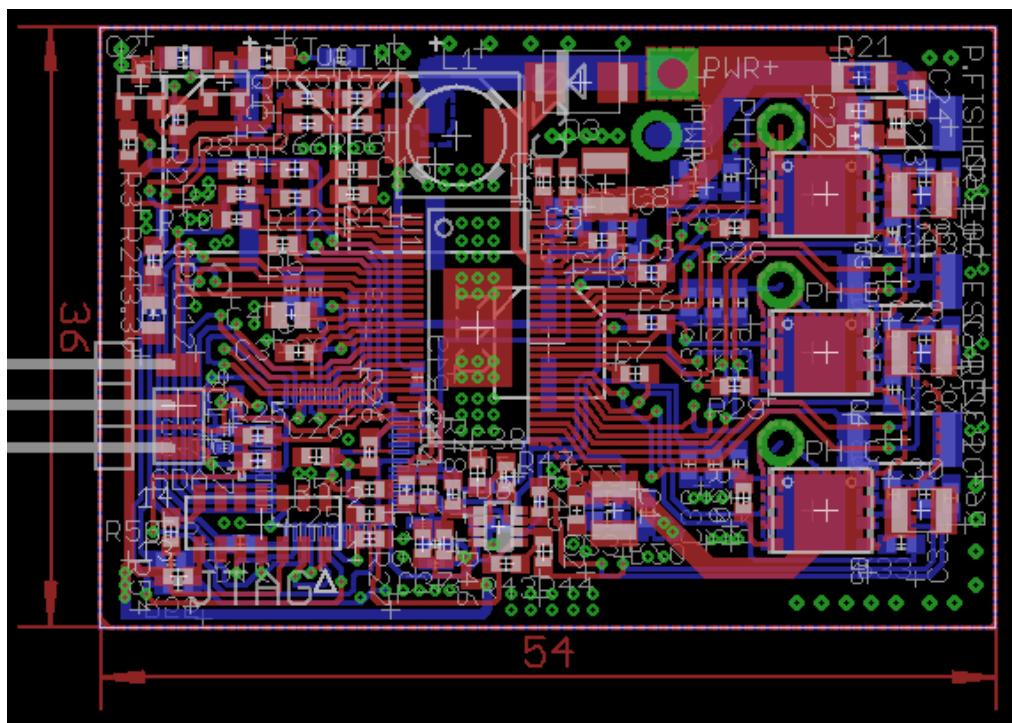
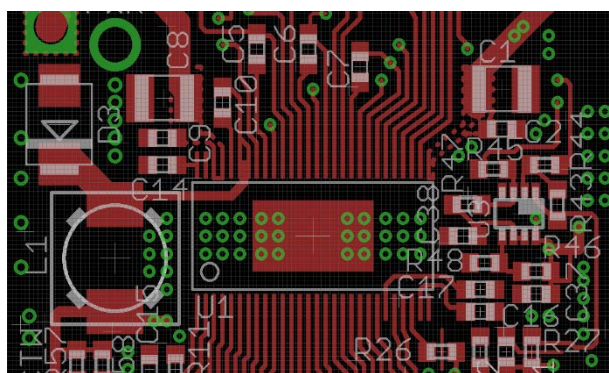


Figure 42. Custom FOC controller (Revision 2C) PCB layout.

DRV8301 Pre-Driver

A custom footprint was developed in Eagle CAD for the DRV8301, this was verified on the *footprint test board*. The DRV8301 datasheet outlines several criteria for the DRV8301 pre-driver and



associated components regarding how they should be laid out on the PCB. These criteria include the placement of C_1 , C_2 , C_4 , C_8 , C_0 , C_{16} and C_{17} which should be placed as close to their corresponding pins as possible with a low impedance path to the device. The placement

Figure 43. DRV8301 Pre-Driver and Associated Components (Revision 2C).

of these components (for revision 2C) may be seen in Figure 43 to the left.

Figure 43 also shows several (30*0.3mm) vias placed directly on or immediately beside a large landing area. This was done to accommodate the power pad on the bottom of the DRV8301 as recommended in the device datasheet.

The power pad serves as the only ground pin for the device and often must dissipate substantial amounts of heat energy, this is the reason for the large number of vias located under the power pad. This was a major problem with initial prototyping of the boards as the mill at CQU only supported large vias (0.6mm minimum) and does not support through-plating. This meant that any thermal advantage gained by adding vias under the power pad was lost. This fact was simply ignored for earlier prototypes as one of the ultimate goals of the project was to have a PCB professionally fabricated, which would allow 0.3mm vias to be through-plated. However, this limitation did mean that overly-long high current runs were avoided with prototypes developed using CQU's mill. The prototype (revision 2A) was still able to reach its 10A continuous (RMS) current rating.

TMS320F28027F Microcontroller

It was also necessary to create a custom footprint for the F28027F microcontroller used. The microcontroller placement was largely a result of board minimisation and was actually moved to the bottom side of the custom FOC Controller from revision 2 onwards. This can be seen in Figure 45 to the left. Figure 45 also shows several vias placed immediately beneath where the microcontroller is seated. While most of these are simply stitching for the ground plane, some are connecting top and bottom layer signals. This was not possible on any of the prototypes milled at CQU because the vias had to be manually joined (top to bottom) which created an uneven landing surface for the device. The ability to have through plated Vias beneath components allowed the board size to be further reduced from revision 2B (and earlier) to revision 2C.

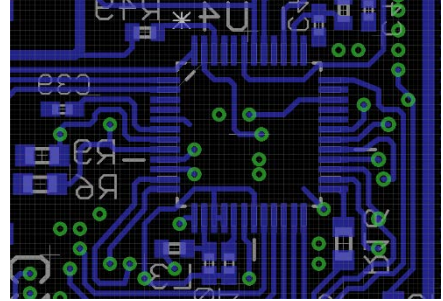


Figure 45. F28027F MCU Placement (Revision 2C).

microcontroller placement was largely a result of board minimisation and was actually moved to the bottom side of the custom FOC Controller from revision 2 onwards. This can be seen in Figure 45 to the left. Figure 45 also shows several vias placed immediately beneath where the microcontroller is seated. While most of these are simply stitching for the ground plane, some are connecting top and bottom layer signals. This was not possible on any of the prototypes milled at CQU because the vias had to be manually joined (top to bottom) which created an uneven landing surface for the device. The ability to have through plated Vias beneath components allowed the board size to be further reduced from revision 2B (and earlier) to revision 2C.

CSD18533Q5A MOSFETs and Sense Resistors

A custom footprint was also required for the power MOSFETs used. This can be seen in Figure 46 below. A large exposed pad can be seen on each of the FET landing areas, this is because TI's

NexFET™ incorporates a PowerPad™ not dissimilar to that of the DRV8301 pre-driver. Vias could be placed on the PowerPad landing area to increase thermal dissipation

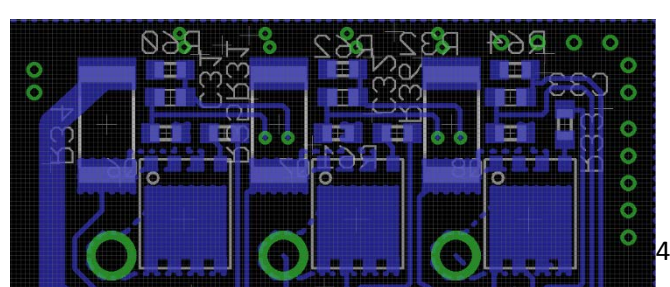


Figure 46. Low Side MOSFET Placement (Revision 2C).

(see DRV8301), but, in this case the layout did not allow for it. Board revision 1 (see Figure 52) did utilise vias on the PowerPAD™ landing area but this design did not allow the MOSFETs to be placed on opposite sides of the board (as in later revisions) which meant that a significantly larger overall board size was required.

The current shunt resistors (R_{34} , R_{35} and R_{36}) can also be seen in Figure 46. These resistors must be capable of sinking the entire phase current flowing from the low side MOSFET through to ground. The ground side of these resistors is grounded using the 'main' ground polygon (plane). Ordinarily,

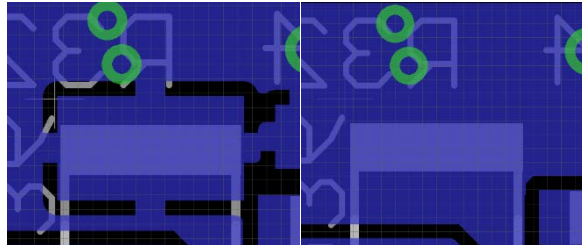


Figure 47. R_{36} With (Left) and Without (Right) Thermal Relief.

thermal relief (see Figure 47 - left) is added by default when the ground polygon is created. This is so that components can be more easily soldered (copper plane acts as a heat sink making soldering difficult), but this also increases the effective impedance to ground, effectively limiting the power rating of the components. The same current must also flow through the side of the

current shunt resistors connected to the low side MOSFET drain. This means that thermal relief cannot be applied on either side of the current shunt resistors. From Revision 2 onwards, no thermal relief was applied to these resistors, and, large copper planes (created using polygons) are used to connect all high current devices. In addition, the shunt resistors were placed immediately beside the low side MOSFET (see Figure 46) to ensure a minimum impedance path.

Differential, Power and Ground Traces

There are several differential signals required for the custom FOC controller. These signals are used for current feedback and run directly from the high and low sides of the shunt resistors to their respective op-amps, DRV8301 for phases A and B and an external op-amp for phase C. R_{59} to R_{64} (See Appendix I - *FOC Speed Controller Full Schematic (4/5)*) are 0Ω jumper resistors used to allow Eagle CAD to treat the signals as true differential signals. These resistors are only required because Eagle does not support joining nets and does not directly support a ground differential trace. Having the signals recognised as differential by Eagle allows the use of Eagle's differential signal router. This essentially routes the two differential signals simultaneously to minimise any difference in signal length, an important factor for differential signals. Figure 48 below shows the differential signals and the lengths of the traces.

Eagle: Wire length of Layout
EAGLE Version 6.4.0 Copyright (c) 1988-2013 CadSoft
List of signals with length and its max. frequency / current
exported from C:/Users/Patrick/Documents/eagle/FOC_ESC/ESC_Schematic.brd
at 9/05/2014 8:04:00 PM

Cu thickness = 0.035 mm

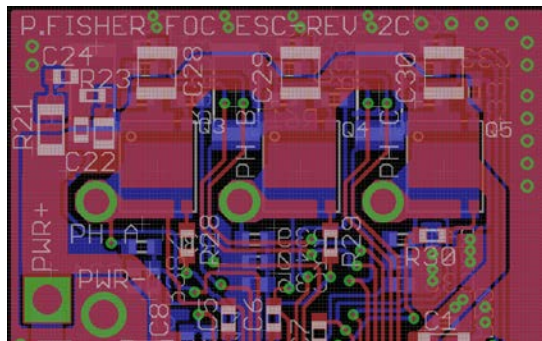
Signal	f max. [MHz]	l [mm]	A [mm ²]	R [mOhm]	w min [mm]	w max [mm]	I _{max} [A]
+3.3V	1592.52	188.255	0.009	368.46	0.254	0.610	0.80
+INA	77726.65	3.857	0.009	7.55	0.254	0.254	0.80
+PVDD	4201.06	71.363	0.005	232.79	0.152	3.048	0.50
A_ISENSE_N	7132.40	42.034	0.009	82.27	0.254	0.254	0.80
A_ISENSE_P	6983.95	42.927	0.009	84.02	0.254	0.254	0.80
B_ISENSE_N	9080.84	33.015	0.007	80.77	0.203	0.254	0.65
B_ISENSE_P	8976.36	33.399	0.007	81.71	0.203	0.254	0.65
BIAS/VDD_SPI	28365.56	10.569	0.009	20.69	0.254	0.254	0.80
C_ISENSE_N	8737.62	34.311	0.007	83.95	0.203	0.254	0.65
C_ISENSE_P	8817.84	33.999	0.009	66.55	0.254	0.254	0.80

Save Close

Figure 48. Differential Signal Parameters.

Note, in Figure 48 above, it appears as though multiple width traces are used for the differential signals. This is not the case. The differential signal was increased from 0.203mm to 0.254mm and some sections of 0.203mm trace still exist under component pads. There is no physical trace of copper that is less than 0.254mm on the custom FOC controller PCB.

High current carrying traces must be designed properly to ensure the controller will perform as expected. The custom FOC controller has several high current traces supplying the three-phase



board (in all design revisions) to minimise the chances of transients entering signal traces. This also allows for maximum width traces to be used without resulting in an overly-large board. Additionally, it allows for a much greater ground plane to be applied as it (the ground plane) is not interspersed with small passive components (resistors, capacitors, etc) which limit the amount of ground plane copper. Figure 49 above shows 2mm (drill) vias used for the main ground and power lines. These also serve to connect the top and bottom power and ground plane as was done for the phase outputs. No thermal relieve is applied to the main power and ground connections for the reasons discussed above. This did make soldering particularly difficult as there was a substantial amount of copper on both the top and bottom layers of the power and ground connection (which acts like a heat sink).

Additionally, great care was taken to ensure that no high impedance ground loops existed in the board design (particularly for revision 2 onwards). It can be seen in Figure 42, that for almost every grounded component, there are several paths for ground currents to flow and none are particularly lengthy or high impedance (i.e. trace width is significant). The grounding design has been validated in that no issues that arose during testing were discovered to be related to poor ground design.

Placement Sensitive Components

In addition to placement critical components already discussed, there are several voltage divider

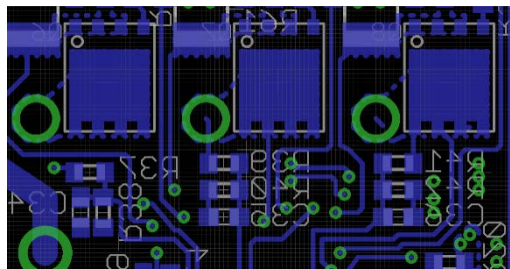


Figure 50. Phase Voltage Sense Dividers.

components whose placement on the board was a significant design choice. Phase voltage sense resistors (R_{37} to R_{43}) and capacitors (C_{34} to C_{36}) can be seen immediately below their respective phase output in Figure 50 to the left. The traces to the ADC were kept as short as possible in an effort to minimise any noise pick up. The traces were also intentionally routed away from any inductors for this reason. These lines also must run across a transient suppression IC (U2). The placement of

this IC (U2) was not critical and was made such that the track length from the voltage dividers to the MCU was as short and direct as possible.

There are several other placement sensitive components on the custom FOC controller board. Notably, a large inductor, L_1 , used for the buck converter, bus capacitors C_{11} , C_{21} and C_{22} and a shottky diode D_3 used for the buck converter. Care was taken to ensure that these components were effectively placed. For example, L_1 was not placed above any noise sensitive signals to minimise noise injection from this component. In addition, components were grouped according to the schematic. This allows for a more compact board design and minimises the number of lengthy traces on the board.

JTAG Header

One of the most significant secondary elements is JTAG, and more specifically, the header used. The

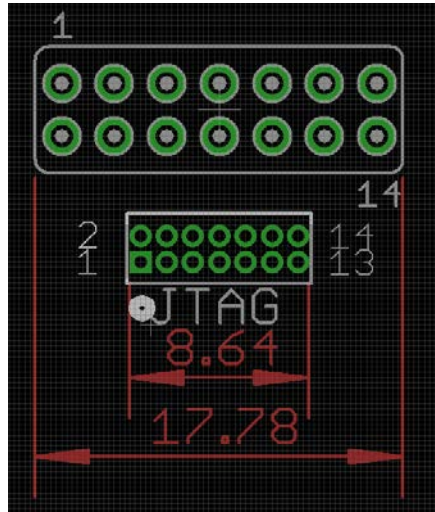


Figure 51. 2.54mm and SAMTEC Headers.

controller board.

JTAG header used prior to revision 2C was a standard 2.54mm double row male header. This header took up a substantial amount of board space and it was deemed necessary to either remove it completely or replace it with a much smaller option. Given the nature of the project and its potentially experimental uses, it was decided that the JTAG header should remain on all revisions of the board. A micro header by SAMTEC was found with a substantially reduced footprint, this can be seen in comparison to a standard 2.54mm header in Figure 51 to the left. The micro header by SAMTEC is also surface mount (as opposed to through-hole) which allowed the header to be placed immediately above (opposite side) the MCU. This was not possible with through-hole headers and allowed a further reduction in the size of the custom FOC

5.3.8 Prototyping

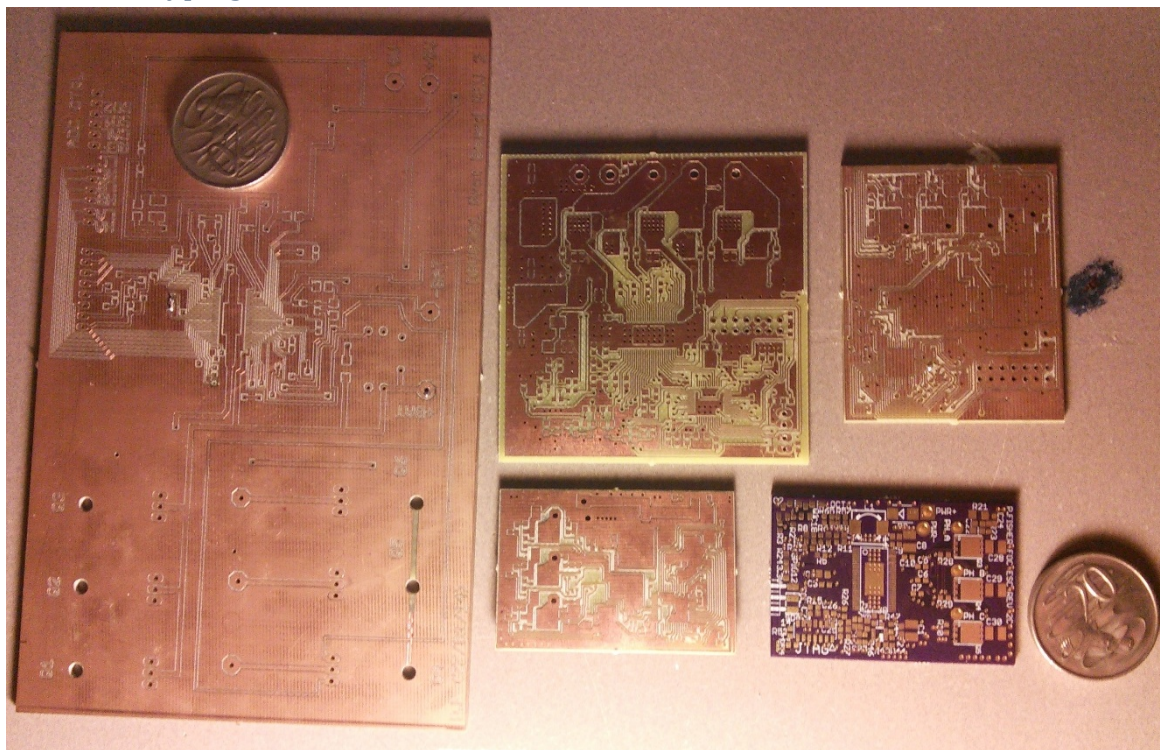


Figure 52. Custom Motor Controller Unpopulated Boards.

Figure 52 starting from left (largest board) and moving clockwise;

- Footprint test board;
 - Used to verify several custom footprints including the DRV8301 pre-driver;
- Revision 1;
 - Never populated;

- Revision 2A;
 - Fully populated and successfully tested;
- Revision 2B;
 - Never populated;
- Revision 2C;
 - Fully populated and successfully tested.

5.3.8.1 *Unpopulated Prototype Boards*

The first and largest PCB that can be seen in Figure 52 above was used to assess the performance of the CNC mill at CQU and verify some of the custom footprints created (primarily the DRV8301). The DRV8301 landing area which can be seen clearly in the figure has several 8mil traces extending from it. The 8mil traces were found to be broken in several locations by the Mill. In response, all 8mil traces were increased to 10mil width which allowed the mill to route the circuit perfectly. This change is present in all revisions of the custom controller, traces for revision 2C onwards could be changed back to 8mil if necessary, provided they are professionally fabricated. In addition to discovering the limitation of the mill at CQU, the footprint developed for the DRV8301 (and some secondary components) was verified.

Revision 1 was initially intended to be populated and tested. However, while waiting for parts to arrive, several non-critical PCB design issues were discovered. The most significant design flaw was the poor differential signal routing and the landing areas for the power supply leads. The differential signals were routed (not in pairs as in revision 2 onwards) unevenly and had unnecessarily long traces. The power pads (which can be seen at the top left) had only very small copper landing areas and the width of the traces to the power inverter were arbitrarily chosen and too small for the required current. A decision was made to address these issues and re-mill the board before attempting to populate any boards. This resulted in significant board changes, for example, half of the three-phase inverter was moved to the bottom side of the PCB, the 0Ω jumper resistors were added to allow for true differential routing and many other general design improvements were made. The new board was designated revision 2A which was the first prototype to be successfully tested.

High Performance Brushless DC Motor Control

5.3.8.2 Revision 2A

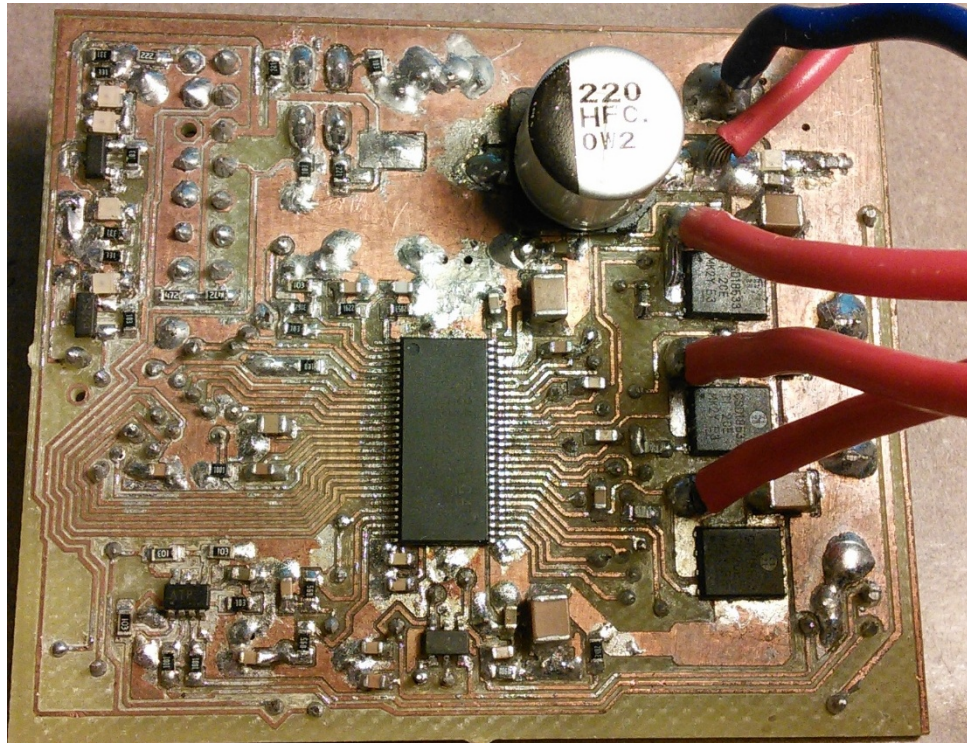


Figure 53. Custom FOC Controller Revision 2A Top Side.

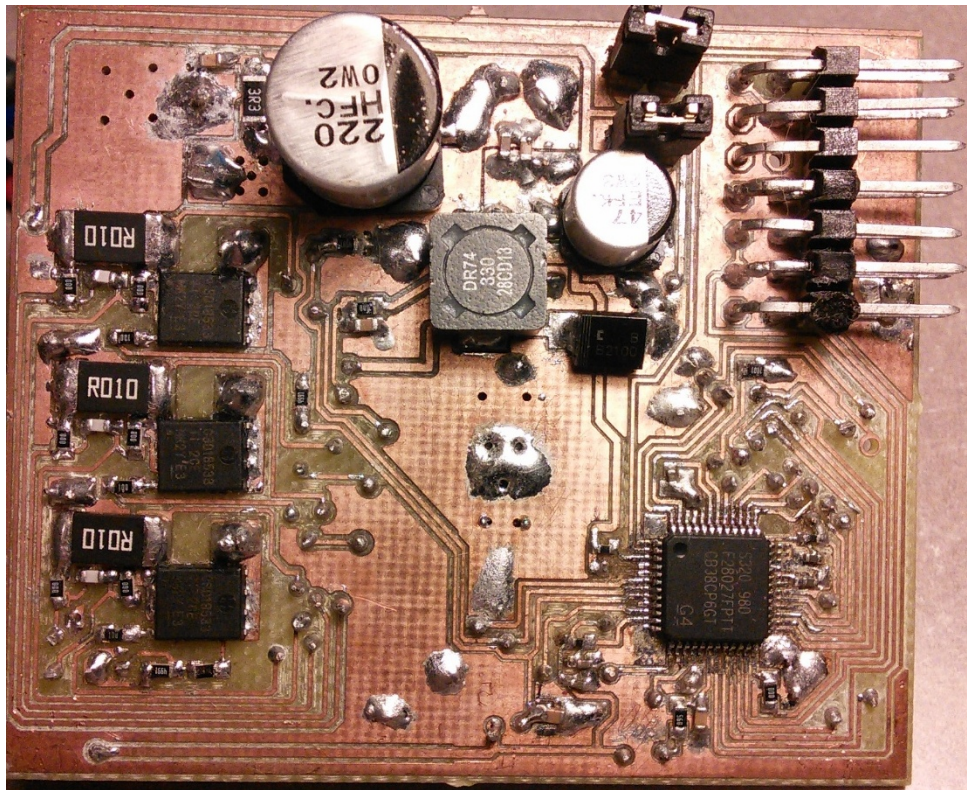


Figure 54. Custom FOC Controller Revision 2A Bottom Side.

Revision 2A was the first revision of the Custom FOC Controller to be fully populated and tested. This board was fabricated using the mill at CQU without issue. However, using the mill at CQU did mean that the board had no solder mask or silk screen and all vias had to be joined manually. Components were placed with continual reference to the Eagle board layout and were methodically marked off a list once placed. In addition, due to the lack of solder mask, great care was taken to avoid bridging components and traces.

The DRV8301, MOSFETs and microcontroller were soldered using solder paste and hot air. All other components were hand placed and soldered. The shunt resistors proved difficult to solder due to the large copper planes, connecting the low side MOSFET and the current sense resistor, acting like a heat sink. Because several small (0603) passive devices were already mounted around the shunt resistor, hot air could not be used (0603 devices would likely fall off) and instead, a large chisel tip iron was used to heat up the entire copper plane.

A decision was made to populate the board in sections in an attempt to maximise the chances of success. The first ‘section’ to be populated was the DRV8301 pre-driver and associated buck converter components. This was done so that the 3.3V output could be tested before potentially damaging the voltage sensitive microcontroller. The first test on this section was unsuccessful as it was found that the buck converter was regulating at 5.65V and not the required 3.3V. After verifying the buck converter passive component values were correct, the chip was removed with hot air and it was found that the PowerPad™ was not soldered to the ground plane. This resulted in the ground floating up ($\sim 0.5V$) resulting in a high reference voltage and subsequently the high output voltage. After reviewing the reflow profile found in the device datasheet, it was found that temperatures initially used were not high enough. This was adjusted and upon re-testing, the buck converter was regulating at the desired voltage.

The next ‘section’ to be populated was the microcontroller and associated components (including JTAG). No problems were encountered and the operation of the microcontroller was verified by writing a small program to oscillate some GPIOs from high to low.

Finally, the MOSFETs and all remaining components were placed on the board. At this point, InstaSPIN was tried, unsuccessfully. However, no fault was reported by either the DRV8301 (active low output) or the microcontroller and InstaSPIN appeared to be running. It was found that the DRV8301 was not responding to PWM signals from the microcontroller and that it had locked the MOSFETs in a high impedance state. All feedback signals (to the DRV8301) were checked and verified and the fault output was investigated to see why an apparent fault was not being flagged. A solder bridge was found which connected a via on the fault line to the main +3.3V line. When this was cleared, InstaSPIN responded to the fault (entering a CTRL Fault state) and the red fault LED was illuminated. Several days were spent troubleshooting the controller (checking all signals that could result in a fault being reported by the DRV8301) but no issues were discovered. The DRV8301 was replaced and the top layer of the board was reflowed. This resulted in the controller successfully spinning and even identifying the troublesome PropDrive BLDC motor! Whether the DRV8301 was faulty from multiple reflows and a fault line short circuit or a solder bridge was cleared when the top-layer was reflowed remains unclear.

Revision 2A was tested up to its design rating of 10A continuous and was also able to identify several BLDC motors (which the development board was not able to do). The controller was also able to

High Performance Brushless DC Motor Control

commute BLDC motors at considerably lower speeds (~100RPMs) than had been possible during the initial evaluation. Notwithstanding the considerable time taken to achieve a fully-functional controller (two weeks), the prototype board was considered a success and work began on a revision of the PCB to be professionally fabricated.

5.3.8.2 Revision 2C

Revision 2C of the custom FOC Controller may be seen fully populated in the photographs below.

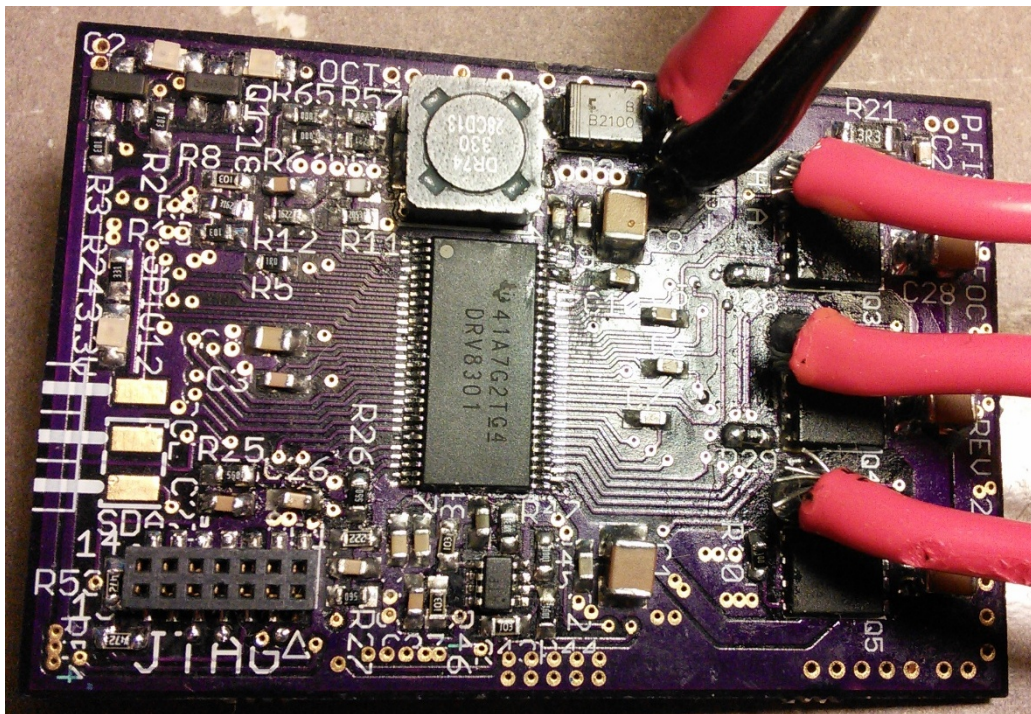


Figure 55. Custom Controller Revision 2C Top Side.

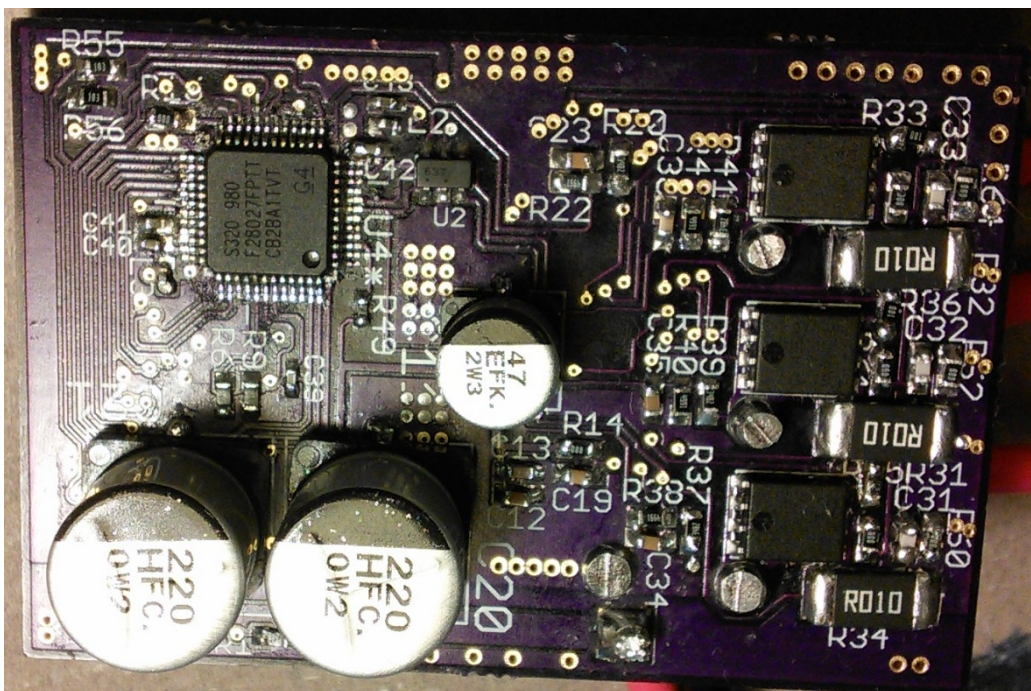


Figure 56. Custom Controller Revision 2C Bottom Side.

Revision 2C of the Custom FOC Controller required no major circuit changes from revision 2A. Some secondary system components, most noticeably the JTAG header, were changed but the fundamental operation of the controller remained unchanged. The major changes from revisions 2A to 2C were, differential signal routing optimisation, some component repositioning, JTAG header minimisation and a professionally fabricated PCB.

In contrast to Revision 2A, Revision 2C was fully populated (4hrs) before any power was applied. At this point, the output of the buck converter was verified at 3.3V and the microcontroller was successfully tested by running a JTAG integrity test. InstaSPIN – FOC was then loaded and tested at which point a fault was reported. Checking the SPI registers, it was found that the fault was related to the power inverter, and by looking into this, the fault was found to be a result of the gates of the transistors not being soldered to their respective pads correctly. This was most likely a result of mistakenly not applying solder paste to the gate pin or pad. With this issue fixed, the board was able to identify and spin motors. For a full breakdown of capability of the custom FOC controller, see chapter 6 *Results and Discussion*.

5.3.9 InstaSPIN™-FOC User Configuration

All InstaSPIN™-FOC user configuration is done in a single header, *user.h*. This header allows InstaSPIN to be highly configurable and everything from identification ramp times to maximum bus current to PWM frequency and everything in between is set here. The correct configuration of user parameters, located primarily in *user.h*, is critical to the performance of the controller and requires a great deal of consideration. Configuring *user.h* for the Custom FOC Controller proved to be a somewhat experimental process and the *user.h* header was continually evaluated and updated throughout the entire course of the research. Experience gained with the TI development board initially was invaluable and dramatically decreased the time required to correctly configure the *user.h* file for the custom FOC controller.

The full user.h header that was used may be seen in Appendix III.

5.3.9.1 Software Execution Timing

The F28027F microcontroller has a maximum clock speed of 60MHz, driven by the internal crystal (10MHz) and a phased-locked loop (PLL). The Custom FOC Controller was clocked at this speed by **#define USER_SYSTEM_FREQ_MHz (60.0)**.

InstaSPIN-FOC operates around a main interrupt service routine triggered at a configurable frequency, f_{ISR} . This frequency is decimated further to run particular control elements. **USER_NUM_ISR_TICKS_PER_CTRL_TICK** is the first decimation factor seen in *user.h* and decimates the interrupt frequency to create an execution frequency for the top-level controller. This was set to (1), meaning that the controller clock rate is the same as the PWM frequency. The next decimation factor is **USER_NUM_CTRL_TICKS_PER_CURRENT_TICK**, this sets the execution frequency for the current controllers by the equation that follows:

$$f_{CURRENT} = \frac{1}{numCtrlTicksPerCurrentTic} * \frac{1}{numIsrTicksPerCtrlTic} * f_{ISR} \quad \text{Equation 38}$$

USER_NUM_CTRL_TICKS_PER_CURRENT_TICK was set to (1), from Equation 38, this sets $f_{CURRENT}$ to the main interrupt service routine frequency, f_{ISR} .

Similarly, ***USER_NUM_CTRL_TICKS_PER_SPEED_TICK***, is used to set the execution frequency for the speed controller, this was set to (10) in order to best match the PWM frequency. f_{SPEED} is set as per Equation 38 with the exception that *numCtrlTicksPerCurrentTic* is changed to ***USER_NUM_CTRL_TICKS_PER_SPEED_TICK***.

The next decimation factor is ***USER_NUM_CTRL_TICKS_PER_EST_TICK***, this decimates the top-level controller frequency to create an execution frequency for the estimator. This was set to (1), meaning the estimator frequency, f_{EST} is set to the main interrupt service routine, f_{ISR} .

Finally, a decimation for the trajectory generator, ***USER_NUM_CTRL_TICKS_PER_TRAJ_TICK***, must be set. This was set to (10) and the frequency f_{TRAJ} is set by making the established alteration to Equation 38 as shown for f_{SPEED} .

The PWM frequency generated is one of the most critical user set parameters within *user.h*. This is set by **#define USER_PWM_FREQ_kHz**, in this case to (45). This is above TIs recommended setting of (30) but was found to work well with small hobby BLDC motors. Figure 57 below shows the phase-ground waveform for the custom FOC controller.

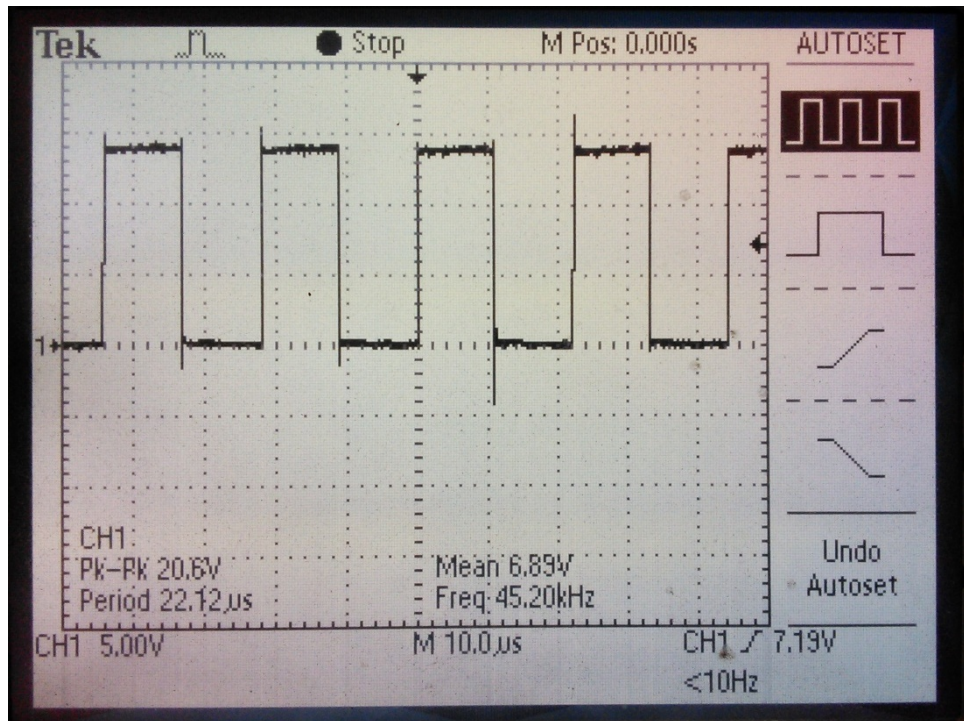


Figure 57. Phase-Gnd Waveform: Custom FOC Controller.

This waveform is repeated for the remaining two phases. The 45kHz PWM is further ‘modulated’ depending on the torque or speed set-point to achieve the required rotating stator flux (these are synchronous motors – no slip). An attempt was made to capture the ‘modulation’ (considerably slower than 45kHz) signal using fast Fourier transforms on an oscilloscope but was unsuccessful.

5.3.9.2 InstaSPIN-FOC Hardware Parameters

There are several hardware parameters that are required for InstaSPIN-FOC to operate correctly on the Custom FOC Controller.

USER_IQ_FULL_SCALE_FREQ_Hz defines the full scale frequency for the IQ variable in Hz. This parameter must be set larger than the maximum speed expected from the motor. This was initially set to (800) by default (TI) but was changed to (**4 * USER_VOLTAGE_FILTER_POLE_Hz**) to allow for the Kv (thousands RPM Volt) rating of all motors evaluated to be tested. **USER_VOLTAGE_FILTER_POLE_Hz** is set to (364.68), this is the voltage filter pole and is explained in section 5.3.4 Voltage Sense above. Additionally, the number of voltage and current sensors can be set directly in *user.h* - **#define USER_NUM_CURRENT_SENSORS, #define USER_NUM_VOLTAGE_SENSORS**. These are both set to (3) for obvious reasons.

Full scale voltage and current feedback is required to be set in *user.h*. This relates to the scaling discussed in section 5.3.3 Current Sense, namely, what a full (or empty) ADC result register indicates in terms of phase voltage or current. In this case, a 0V (0x00;) reading signifies -16.5A and a +3.3V (0xFF;) reading signifies a +16.5A reading for phase current feedback. Hence, **#define USER_ADC_FULL_SCALE_CURRENT_A**, is set to (33). Additionally, the parameter **USER_IQ_FULL_SCALE_CURRENT_A** set to (20) to reflect the 10A (bidirectional) soft limit of the custom FOC controller, this limit can be set to whatever limit is required, for instance, if it was desired that the board supplied no more than 6A (RMS) continuous, this parameter would be set to (12). Likewise, the maximum feedback voltage must be set for correct scaling. From a hardware perspective these settings are discussed in section 5.3.4 Voltage Sense. Hence, **#define USER_ADC_FULL_SCALE_VOLTAGE_V** was set to (26.314). Finally, the full scale voltage for the custom FOC controller was set to (24) by **#define USER_IQ_FULL_SCALE_VOLTAGE_V**. Like the full scale current, this parameter can be set to any value (<26.314) if it is known that the voltages will not exceed the set value. For example, when testing the Custom FOC Controller, this was set to (16) such that the absolute maximum resolution was achieved. If either the phase of bus voltage exceeds this value, the register will overflow resulting in a destructively inaccurate reading (and, obviously poor performance).

5.3.9.3 InstaSPIN-FOC Motor Parameters and ID Settings

A user motor is added to InstaSPIN by the following declaration **#define USER_MOTOR My_Motor**, the following parameters can then be set in **#elif (USER_MOTOR USER_MOTOR == My_Motor)**:

#define USER_MOTOR_TYPE

This defines the type of motors, in this case, this parameter is set to *MOTOR_Type_Pm* to reflect that the motors are synchronous permanent magnet motors. Theoretically, there is no reason why the board (as is) could not be used to drive (very small) asynchronous induction motors, in which case the parameter would be set to *MOTOR_Type_Induction*.

#define USER_MOTOR_NUM_POLE_PAIRS

This parameter is used to calculate rotor speed and is simply the number of poles (permanent magnets) divided by two. Motors with 2 pole pairs all the way up to 11 pole pairs have been used with the Custom FOC Controller.

#define USER_MOTOR_Rr

This is the rotor coil resistance, identifiable, but not used for the Custom FOC Controller (there are no rotor coils), hence it was set (Null).

#define USER_MOTOR_Rs

This is the identified phase-neutral winding resistance for star equivalent circuits in Ohms. This is unique for every motor and can only be populated after identification has been run or with a datasheet value.

#define USER_MOTOR_Ls_d

For the BLDC motors used, this is the average stator inductances in Henrys. This parameter is slightly different for induction motors. Again, this value is found using InstaSPIN's ID routines.

#define USER_MOTOR_Ls_q

For the BLDC motors used, this is identical to the **#define USER_MOTOR_Ls_d** explained above. Hence, the two values are always identical.

#define USER_MOTOR_RATED_FLUX

This is the total flux linkage between the rotor and the stator in Webers (Volts*Seconds) and is found by automatic identification.

#define USER_MOTOR_MAGNETIZING_CURRENT

Not applicable for BLDC motors, set (Null).

#define USER_MOTOR_RES_EST_CURRENT

This is the maximum current used for Rs identification. This is user set, typically to about 10-20% of the rated motor current.

#define USER_MOTOR_IND_EST_CURRENT

This is the maximum current used for Ls identification. This is user set, ideally, just enough to make the rotor turn (experimental).

#define USER_MOTOR_MAX_CURRENT

This sets the maximum current command output of the speed PI controller to the torque PI controller during run-time and ID.

#define USER_MOTOR_FLUX_EST_FREQ_Hz

This is used during motor ID and sets the maximum commanded speed (during ID), recommended 10% of rated motor speed in Hz.

5.9.3.9 Added Abstractions

To allow the developed controller to be used with typical RC equipment, it was necessary to develop a method for responding to RC signals. RC signals are 50Hz 1-2ms high time signals which command the motor controller to increase or decrease the torque set-point. Revision 2C of the Custom FOC Controller has GPIO12 broken out for specifically this purpose. The full code for the 50Hz PWM 'read' may be seen in Appendix III but the basic principal is outlined in the pseudo code below:

1. Configure PIE for interrupt on both high and low GPIO12 transitions;
2. On low to high transition, start 32bit (60Mhz) timer;
3. On high to low transition, stop 32bit (60Mhz) timer;
4. Calculate the per-unit set-point request;
5. Check the set-point request is valid;
6. Set the commanded set-point;

The code developed has been successfully tested.

In addition to GPIO12, both SCL and SDA have been broken out (Revision 2C) such that I2C may be used instead of 50Hz PWM. This is because I2C is quite a common protocol for experimental craft that may benefit from the controller developed. In addition, I2C allows InstaSPIN data to be transmitted by the controller, this data includes rotor speed, torque and even motor temperature (all gathered sensorlessly). The benefits of this are obvious. While some I2C abstractions have been written (and can be seen in Appendix III), this work (at the time of writing) is not yet complete.

6 Results and Discussion

The performance of the custom FOC controller was evaluated using several hobby BLDC motors. Additionally, several commercial controllers from mid-high performance (Plush 40) to low-performance (HobbyKing ss) were compared with the custom motor controller.

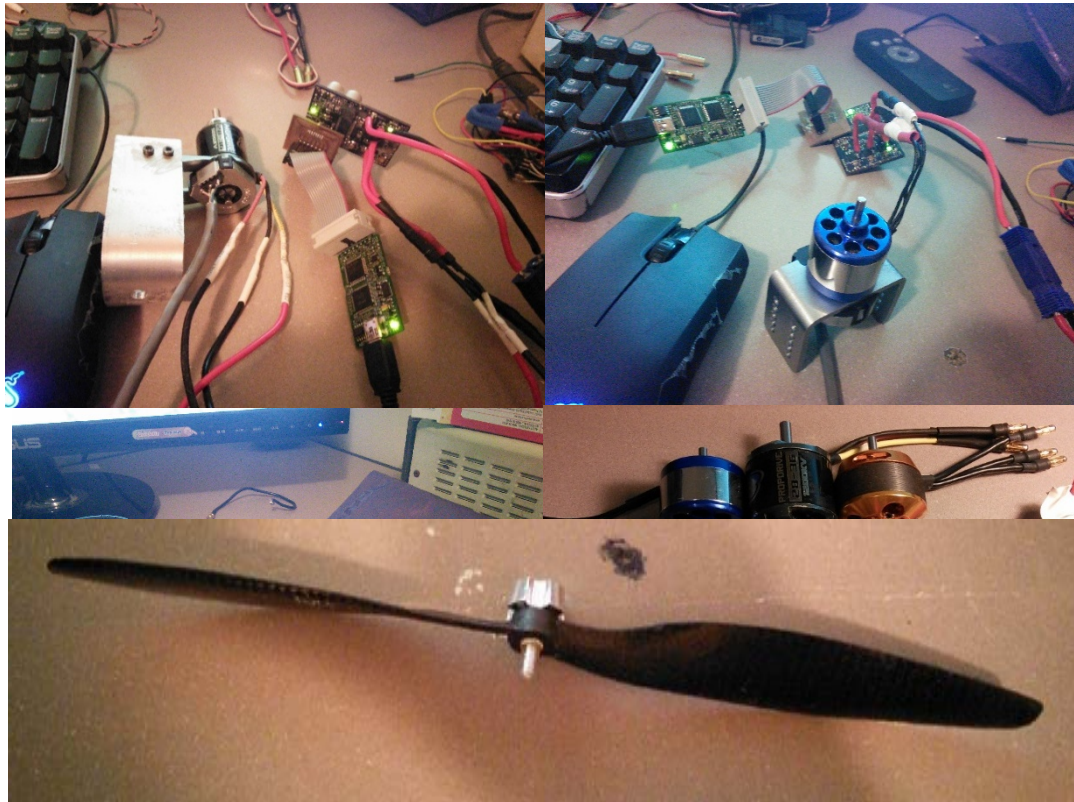


Figure 58. Evaluated Motors, Controllers and Loads.

Figure 58 starting from top-left and moving clockwise;

- PropDrive 1200Kv Outrunner Motor with Custom FOC Controller.
- 2728 1000Kv Outrunner Motor with Custom FOC Controller.
- All motors and controllers tested.
- Load: 12*4.5" model aeroplane propeller.
- Unknown motor with FOC Controller.

The rotary encoder can be seen mounted under each motor in Figure 58 above.

The data that follows has not been altered in anyway, it has merely been presented in a more coherent form than what it was collected in. In addition, while the data is not averaged at all, the tests were run several times to ensure that all results were consistent across multiple runs.

6.9 Test Motors and Controllers

Several hobby BLDC motors and electronic controllers were selected at random for evaluation. These motors and controllers are typically used for hobby and academic purposes in model helicopters, aeroplanes, boats and multicopters. A motor with no known parameters (not even the brand) was obtained to assess the capability of the controller to identify and drive a motor without any name plate data. The ‘unknown’ motor poles were simply counted (permanent magnets can be clearly seen through ventilation holes) and a continuous current rating of 10A was assumed. It is believed this is a very conservative rating given the physical size of the motor. This is the only data that is absolutely essential for the Custom FOC Controller and is always provided by the manufacturer.

Table 7 and Table 8 below show the known parameters of the selected motors and controllers.

Table 7. Selected Hobby Motors and Known Parameters.

	NTM PropDrive 28-36	Unknown Motor	2728 Brushless Outrunner
Rated Kv (kRPM*v)	1200	?	1000
#Poles	6	14	14
Power (W)	530	?	250
Max Current (A)	36	10	18
Nominal Operating Voltage (V)	14	?	14

Table 8. Selected Motor Controllers and Known Parameters.

	Turnigy Plush 40	Turnigy Plush 10	Hobbyking SS
Rated Voltage (V)	25	20	12.6
Continuous Current (A)	40	10	8
Burst Current	55	12	10

Note, the Hobbyking ss (HK-10) was destroyed by overcurrent. All data, although minimal, gathered using this controller is provided.

6.10 Identification Results

All motors were first identified using the custom motor controller developed (version 2C as pictured). All motors identified successfully with very consistent results over multiple identification runs. The results may be seen in Table 9 below.

Table 9. Identification Results.

	NTM PropDrive 28-36	Unknown	2728 Brushless Outrunner
Stator Resistance ($m\Omega$)	53.88501	65.27009	93.52004
Quadrature Inductance (μH)	8.263837	7.773364	13.37453
Direct Inductance (μH)	8.263837	7.773364	13.37453
Rated Flux (mV/Hz)	10.08105	3.875713	4.709641

This is in contrast with the TI development kit initially tested which would not successfully identify any of the three motors outlined in Table 9 above. The success in motor identification is due to the custom board voltage and current feedback being scaled for much more suitable levels for these motors. Because all of the tested motors are rated at or less than 14V, the *user.h* parameter `#define USER_IQ_FULL_SCALE_VOLTAGE_V` was changed from the board limit (24V) to (16V). This allows for slightly more resolution to be garnered from the same hardware. However, no substantial difference was seen in identification results for any of the motors tested.

6.11 Unloaded

The motors were initially tested un-loaded and the results for these tests can be seen in the table and figures below.

Table 10. Unloaded Motor Results.

High Performance Brushless DC Motor Control

Transition time zero to full speed (s)	0.49	0.51	0.39	0.76	0.61	0.54	0.69	0.68	0.54	0.61	NA	NA
Maximum Bus Current (A)	1.14	1.7	1.14	2.15	2.62	1.21	4.4	3.3	1.34	2.42	NA	NA

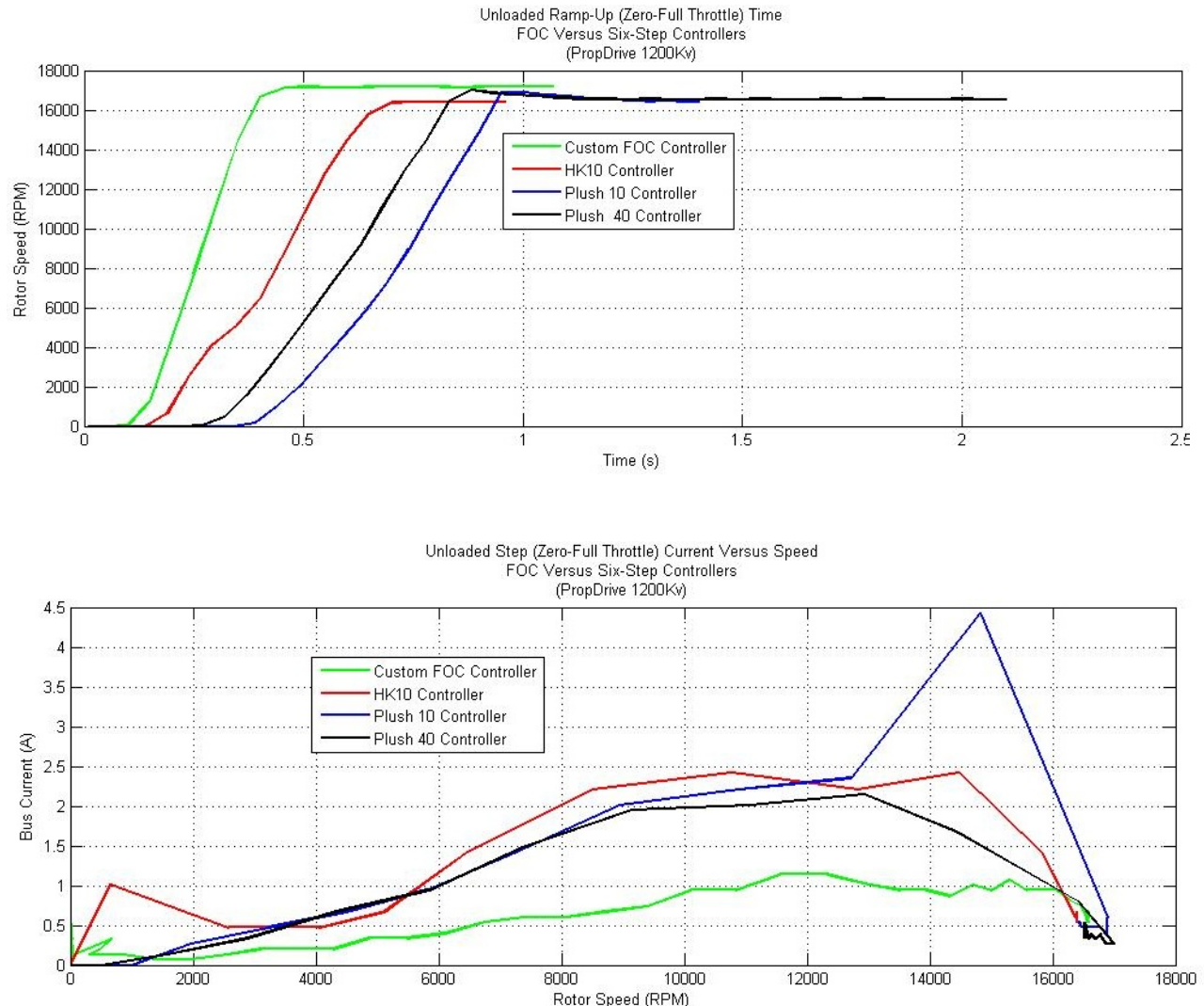


Figure 59. PropDrive Motor Unloaded Data.

Note, the apparent anomaly seen in the Current Versus Speed graph above is simply a result of the 1Hz oscillation resulting from InstaSPINs Forced Angle coupled with a single spurious Bus Current reading and should be ignored.

High Performance Brushless DC Motor Control

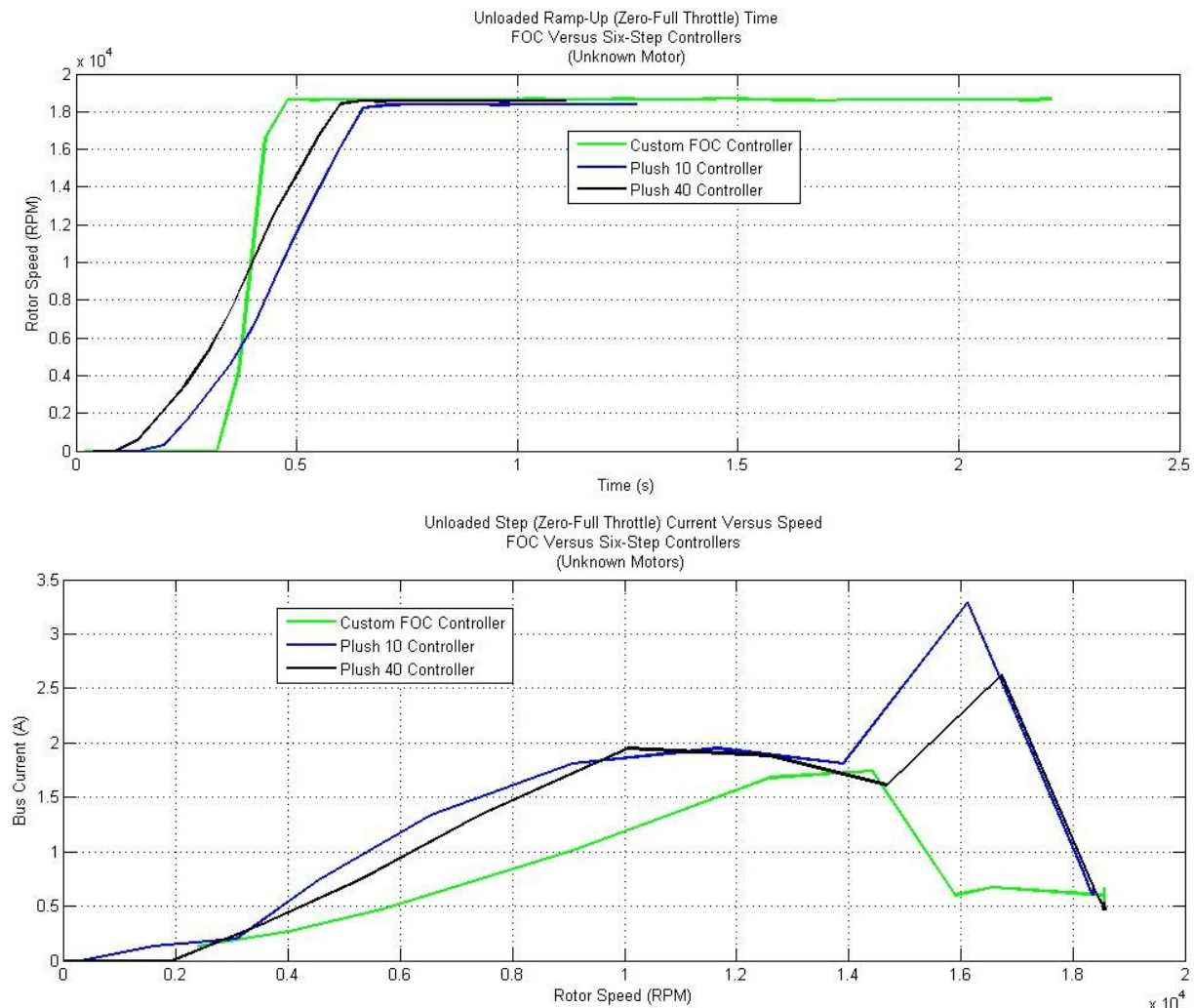


Figure 60. Unknown Motor Unloaded Data.

High Performance Brushless DC Motor Control

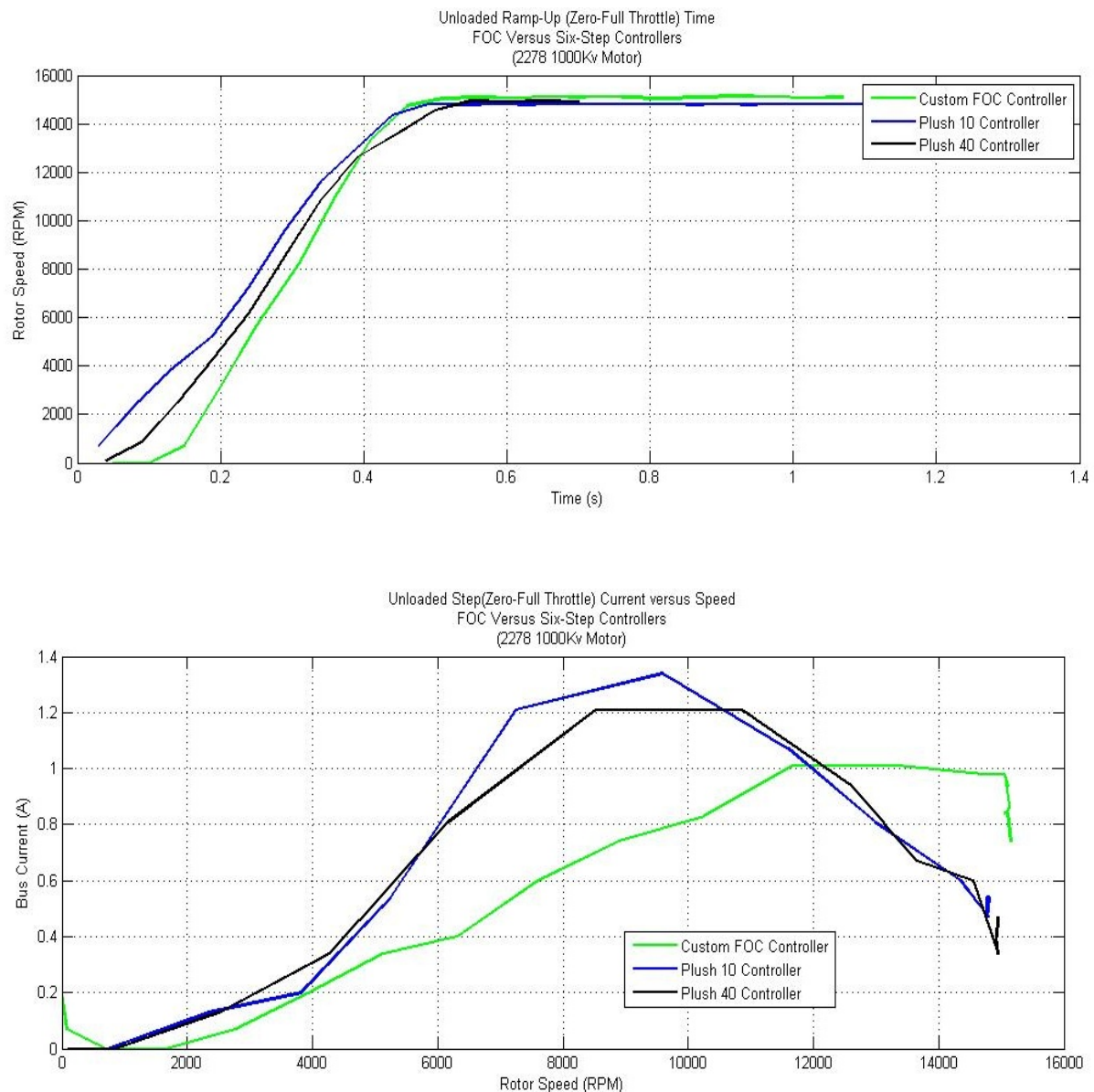


Figure 61. 2278 Motor Unloaded Data.

Several conclusions can be drawn from the unloaded motor test results shown above. The most significant difference between the custom FOC controller and the commercial controllers tested was the ability of each controller to commutate at very low speeds. The FOC controller was able to control all motors at speeds around 100RPM and, in addition, utilising InstaSPIN's speed loop the motors could develop significant torque at these low RPMs. The low speed torque test was conducted by adding lateral resistance to the rotor by hand and subjectively noting the response. This was done because a suitable programmable load could not be developed in the time frame. While this test provides no empirical data, it did clearly show that the FOC controller could produce substantial torque even at low RPMs. In contrast, the commercial controllers tested were not able to commutate an unloaded BLDC motor at speeds below 1500RPM, and, at these RPMs, the motors produced very little torque and would stall when the rotor was touched. It should be noted that significant torque is only developed at low RPM by the FOC controller when the speed loop is used, for obvious reasons. Commercial controllers do not utilise closed loop speed controllers, explaining why they are not able to develop torque while unloaded at low RPMs. However, the ability to produce high torque at low RPMs does have uses, for instance, in submersible vehicles where costly mechanical gear boxes are currently used to meet this need.

The custom FOC board was also able ramp the motors up to their top speed considerably faster than the commercial controllers were capable of. On average, the custom FOC controller was 35% faster at transitioning a motor from zero to full speed. In addition, the unloaded speed of each motor under FOC control was faster than any commercial controller tested. Referring to the Rotor Speed/Time graphs shown in Figure 59, Figure 60 and Figure 61, it can be seen that the FOC controller has not only a much quicker ramp-up time, but is also a cleaner and more controlled response. PI loop gains were set by the identified motor parameters directly and not tuned. The performance of the controller serves as validation for the identified parameters. In addition, with PI loop gain fine tuning, the performance, and particularly, the transition time could be further improved. While PI loop gains were fine-tuned during initial InstaSPIN evaluation, it was decided that they would not be tuned beyond automatic InstaSPIN automatic tuning, to show the capability of the Custom FOC Controller with very little user intervention.

Finally, the rotor speed versus bus current graphs provide an excellent comparison of the efficiency of the FOC controller relative to the efficiency of the commercially available tested controllers. In every case, the peak current required by the FOC controller to get the motor to its rated speed was substantially less than what was used by the commercial controller. Interestingly, the Plush 10 controller tested suffered from particularly high current spikes. Given the very quick response times of all of the motor/controller combinations tested (<1s) and the 50mS sampling time, these spikes are often only a single data point. However, these are not spurious data points as the controller/motor combinations have been tested multiple times with consistent results. In fact, it is likely that the current spikes are not the maximum bus current present but are sampled at either side of the *true* peak.

In every metric tested for the unloaded motor/controller combinations, the custom FOC controller had the best performance. In some cases, the performance increases were substantial as compared to the commercial controllers, in particular, the minimum stable rotor speed and ramp up time from zero to full speed. In addition, the Rotor Speed Versus Bus Current graphs provided show that the custom FOC controller averages substantially less bus current usage than any of the commercial controllers tested.

6.12 Loaded

The motors were loaded with a 10*4.5"R aeroplane propeller (shown in Figure 58) to provide a consistent torque to the motors tested. A propeller is a very suitable load for testing of this nature as it provides a torque relative to the rotor speed. In addition, the torque produced for a certain speed is the same regardless of the motor the propeller is attached to. Further, to allow for accurate comparison between controller (as much as possible), the speed controllers were (not actively) current limited to 10A such that all of the controllers and motors could be tested over the same range. Again, the same bench power supply was used across all test to ensure comparisons made were valid.

Table 11, Figure 62, Figure 63 and Figure 64 below shows the response of the motors and controllers from a zero to 10A set-point.

Table 11. Loaded Motor Results.

Controller:	InstaSpin FOC			Plush 40			Plush 10		
Motor:	NTM PropDrive 28-36	Unknown	2728 Brushless Outrunner	NTM PropDrive 28-36	Unknown	2728 Brushless Outrunner	NTM PropDrive 28-36	Unknown	2728 Brushless Outrunner
Minimum Stable Rotor Speed (RPM)	80	70	75	1150	850	820	1050	750	920
Maximum Stable Rotor Speed (kPRM)	5.95	4.65	4.8	5.90	4.60	4.57	5.4	4.3	4.6
Transition time zero to full speed (s)	0.51	1.12	1.12	1.12	1.27	1.23	1.1	1.53	1.12
Maximum Bus Current (A)	10.87	9.93	10.07	13.56	18.46	12.21	10.87	12.62	13.56

High Performance Brushless DC Motor Control

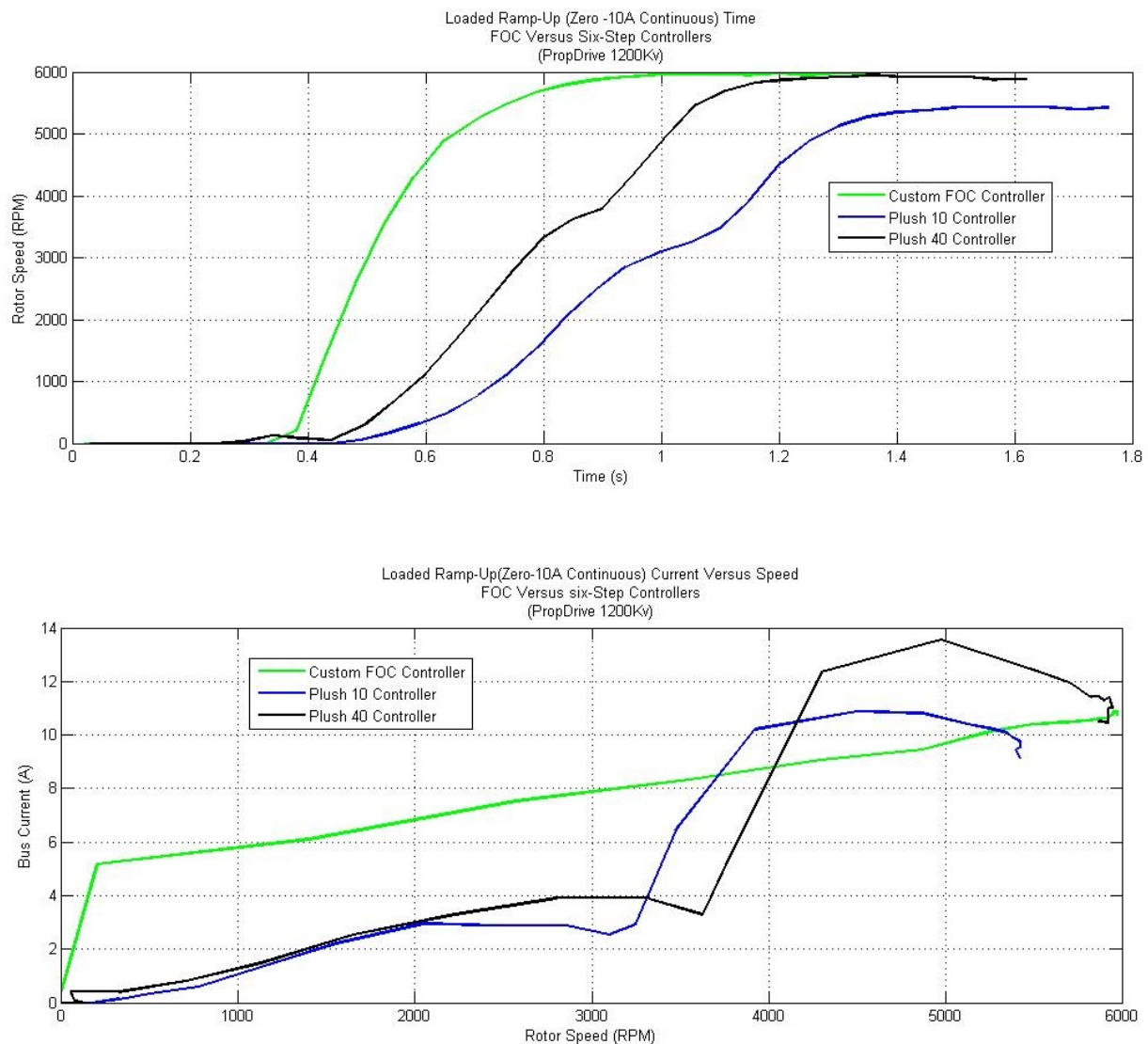


Figure 62. PropDrive Motor Loaded Data.

High Performance Brushless DC Motor Control

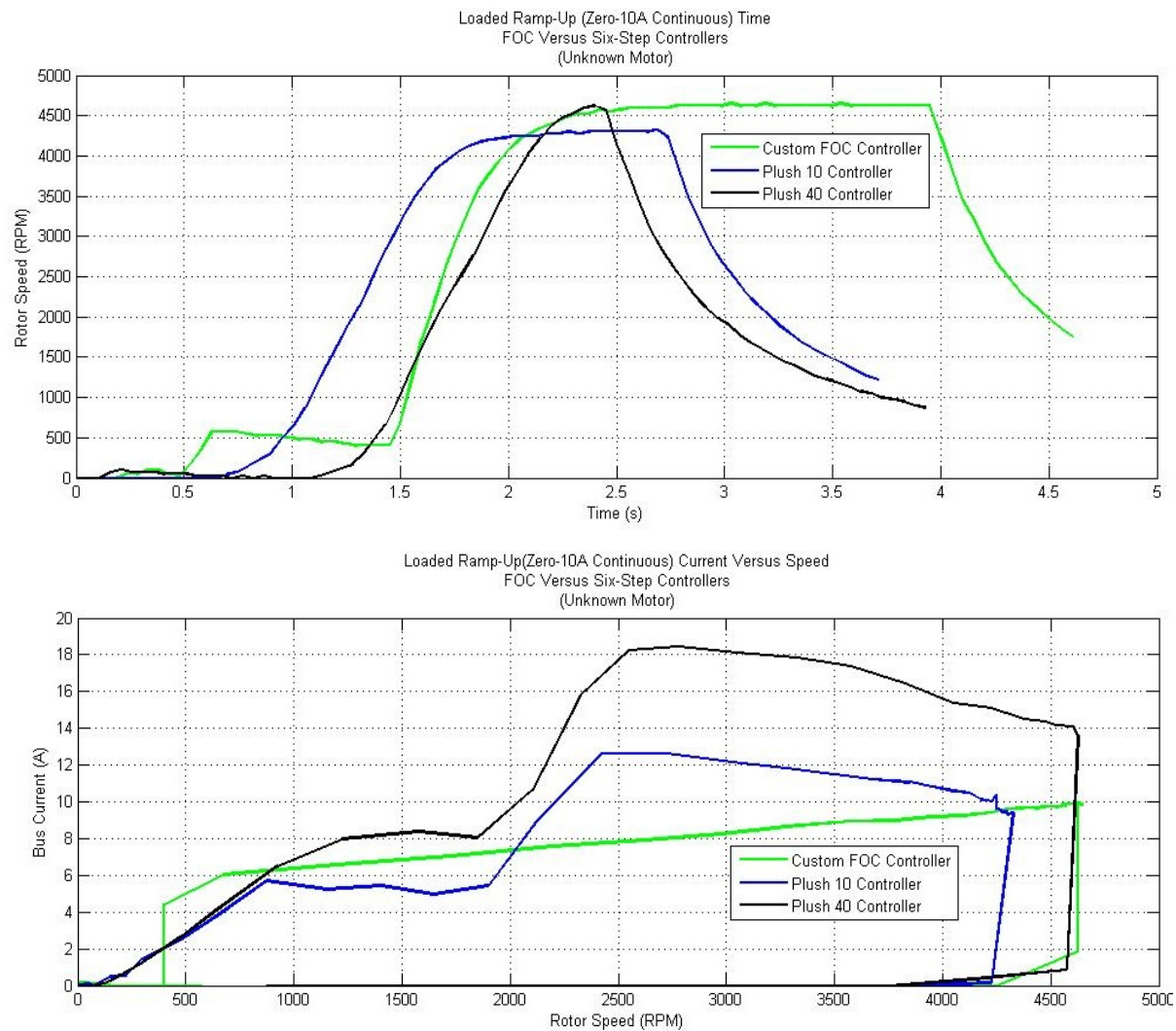


Figure 63. Unknown Motor Unloaded Data.

Note, the custom FOC controller in the figure above was spinning down from a previous test, hence the starting point of 500RPM.

High Performance Brushless DC Motor Control

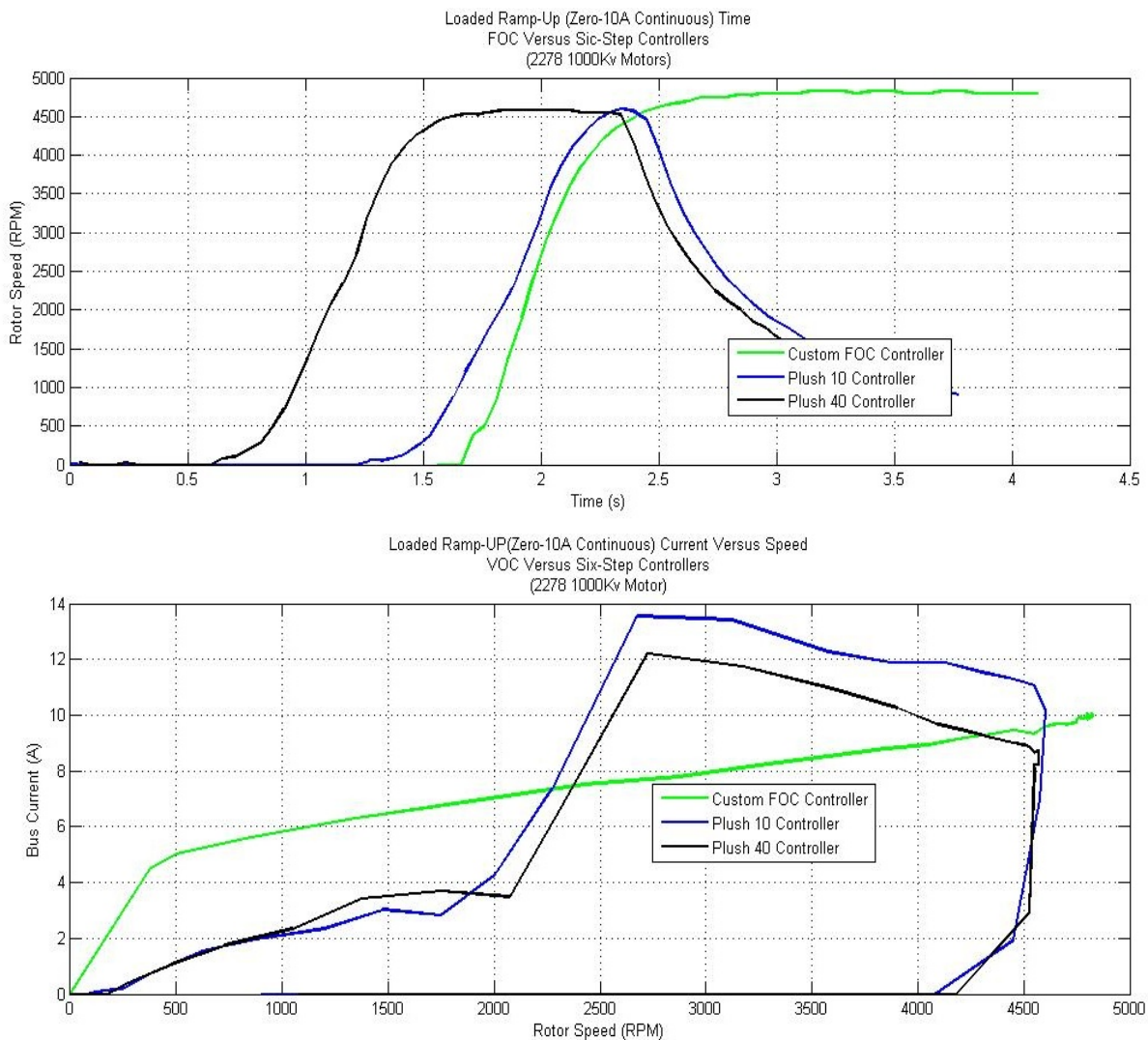


Figure 64. 2278 Motor Loaded Data.

Figure 65 below shows the results of multi-step ‘efficiency’ testing on the motor controller combinations. This test was conducted by choosing 20 speeds and adjusting the torque set-point of each controller until that speed was reached. This allows for a comparison of the efficiencies of the motors at each speed set-point under steady-state conditions. This differs from the single-step tests above in that the aim of the controller is to maintain the set-torque and not to reach a specific set-point in a minimum time.

High Performance Brushless DC Motor Control

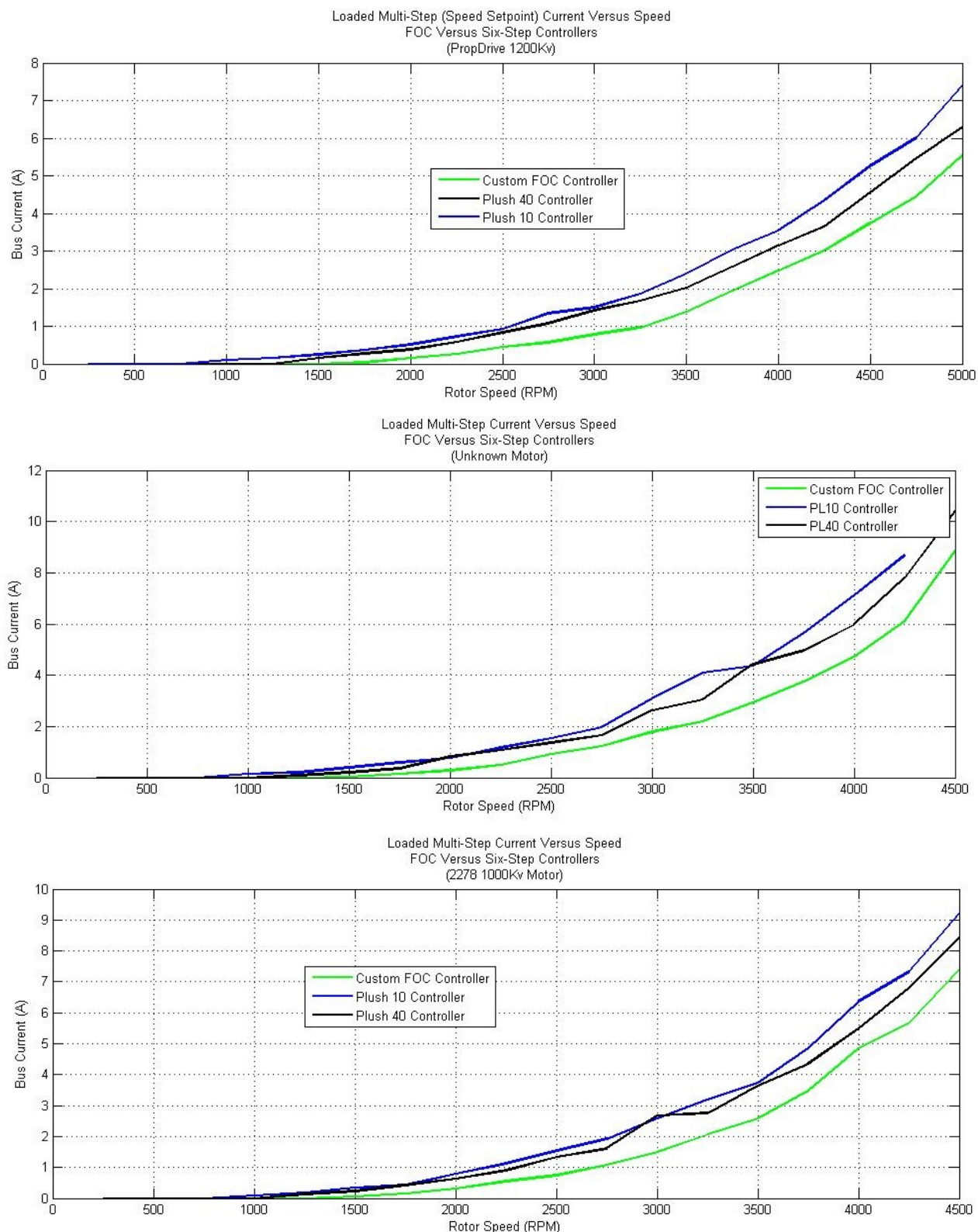


Figure 65. Multi-Step Response of controller/motor combinations.

With the motors loaded with a 10*4.5"R aeroplane propeller the results tell a similar story to the unloaded data. Referring to Table 11, it can be seen that once more, the custom FOC controller has outperformed the commercial controllers tested. Notably, the response time for the PropDrive motor was almost twice as fast as either of the commercial controller tested. The custom FOC controller was able to commutate all of the tested motors at dramatically lower speeds than either of the six-step controllers were capable of. Additionally, the FOC controller was also confined to the 10A limit far more effectively than either of the other tested controllers which had substantial current spikes.

In all cases, FOCs control response was much smoother than the commercial controllers. This is evident in the top graphs of Figure 62, Figure 63 and Figure 64. The rotor speed versus bus current also shown in the figures outlined shows that the FOC controller's current draw spikes initially but maintains a relative constant current draw across the full speed range. This is in clear contrast with the commercial controllers which have a significant spike at about half the maximum commanded speed. Also note that the graphs tendency to fold back in on itself is not a result of spurious data points, but is merely a representation of the controllers being commanded to zero torque and the motors spinning under their own inertia.

Using the Multi-Step response data shown in Figure 65 and removing very low current draw data (the comparisons at the very low end skew the data in FOCs favour as a very small difference in current draw (<50mA) can easily result in several 100% relative efficiency increases even though the actual current draw is not significantly different) the commercial controllers on average drew 30.41% more current than the custom FOC controller when used to drive the PropDrive motor. Similarly, the commercial controllers used, on average, 49.1% more than the custom FOC controller while driving the unknown motor and 40.9% more while driving the 2278 motor. These efficiency increases are substantial, and, while they are repeatable (using the same sensors) and certainly provide strong evidence for the increases in efficiency the FOC controller offers, it is doubtful if a comprehensive test suite (as suggested in section 7.9 Recommendations for Future) would show such a profound efficiency increase. For example, in the 2278 motor multi-step response shown in Figure 65 above, there is clearly a spike in the Plush 40 Controller's curve, and while this test was conducted several times, it is possible this is a spurious data point skewing the results in the Custom FOC Controllers favour. However, no serious test methodology flaws are known and doubts regarding the profound efficiency increases seen stem solely from intuition.

6.13 Cost and Physical Comparison

The total cost for the custom FOC controller, not including manufacturing and other secondary costs may be seen in Appendix II. The cost for a single board (\$75USD) is considerably high, however, when working with mass production quantities of components, this cost drops dramatically (\$25USD). In comparison, the Turnigy Plush 10, Plush 40 and Hobby King SS 8-10A cost \$10, \$22 and \$6.5 respectively. Adding manufacturing costs and general overhead, the custom FOC controller will not be able to compete in terms of price with commercial six-step controllers. However, the custom FOC controller was not intended as a direct competitor to currently available six-step controllers. It was designed for high-end applications (autonomous vehicles for example) which require efficiency and performance that the current generation of commercial controllers cannot meet. In this respect, the custom FOC controller is relatively cheap. This is because the FOC controller does not require any external sensors to achieve very efficient and high precision control.

In terms of physical size, the current revision (2C) of the Custom FOC Controller is significantly larger than any of the commercial controllers tried. It is believed that a further revision could shrink the current size of the Custom FOC Controller further, and, moving to a four layer board, further still. However, the Custom FOC Controller will not be able to achieve the same compactness as commercial six-step controllers, in no small part due to the large footprint of the DRV8301 pre-driver. This device could be removed and exchanged for discrete components to reduce the board size, but this would remove most of the safety features of the board. Most potential applications for the Custom FOC Controller are experimental and benefit from the numerous protection elements this device offers. It was therefore decided that the pre-driver should not be removed and that the larger board size should be kept.

7 Conclusions and Recommendations for Future Work

Field Oriented Control has been shown to be a superior control methodology to six-step control for small BLDC motor controllers. This has been proven by designing and comparing a custom FOC based controller against several currently available commercial options which utilise six-step control. The tests revealed the custom FOC controller consistently outperforming the selected six-step controllers in all areas tested. The most dramatic advantage of the FOC Controller is its ability for low speed commutation. However, the cost of the custom FOC controller was significant when compared with off-the-shelf six-step controllers. In addition, the physical size of the custom controller was significantly larger (see photographs) but this was to be expected given the footprint of the pre-driver used.

The Custom Controller developed is highly customisable and can be used anywhere commercial BLDC controllers are currently used and in many applications where commercial BLDC controllers are not suitable. A full JTAG header has been added to every revision of the Custom FOC Controller, and is recommended for all future revisions. This allows all aspects of InstaSPIN-FOC to be used with the controller, including much functionality that was not tested during this research.

7.9 Recommendations for Future Work

Perhaps the biggest shortcoming of this research is the limitations of the evaluation of the controller's performance. Many tests that were planned were not conducted due to a lack of time and required lab-equipment. These tests include vibration testing and controller efficiency as well as several less crucial tests such as the thermal response of the controller. It is recommended that a comprehensive test suite be developed to evaluate the motor controller on its own merits rather than against commercial controllers. The controller's efficiency could be determined accurately by connecting the test motor to a second brushless DC motor with a three-phase programmable load connected across its phase leads. This will allow very accurate torque output measurements and would provide a value for the overall efficiency of the controller/motor combination with a small error margin (mechanical/electrical losses of the load motor).

It is also recommended that the power stage of the controller be revised to allow the continuous current rating of the controller to be increased. This is because, for anything but multicopters, the current rating of the controller is actually quite low. This would not replace the current board (which is a good size for most multicopters) but would just be a higher current version of the same board to allow its use in larger applications. To do this, it is recommended that the MOSFETs be changed to either CSD18532NQ5B (TI NexFET) or BSC016N04LS G (Infineon). In addition, it would be necessary to properly scale the current sense feedback (including shunt resistors) to the new range. Finally, the power traces should be increased on all boards including, revision 2C.

Revision 2C has both SDA and SCA broken out to allow I₂C to be used as the communications protocol instead of traditional 50Hz PWM (GPIO is broken out for this purpose). This would allow bi-directional communications meaning that data available to the Custom FOC Controller would become available to the 'master' controller. This data includes rotor speed, torque output, bus voltage and even motor temperature. It would also allow controller fault reporting to the master

device. I2C abstractions have been started but not finished and the beginnings of these abstractions may be seen in Appendix III.

Finally, the full potential of the Custom FOC Controller and InstaSPIN FOC has not yet been tested. This, again is due to time limitations caused by unexpectedly long development times. The Custom FOC Controller has the (untested) ability to actively break motors using programmable down speed curves, ramp-up motors on user defined curves, apply over-modulation to move the modulation waveform away from SVPWM and towards trapezoidal, and, field weakening could be used to allow a motor to run up to a theoretical speed of 1.5 times its own rating. This is all possible using the Custom FOC Controller as is, and, sample code for all of this (and more) is provided by Texas Instruments in MotorWare™12 (some minimal changes would be required). In fact, the Custom FOC Controller is very suitable for use as a stand-alone BLDC motor controller development board.

Bibliography

- Acroname, 2007. *Description of Pulse With Modulation*. [Online]
Available at: <http://www.acroname.com/robotics/info/concepts/pwm.html>
[Accessed 09 September 2013].
- Akin, B. & Bhardwaj, M., 2013. *Sensorless Field Oriented Control of 3-Phase Permanent Magnet Synchronous Motors (Application Report SPRABQ3)*, s.l.: Texas Instruments.
- ATMEL, 2007. *AVR449: Sinusoidal driving of 3-phase permanent magnet motor using ATiny261/461/861 (Application Note)*, San Jose: ATMEL.
- AttoPilotInternational, 2011. *Compact DC Voltage and Current Sense PCB with Analog Output (Datasheet)*, s.l.: AttoPilot International LLC.
- Cassadei, D., Profumo, F., Serra, G. & Tani, A., 2002. FOC and DTC: Two Viable Schemes for Induction Motors Torque Control. *IEEE TRANSACTIONS ON POWER ELECTRONICS*, 17(5), pp. 779-787.
- Copley Controls Corp, n.d. *What is 'Field Oriented Control' and what good is it?*, s.l.: Copley Controls Corp.
- Covey, G., 2011. *Brushless Basics*. [Online]
Available at: http://www.rcuniverse.com/magazine/article_display.cfm?article_id=1344
[Accessed 18 04 2014].
- CUI INC, 2010. *AMT 102 & 103 capacitive encoder*. [Online]
Available at: <http://www.cui.com/catalog/resource/1333>
[Accessed 27 January 2014].
- Dan, S., 2008. *Clarke's and Park's Transformations*, Hangzhou: College of Electrical Engineering, Zhejiang University.
- Garcia, X. T. et al., n.d. COMPARISON BETWEEN FOC AND DTC STRATEGIES FOR PERMANENT MAGNET SYNCHRONOUS MOTORS. *Advances in Electrical and Electronic Engineering*, pp. 76-81.
- Ilioudis, C. V. & Margaris, I. N., 2008. PMSM Sliding Mode Observer for Speed and Position Estimation Using Modified Back EMF. *13th International Power Electronics and Motion Control Conference*, pp. 1105-1110.
- Inoue, Y., Morimoto, S. & Sanada, M., 2011. Comparative Study of PMSM Drive Systems Based on Current Control and Direct Torque Control in Flux-weakening Control Region. *IEEE International Electric Machines & Drives Conference (IEMDC)*, pp. 1094-1099.
- Jacob, J., Alex, S. S. & Daniel, A. E., 2013. Speed Control of Brushless DC Motor Implementing Extended Kalman Filter. *International Journal of Engineering and Innovative Technology (IJEIT)*, 3(1), pp. 305-308.
- John, J. P., Kumar, S. S. & Jaya, B., 2011. Space Vector Modulation based Field Oriented Control Scheme for Brushless DC Motors. *IEEE*, pp. 346-351.

- Kummerl, S., 2011. *PowerPAD™ Thermally Enhanced Package*. Dallas: Texas Instruments.
- Lee, H. & Lee, J., 2013. Design of Iterative Sliding Mode Observer for Sensorless PMSM Control. *IEEE TRANSACTIONS ON CONTROL SYSTEMS TECHNOLOGY*, 21(4), pp. 1394-1399.
- Lee, S. & Lemley, T., n.d. A COMPARISON STUDY OF THE COMMUTATION METHODS FOR THE THREE-PHASE PERMANENT MAGNET BRUSHLESS DC MOTOR, Pennsylvania: Pennsylvania State University & Moog Inc.
- Lepka, J., 2009. *Sensorless PMSM Drive for Dishwasher Pump Using Freescale MC56F8006 Device*. [Online]
- Available at: <http://dev.emcelettronica.com/sensorless-pmsm-drive-dishwasher-pump-using-freescale-mc56f8006-device-12>
[Accessed 11 September 2013].
- Liu, Y. & Zhu, Z. Q., 2008. Direct Torque Control of Brushless DC Drives With Reduced Torque Ripple. *IEEE TRANSACTIONS ON INDUSTRY APPLICATIONS*, 41(2), pp. 599-608.
- Lock, T., 2012. *qut-brushless-controller*. [Online]
- Available at: <https://code.google.com/p/qut-brushless-controller/wiki/mosfetdrive>
[Accessed 15 September 2013].
- Merzoug, M. S. & Naceri, F., 2008. Comparison of Field-Oriented Control and Direct Torque Control for Permanent Magnet Synchronous Motor (PMSM). *World Academy of Science, Engineering and Technology*, Volume 21, pp. 299-204.
- Microcontroller Solutions, n.d. *Sensorless BLDC Motor Control with Back-EMF Filtering Using a Majority Function*. [Online]
- Available at:
<http://www.digikey.com/us/en/techzone/microcontroller/resources/articles/sensorless-bldc-motor-control.html>
[Accessed 03 September 2013].
- Ozturk, S. B. & Toluyat, H. A., 2007. Direct Torque Control of Brushless DC Motor with Non-sinusoidal Back-EMF. *IEEE*, pp. 165-171.
- Paturca, S. V., Covrig, M. & Melcescu, L., 2006. Direct Torque Control of Permanent Magnet Synchronous Motor (PMSM) – an approach by using Space Vector Modulation (SVM). *Conf. on Electric Power Systems, High Voltages, Electric Machines*, Volume 6, pp. 111-116.
- SERL, 2014. *SERL Quadrotor Research Platform*. [Online]
- Available at: <http://systemsengineeringresearchlaboratory.org/projects/current-projects/srl-quadrotor/>
[Accessed 10 May 2014].
- Spurgeon, S. K., 2008. Sliding mode observers: a survey. *International Journal of Systems Science*, 39(8), pp. 751-764.

High Performance Brushless DC Motor Control

Terzic, B. & Jadric, M., 2001. Design and Implementation of the Extended Kalman Filter for the Speed and Rotor Position Estimation of Brushless DC Motor. *IEEE TRANSACTIONS ON INDUSTRIAL ELECTRONICS*, 48(6), pp. 1065-1073.

Texas Instruments, 2011. *Three Phase Pre-Driver with Dual Current Shunt Amplifiers and Buck Regulator*. [Online]

Available at: <http://www.ti.com/lit/ds/symlink/dr8301.pdf>
[Accessed 23 March 2014].

Texas Instruments, 2013. *Breakthrough InstaSPIN™-FOC motor control technology is here!*, Dallas: Texas Instruments.

Texas Instruments, 2013. *TMS320F28026F, TMS320F28027F InstaSPIN™-FOC Software Technical Reference Manual*. Texas: Texas Instruments.

Texas Instruments, 2013. TMS320F2802xF InstaSPIN™-FOC, TMS320F2806xF InstaSPIN™-FOC, TMS320F2806xM InstaSPIN™-MOTION User's Guide. In: *Hardware Prerequisites*. Dallas: Texas Instruments, pp. 144-153.

Texas Instruments, 2013. Tuning the FAST Current Loop. In: *InstaSPIN Projects and Labs User's Guide*. Texas: Texas Instruments, pp. 69-73.

Texas Instruments, 2014. *Motor Drive BoosterPack featuring DRV8301 and NexFET™ MOSFETs*. [Online]

Available at: <http://www.ti.com/tool/boostxl-drv8301>
[Accessed 23 March 2014].

Torres, D., 2009. *Comparing motor-control techniques*. [Online]

Available at: <http://www.ecnmag.com/articles/2009/10/comparing-motor-control-techniques>
[Accessed 05 September 2013].

Ungurean, A., Coroban-Schramel, V. & Boldea, I., 2010. Sensorless control of a BLDC PM motor based on I-f starting and Back-EMF zero-crossing detection. *International Conference on Optimization of Electrical and Electronic Equipment*, Volume 12, pp. 377-382.

Virginia Tech, n.d. *SPACE VECTOR MODULATION FOR THREE-LEG VOLTAGE*. [Online]

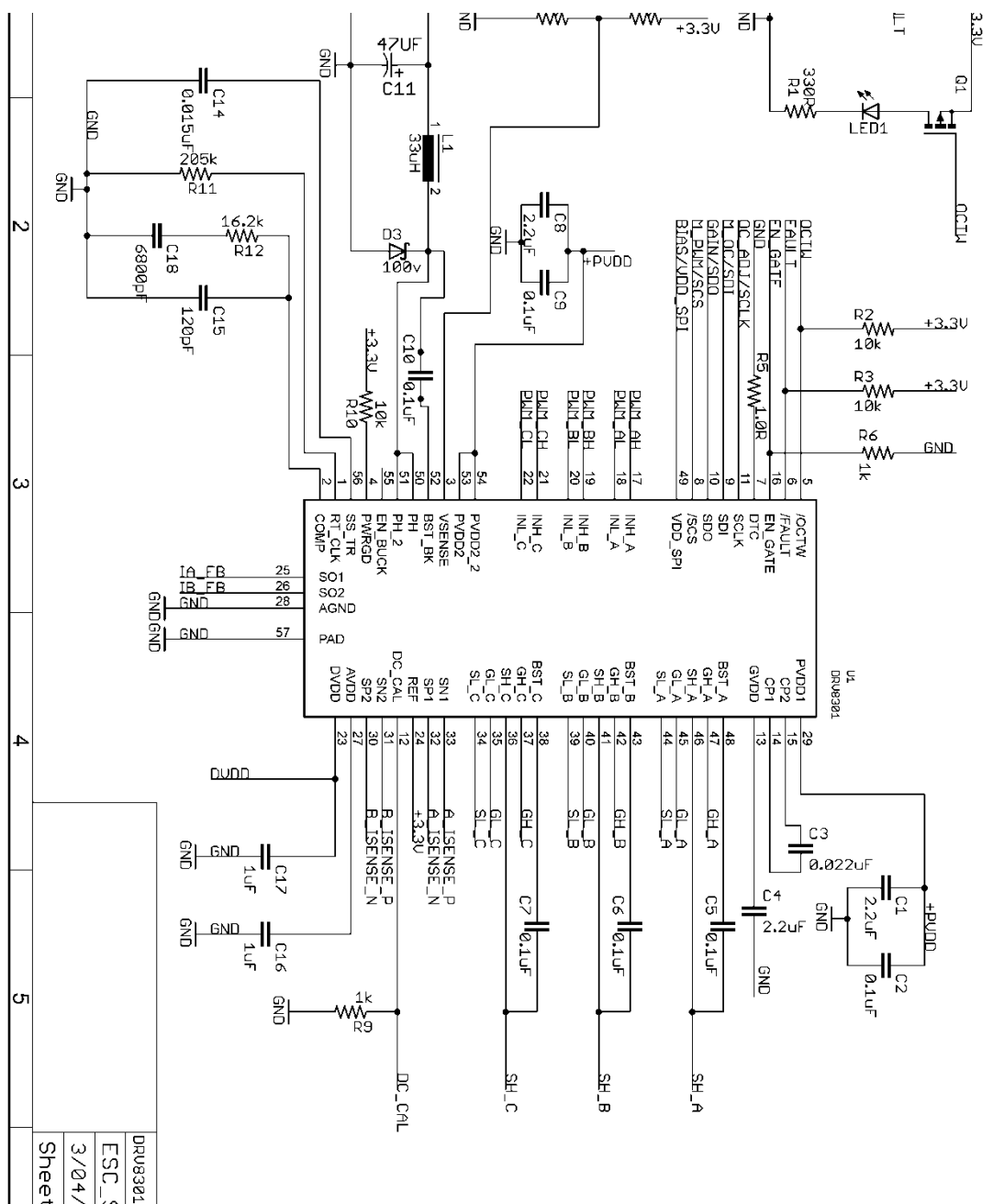
Available at: <http://scholar.lib.vt.edu/theses/available/etd-2798-1216/unrestricted/chap2.pdf>
[Accessed 20 September 2013].

Yedamale, P., 2003. *Brushless DC (BLDC) Motor Fundamentals*, Chandler: Microchip.

Zambada, J. & Deb, D., 2010. *Sensorless Field Oriented Control of a PMSM (AN1078)*, Chandler: Microchip.

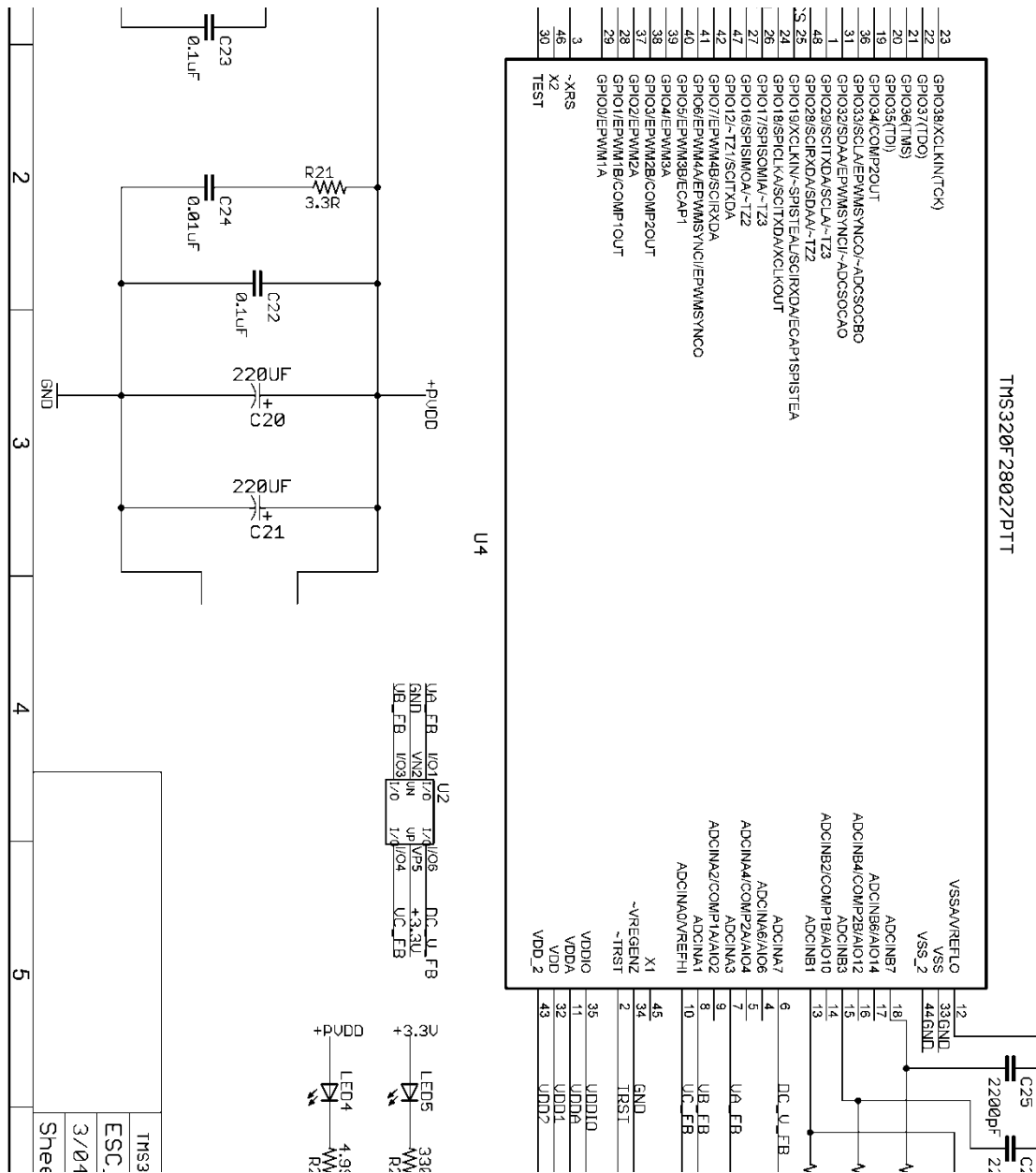
APENDIX I

FOC Speed Controller



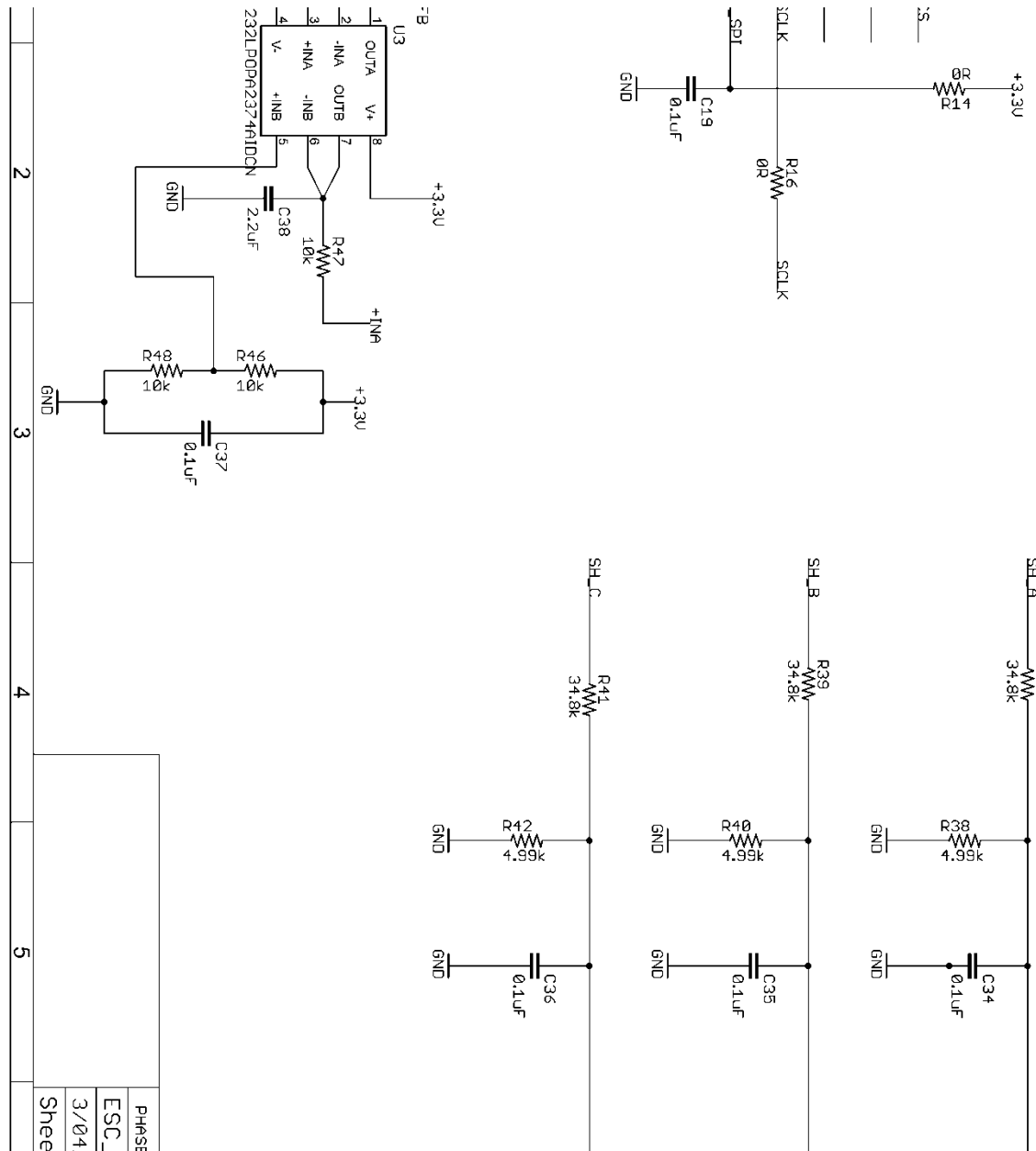
FOC Speed Controller Full Schematic (2/5)

High Performance Brushless DC Motor Control



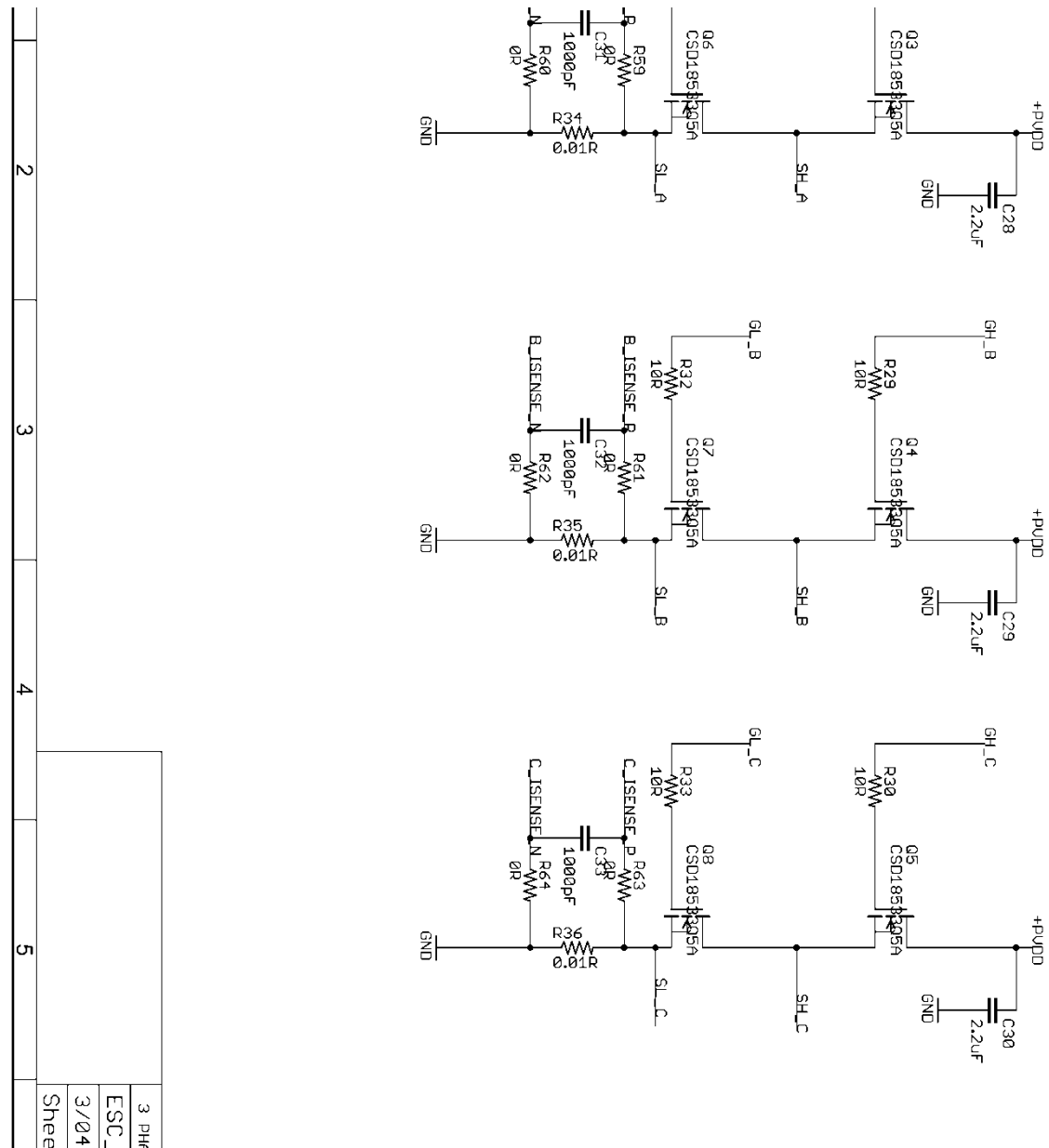
FOC Speed Controller Full Schematic (3/5)

High Performance Brushless DC Motor Control



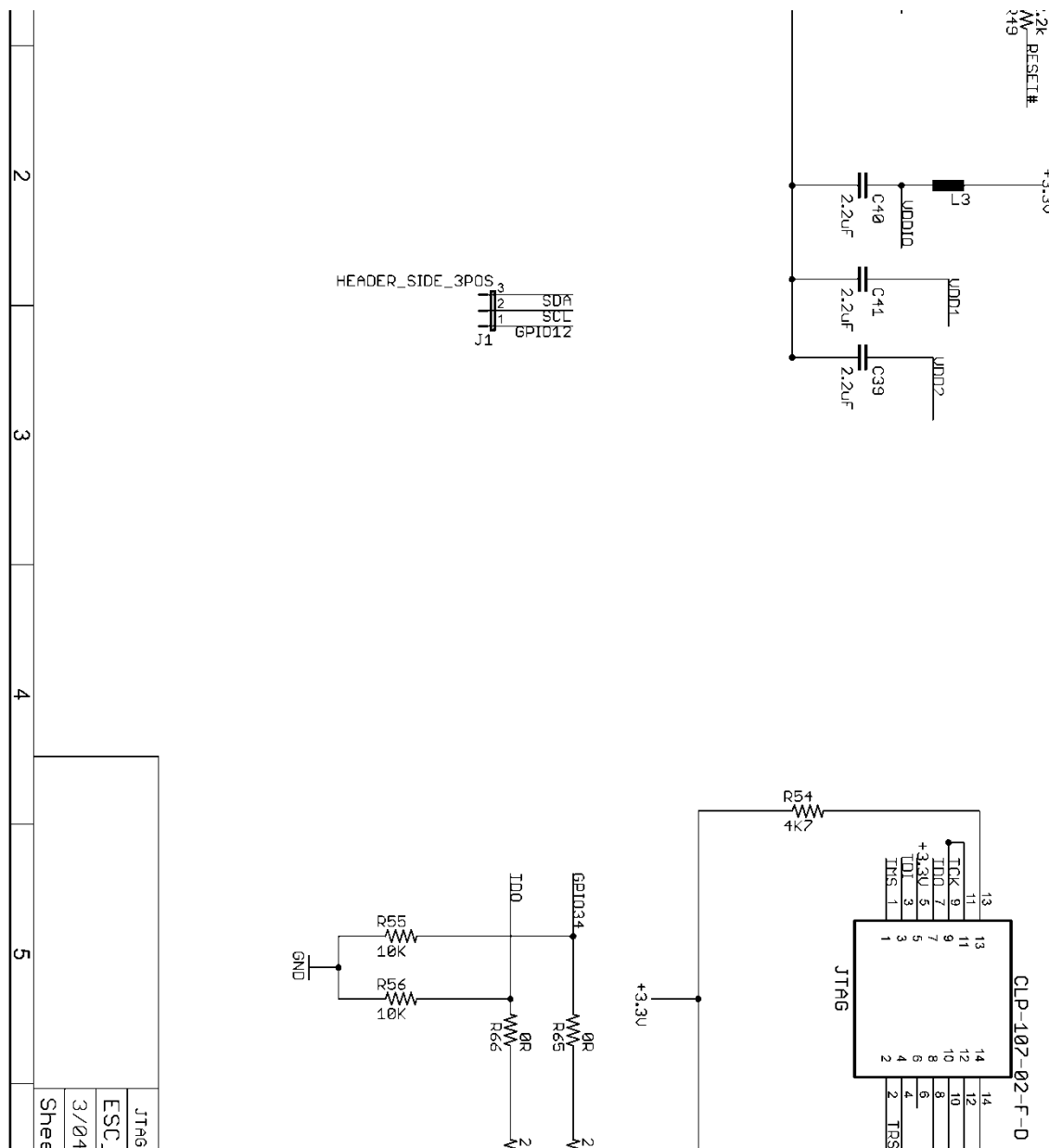
FOC Speed Controller Full Schematic (4/5)

High Performance Brushless DC Motor Control



FOC Speed Controller Full Schematic (5/5)

High Performance Brushless DC Motor Control



Appendix II

Cost of custom FOC controller bill of materials (BOM)

Total Cost (\$USD)	\$ 75.061	Total Cost (Mass Production)(\$USD)	\$ 24.601	Total Boards	1							
Part	Quantity	Value	Description	PackageReference	PartNumber	Manufacturer	Digi-Key PN	Cost/1 (\$USD)	Bulk Cost/1(\$USD)	Cost(\$USD) = B8*18	Bulk(\$USD) = E	Notes
C20, C21	2	220uF	CAP, AL, 220uF, 50V, +/-20%, 0.3 ohm, SMD	SMT Radial G	EEE-FC1H221P	Panasonic	PCE4016CT-ND	\$ 1.050	\$ 0.318	\$ 2.100	\$ 0.64	
C11	1	47uF	CAP, AL, 47uF, 25V, +/-20%, 0.36 ohm, SMD	SMT Radial D	EEE-FK1E470P	Panasonic	PCE3804CT-ND	\$ 0.560	\$ 0.119	\$ 0.560	\$ 0.12	
C14	1	0.015uF	CAP, CERM, 0.015uF, 50V, +/-10%, X7R, 0603	0603	GRM188R71H153KA01	MuRata	490-1514-1-ND	\$ 0.100	\$ 0.012	\$ 0.100	\$ 0.01	
C24	1	0.01uF	CAP, CERM, 0.01uF, 100V, +/-10%, X7R, 0603	0603	C1608X7R2A103K	TDK	445-1304-1-ND	\$ 0.100	\$ 0.012	\$ 0.100	\$ 0.01	
C3	1	0.022uF	CAP, CERM, 0.022uF, 50V, +/-10%, X7R, 0603	0603	C1608X7R1H223K	TDK	445-1312-1-ND	\$ 0.100	\$ 0.046	\$ 0.100	\$ 0.05	
C2, C9, C22	3	0.1uF	CAP, CERM, 0.1uF, 100V, +/-10%, X7R, 0603	0603	GRM188R72A104KA35	MuRata	490-3285-1-ND	\$ 0.200	\$ 0.047	\$ 0.600	\$ 0.14	
C23, C34, C35, C36, C37	4	0.1uF	CAP, CERM, 0.1uF, 16V, +/-5%, X7R, 0603	0603	C0603C104J4RACTU	Kemet	399-1097-1-ND	\$ 0.110	\$ 0.016	\$ 0.440	\$ 0.06	
C12, C19	2	0.1uF	CAP, CERM, 0.1uF, 25V, +/-10%, X7R, 0603	0603	C1608X7R1E104K	TDK	445-1316-1-ND	\$ 0.100	\$ 0.005	\$ 0.200	\$ 0.01	
C5, C6, C7, C10	4	0.1uF	CAP, CERM, 0.1uF, 50V, +/-10%, X7R, 0603	0603	C1608X7R1H104K	TDK	445-1314-1-ND	\$ 0.100	\$ 0.008	\$ 0.400	\$ 0.03	
C31, C32, C33	3	1000pF	CAP, CERM, 1000pF, 50V, +/-5%, COG/NP0, 0603	0603	C0603C102J5GAC	Kemet	399-3293-1-ND	\$ 0.100	\$ 0.011	\$ 0.300	\$ 0.03	
C15	1	120pF	CAP, CERM, 120pF, 50V, +/-5%, COG/NP0, 0603	0603	GRM1885C1H121JA01	MuRata	490-1429-1-ND	\$ 0.100	\$ 0.019	\$ 0.100	\$ 0.02	
C13	1	1uF	CAP, CERM, 1uF, 25V, +/-10%, X5R, 0603	0603	C1608XR1E105K080A	TDK	445-5146-1-ND	\$ 0.130	\$ 0.019	\$ 0.130	\$ 0.02	
C16, C17	2	1uF	CAP, CERM, 1uF, 25V, +/-10%, X5R, 0603	0603	GRM188R61E105KA12	MuRata	490-3897-1-ND	\$ 0.120	\$ 0.082	\$ 0.240	\$ 0.16	
C1, C8, C28, C29, C30	5	2.2uF	CAP, CERM, 2.2uF, 100V, +/-10%, X7R, 1210	1210	GRM32ER72A225KA35	MuRata	490-3385-1-ND	\$ 1.260	\$ 0.522	\$ 6.300	\$ 2.61	
C38	1	2.2uF	CAP, CERM, 2.2uF, 10V, +/-20%, X5R, 0603	0603	C0603C225MBPACTU	Kemet	399-4912-1-ND	\$ 0.390	\$ 0.083	\$ 0.390	\$ 0.08	
C4	1	2.2uF	CAP, CERM, 2.2uF, 25V, +/-10%, X5R, 0805	0805	GRM219R61E225KA12	MuRata	490-1701-1-ND	\$ 0.340	\$ 0.104	\$ 0.340	\$ 0.10	
C25, C26, C27	3	2200pF	CAP, CERM, 2200pF, 16V, +/-10%, X7R, 0603	0603	GRM188R71C222KA01	MuRata	NA - Mouser: 81-GRM188R	\$ 0.297	\$ 0.008	\$ 0.891	\$ 0.02	0 Available.... Alt-> Mouser number: 81
C18	1	6800pF	CAP, CERM, 6800pF, 50V, +/-10%, X7R, 0603	0603	GRM188R71H682KA01	MuRata	490-1508-1-ND	\$ 0.100	\$ 0.010	\$ 0.100	\$ 0.01	
D3	1	100V	Diode, Schottky, 100V, 2A, SMB	SMB	CDBB2100-G	Comchip Technology	641-1109-1-ND	\$ 0.510	\$ 0.163	\$ 0.510	\$ 0.16	
U2	1	NUP4201MR6	IC, 500mV, Transient Voltage Suppressors	SOT	NUP4201MR6	On Semi	NUP4201MR6T1GOSCT-ND	\$ 0.670	\$ 0.214	\$ 0.670	\$ 0.21	
U1	1	DRV8301DCA	IC, 3 Phase Pre-Driver with Dual Current Shunt Amplifiers and Buck Regulator-Hardware Controlled		DRV8301DCA	Texas Instruments	296-29433-1-ND	\$ 6.480	\$ 2.813	\$ 6.480	\$ 2.81	
U3	1	OPA2374AIDCNx	IC, CMOS, R-R I/O Op Amp, Single Supply, 6.5MHz, 585uA	SSOP-8	OPA2374AIDCN	TI	296-18504-1-ND	\$ 2.260	\$ 1.420	\$ 2.260	\$ 1.42	
L1	1	33uH	INDUCTOR SHIELD PWR 33UH SMD	0.300" sq	DR74-330-R	Cooper Bussmann	513-1141-1-ND	\$ 1.400	\$ 0.560	\$ 1.400	\$ 0.56	
LED 4,5	2	GREEN	LED THIN 565NM GRN DIFF 0805 SMD		SML-LXT0805GW-TR	Lumex Opto/Componer	67-1553-1-ND	\$ 0.470	\$ 0.070	\$ 0.940	\$ 0.14	
LED 1	1	YELLOW	LED THIN 585NM YEL DIFF 0805 SMD		SML-LXT0805YW-TR	Lumex Opto/Componer	67-1554-1-ND	\$ 0.430	\$ 0.064	\$ 0.430	\$ 0.06	
LED 2	1	RED	LED THIN 660NM SUPRED DIFF0805SMD		SML-LXT0805SRW-TR	Lumex Opto/Componer	67-1555-1-ND	\$ 0.410	\$ 0.060	\$ 0.410	\$ 0.06	
Q1, Q2	2	P_CH	MOSFET P-CH 8V 5.4A SOT23-3		SI2325DS-T1-E3	Vishey Siliconix	SI2325DS-T1-E3CT-ND	\$ 1.200	\$ 0.443	\$ 2.400	\$ 0.89	
Q3, Q4, Q5, Q6, Q7, Q8	6	CSD18533Q5A	MOSFET, N-Chan, 60V, 18A, 6.1 mOhm	QFN-8 POWER	CSD18533Q5A	TI	296-35027-1-ND	\$ 1.810	\$ 0.709	\$ 10.860	\$ 4.25	
R14,	8	0	RES, 0 ohm, 5%, 0.1W, 0603	0603	CRCW06030000Z0EA	Vishay-Dale	541-0.0GCT-ND	\$ 0.074	\$ 0.004	\$ 0.592	\$ 0.03	
R16,R59,R60,R61,R62,R63,R64							CRA2512-FZ-R010ELFCT-ND	\$ 0.670	\$ 0.237	\$ 2.010	\$ 0.71	
R34, R35, R36	3	0.01	RES, 0.01 ohm, 1%, 3W, 2512	2512	CRA2512-FZ-R010ELF	Bourns	541-1.0GCT-ND	\$ 0.074	\$ 0.004	\$ 0.074	\$ 0.00	
R5	1	1.0	RES, 1.0 ohm, 5%, 0.1W, 0603	0603	CRCW06031R00JNEA	Vishay-Dale	541-1.00KHCT-ND	\$ 0.081	\$ 0.006	\$ 0.162	\$ 0.01	
R44, R45	2	1.00k	RES, 1.00k ohm, 1%, 0.1W, 0603	0603	CRCW06031K00FKEA	Vishay-Dale	541-1.0KGCT-ND	\$ 0.074	\$ 0.004	\$ 0.148	\$ 0.01	
R6, R9	2	1.0k	RES, 1.0k ohm, 5%, 0.1W, 0603	0603	CRCW06031K00JNEA	Vishay-Dale	541-10KGCT-ND	\$ 0.074	\$ 0.004	\$ 0.370	\$ 0.02	
R28, R29, R30, R31, R32, R33	5	10	RES, 10 ohm, 5%, 0.1W, 0603	0603	CRCW060310R00JNEA	Vishay-Dale	RG1608P-103-B-T5	\$ 0.530	\$ 0.057	\$ 2.120	\$ 0.23	
R8, R43, R46, R48	4	10.0k	RES, 10.0k ohm, 0.1%, 0.1W, 0603	0603	RG1608P-103-B-T5	Susumu Co Ltd	RG16P10.0KBCT-ND	\$ 0.074	\$ 0.004	\$ 0.296	\$ 0.02	
R2, R3, R10, R47	4	10k	RES, 10k ohm, 5%, 0.1W, 0603	0603	CRCW060310K00JNEA	Vishay-Dale	541-16.2KHCT-ND	\$ 0.081	\$ 0.006	\$ 0.081	\$ 0.01	
R12	1	16.2k	RES, 16.2k ohm, 1%, 0.1W, 0603	0603	CRCW060316K2FKEA	Vishay-Dale	541-205KHCT-ND	\$ 0.081	\$ 0.006	\$ 0.081	\$ 0.01	
R11	1	205k	RES, 205k ohm, 1%, 0.1W, 0603	0603	CRCW0603205KFKEA	Vishay-Dale	541-3.3UACT-ND	\$ 0.380	\$ 0.054	\$ 0.380	\$ 0.05	
R21	1	3.3	RES, 3.3 ohm, 5%, 0.25W, 1206	1206	CRCW12063R30JNEA	Vishay-Dale	541-31.6KHCT-ND	\$ 0.081	\$ 0.006	\$ 0.081	\$ 0.01	
R7	1	31.6k	RES, 31.6k ohm, 1%, 0.1W, 0603	0603	CRCW060331K6FKEA	Vishay-Dale	541-330GCT-ND	\$ 0.074	\$ 0.004	\$ 0.222	\$ 0.01	
R1, R4, R24	3	330	RES, 330 ohm, 5%, 0.1W, 0603	0603	CRCW0603330RJNEA	Vishay-Dale	541-34.8KHCT-ND	\$ 0.081	\$ 0.006	\$ 0.324	\$ 0.02	
R20, R37, R39, R41	4	34.8k	RES, 34.8k ohm, 1%, 0.1W, 0603	0603	CRCW060334K8FKEA	Vishay-Dale	541-4.99KHCT-ND	\$ 0.081	\$ 0.006	\$ 0.405	\$ 0.03	
R22, R23, R38, R40, R42	5	4.99k	RES, 4.99k ohm, 1%, 0.1W, 0603	0603	CRCW06034K99FKEA	Vishay-Dale	541-56GCT-ND	\$ 0.074	\$ 0.004	\$ 0.222	\$ 0.01	
R25, R26, R27	3	56	RES, 56 ohm, 5%, 0.1W, 0603	0603	CRCW060356R00JNEA	Vishay-Dale	541-56GCT-ND	\$ 0.100	\$ 0.015	\$ 0.100	\$ 0.01	

Appendix III

Custom FOC Controller Source Code

Note, the code provided below only constitutes the header or c files that were altered in some way for this project. InstaSPIN™ requires many more header and c files, including;

<i>adc.c/.h</i>	<i>gate.c/.h</i>
<i>clarke.c/.h</i>	<i>gpio.c/.h</i>
<i>clk.c/.h</i>	<i>ipark.c/.h</i>
<i>CodeStartBranch.asm</i>	<i>memCopy.c/.h</i>
<i>cpu.c/.h</i>	<i>offset.c/.h</i>
<i>ctrl.c/.h</i>	<i>osc.c/.h</i>
<i>filter_fo.c/.h</i>	<i>pid.c/.h</i>
<i>flash.c/.h</i>	<i>pie.c/.h</i>
<i>pll.c/h</i>	<i>spi.c/.h</i>
<i>pwm.c/.h</i>	<i>park.c/.h</i>
<i>svgen.c/.h</i>	<i>timer.c/.h</i>
<i>traj.c/.h</i>	<i>usDelay.c/.h</i>
<i>wdog.c/.h</i>	<i>Ram/Flash Linkers</i>

These files can be obtained freely from Texas Instrument's MotorWare™ 11 found at:

<http://www.ti.com/tool/motorware>

SPRT703

IMPORTANT NOTICE

Texas Instruments Incorporated and its subsidiaries (TI) reserve the right to make corrections, enhancements, improvements and other changes to its semiconductor products and services per JESD46, latest issue, and to discontinue any product or service per JESD48, latest issue. Buyers should obtain the latest relevant information before placing orders and should verify that such information is current and complete. All semiconductor products (also referred to herein as "components") are sold subject to TI's terms and conditions of sale supplied at the time of order acknowledgment.

TI warrants performance of its components to the specifications applicable at the time of sale, in accordance with the warranty in TI's terms and conditions of sale of semiconductor products. Testing and other quality control techniques are used to the extent TI deems necessary to support this warranty. Except where mandated by applicable law, testing of all parameters of each component is not necessarily performed.

TI assumes no liability for applications assistance or the design of Buyers' products. Buyers are responsible for their products and applications using TI components. To minimize the risks associated with Buyers' products and applications, Buyers should provide adequate design and operating safeguards.

TI does not warrant or represent that any license, either express or implied, is granted under any patent right, copyright, mask work right, or other intellectual property right relating to any combination, machine, or process in which TI components or services are used. Information published by TI regarding third-party products or services does not constitute a license to use such products or services or a warranty or endorsement thereof. Use of such information may require a license from a third party under the patents or other intellectual property of the third party, or a license from TI under the patents or other intellectual property of TI.

Reproduction of significant portions of TI information in TI data books or data sheets is permissible only if reproduction is without alteration and is accompanied by all associated warranties, conditions, limitations, and notices. TI is not responsible or liable for such altered documentation. Information of third parties may be subject to additional restrictions.

Resale of TI components or services with statements different from or beyond the parameters stated by TI for that component or service voids all express and any implied warranties for the associated TI component or service and is an unfair and deceptive business practice. TI is not responsible or liable for any such statements.

Buyer acknowledges and agrees that it is solely responsible for compliance with all legal, regulatory and safety-related requirements concerning its products, and any use of TI components in its applications, notwithstanding any applications-related information or support that may be provided by TI. Buyer represents and agrees that it has all the necessary expertise to create and implement safeguards which anticipate dangerous consequences of failures, monitor failures and their consequences, lessen the likelihood of failures that might cause harm and take appropriate remedial actions. Buyer will fully indemnify TI and its representatives against any damages arising out of the use of any TI components in safety-critical applications.

In some cases, TI components may be promoted specifically to facilitate safety-related applications. With such components, TI's goal is to help enable customers to design and create their own end-product solutions that meet applicable functional safety standards and requirements. Nonetheless, such components are subject to these terms.

No TI components are authorized for use in FDA Class III (or similar life-critical medical equipment) unless authorized officers of the parties have executed a special agreement specifically governing such use.

Only those TI components which TI has specifically designated as military grade or "enhanced plastic" are designed and intended for use in military/aerospace applications or environments. Buyer acknowledges and agrees that any military or aerospace use of TI components which have **not** been so designated is solely at the Buyer's risk, and that Buyer is solely responsible for compliance with all legal and regulatory requirements in connection with such use.

TI has specifically designated certain components as meeting ISO/TS16949 requirements, mainly for automotive use. In any case of use of non-designated products, TI will not be responsible for any failure to meet ISO/TS16949.

Products	Applications		
Audio	www.ti.com/audio	Automotive and Transportation	www.ti.com/automotive
Amplifiers	amplifier.ti.com	Communications and Telecom	www.ti.com/communications
Data Converters	dataconverter.ti.com	Computers and Peripherals	www.ti.com/computers
DLP® Products	www.dlp.com	Consumer Electronics	www.ti.com/consumer-apps
DSP	dsp.ti.com	Energy and Lighting	www.ti.com/energy
Clocks and Timers	www.ti.com/clocks	Industrial	www.ti.com/industrial
Interface	interface.ti.com	Medical	www.ti.com/medical
Logic	logic.ti.com	Security	www.ti.com/security
Power Mgmt	power.ti.com	Space, Avionics and Defense	www.ti.com/space-avionics-defense
Microcontrollers	microcontroller.ti.com	Video and Imaging	www.ti.com/video
RFID	www.ti-rfid.com	TI E2E Community	
OMAP Applications Processors	www.ti.com/omap	e2e.ti.com	
Wireless Connectivity	www.ti.com/wirelessconnectivity		